Department of Chemistry

SINGLE MOLECULE CONDUCTANCE OF ETHERS AND PEPTIDES

Thesis submitted in accordance with the requirements of the University of Liverpool for the degree of Doctor in Philosophy

by

Lisa Scullion

Supervisor: Prof. R. J. Nichols

September 2010

Abstract

This thesis presents investigations into the electrical properties are several novel 'molecular wires'. Scanning tunnelling microscope (STM) techniques were used to determine the single molecule conductance of seven different molecules including a simple alkane chain, alkanes containing oxygen and sulfur bridges and a selection of peptide sequences. Electrical contact to gold electrodes was achieved through employment of sulfur containing terminal groups such as thioacetates and the amino acid cysteine in the case of peptide molecules.

The first part of this thesis presents the first single molecule conductance measurements of heptanedithioacetate and explores the factors that influence the distance dependence of the *n*-alkanedithiol family. Investigations into central atom substitutions in polymethylene chains produced results to show that a single ether substitution showed behaviour consistent with a double tunnelling barrier system. This work was complemented with DFT calculations and barrier model fitting. Molecules incorporating two oxygen bridges and also one with a central sulfur atom were also studied. The single molecule conductance of all the molecules was found to be higher than their polymethylene analogues. Environmental effects are also presented and it was observed that molecular wires incorporating oxygen atoms had a higher conductance when measured in water environments.

The second part of this thesis is concerned with the conductance measurements of three different synthetic peptide sequences. The first two sequences presented different terminal linking groups which were observed to have minimal effects on the single molecule conductance. STM techniques were then employed to measure electrical properties and thus confirm the pH dependent switching of the final peptide. The switching mechanism was attributed to a conformational change from an α-helical structure to a random coil structure.

Preface

- Chapter 1 presents an introduction to this thesis and describes the background and theory behind molecular electronics. Conductance through single molecules and groups of molecules is discussed in addition to a description of tunnelling in molecular junctions. The operation and main components of a scanning tunnelling microscope are also presented and the progress in the field of single molecule conductance is reviewed.
- Chapter 2 is a description of the main techniques that are used throughout this thesis, including $I(s)$, $I(t)$ break junction and monolayer methods
- Chapter 3 describes the first single molecule conductance measurement of heptanedithioacetate, an overlooked member of the family of *n*-alkanedithiols. The conductance values observed were comparable with other alkanedithiols and found to fit very well into the series. A study of the anomalous length dependence of short alkanedithiols is also presented here.
- An examination of systematic changes in molecular wires and the subsequent effects on conductance values is presented in Chapter 4. Three ether molecules have been synthesised, two with ether oxygens and one thioether. A variety of techniques were used to determine the single molecule conductance of the three molecules. The results of these experiments showed that the substituted molecules showed enhanced electron transport capabilities to those of unsubstituted polymethylene chains. Also investigated, was the effect of environment on current flow through these wires.
- Chapter 5 describes the single molecule conductance measurements of three different peptide sequences. The first two are short alanine based sequences with alternate sulfur and amide linking groups. STM techniques were employed to determine that the linking groups did not have a large influence on the electron transport through the molecules; an observation that was rationalised by the examination of the peptide molecular lengths and conformations within the junction. The electrical properties of the third peptide were studied in different pH environments. At low pH values the peptide sequence was capable of electron transfer as it assumes a helical conformation, at high pH values the peptide adopted a random coil structure which consequently showed no electron transport features. The chapter also presents a review of some of the recent work on peptides within the field of molecular electronics.

Contents

List of Figures

Chapter 1. Introduction

1.1 Molecular Electronics

Incorporation of single molecules or groups of molecules into electronic devices is one of the primary aims of molecular electronics. Traditional solid state electronics is built upon silicon based top-down fabrication methods such as lithography and etching which involve the gradual reduction in dimensions of a larger scale object or pattern. However, current lithographic methods are limited to creating structures with a minimum size of around 10 nm[1] this is due to factors such as entanglement, positioning and reliability. The 'bottom up' method may allow nanoscale structures to be constructed atom by atom, using single molecules or clusters of molecules as integrated components, thus reducing further the size of such structures. Single molecules are attractive candidates as current methods of chemical synthesis allow virtually any design and functionality.

There is a continual demand for greater information storage capacity and faster information retrieval. One of the main driving forces to implement these bottom up methods and induce a paradigm shift in the electronics industry towards molecular electronics is the continuing fulfilment of Moore's law which states that the number of transistors incorporated on a memory chip doubles every year and a half.[2] A continual decrease in the size of transistors and improvements in design factors such as the efficiency of interconnections over the last several decades has allowed this prediction to be adhered to. However, within 10 – 20 years, following this trend, the size of transistors will need to approach close to the atomic scale. Further miniaturization using bottom up methods may enable devices to run at higher speeds and increase the density of active components within the devices,[3,4] it would also combat the rise in processing costs associated with decreasing the size of devices using present day techniques.

The introduction of scanning probe microscopes such as STM and AFM in the 1980s represented a breakthrough for molecular electronics, as they allowed surfaces to be imaged with atomic resolution and presented routes with which to investigate the electrical behaviour of individual molecules contacted to two electrodes. One of the most promising features of the STM is the ability to move and manipulate individual atoms and molecules on surfaces as a result of using an atomically sharp tip coupled with precision control. Building nanostructures atom by atom then becomes a possibility, however for the moment research is focused on using the intrinsic properties of molecules and atoms to form structures and crystals through thermodynamic interactions and self-assembly processes. [1,5,6]

To achieve the construction of devices and circuits on the nanometre scale using molecules, the molecular wires must be capable of electron or hole conduction and have a functionality that enables them to bind to the other elements in the system. They also need to have a defined length in order to bridge gaps between components and produce uniform operations. Development and optimization of such devices requires detailed understanding of the charge transport through molecules. Far from being ohmic in nature, molecular wires tend to facilitate electron transport through a tunnelling mechanism and many different types of molecules display enhanced transport function with respect to vacuum. Research over the last decade or so has been focussed on identifying single molecules that can display properties of electronic components such as switches to eventually replace current components such as field effect transistors.[7-9] Aviram and Ratner first proposed a molecular rectifier in a theoretical paper in 1974[10] where a molecule could behave as a p-n-junction due to a donor-spacer-acceptor structure, although it took almost 20 years before this was realized experimentally. In theory, molecular switches in a two state device could be used to function in a binary mode, where (1) and (0) are used to denote on and off states. Early work on molecular switches included the work by Collier *et al.*[7] where a catenane molecule switches between open and closed states with the applied bias of +2 V and -2 V. This switching is brought about by the

oxidation of a TTF moiety within a structure of two interlocking rings that results in a reversible rotation of one of the rings, the device could be switched on and off repeatedly at ambient temperatures. Haiss *et al.*[11,12] have reported electrochemical switching of a molecule incorporating a viologen group with two alkyl chains on either side, each six carbons in length. The viologen can switch from its oxidized ($bipy^{2+}$) state to the reduced ($bipy^{1+}$) state upon application of electrode potentials in solution, resulting in a change in conductance by a factor of six. More recently light-controlled molecular switching has been reported for diarylethene molecules[13] where the switching from the 'on' to 'off' states is achieved by illumination with visible light. Irradiation with UV light then allows switching back to the 'on' state. This phenomenon is due to the reversible isomerisation of the molecule from a conjugated to a cross-conjugated conformation.

Other molecules which show rectification behaviour[14,15] similar to that found in semiconductor diodes and molecules that exhibit negative differential resistance[12,16] that could be used in low noise amplification and high-frequency oscillators[17] have been examined. As a result, techniques have been developed whereby the molecules can be tethered to electrodes enabling the measurement of current flow through the molecules. Consequently, several methods to measure single molecule conductance have been reported with a certain degree of convergence between experimental results. Examples of experimental approaches include break junctions,[18] crossed nanowires,[19] conducting atomic force microscopy,[20] mercury drop experiments,[21,22] fabrication of nanopores[23-25] and nanoparticle bridge experiments.[26]

1.1.1 Journey to the Nanoscale

Physical properties of bulk systems such as electron transport, reactivity and optical effects are reasonably well understood; their properties are size independent down to a critical limit and are a result of averaged microscopic details. However, when the size of a material decreases below this limit it no longer displays the same properties as that of the bulk

material. For example, below 100 nm, materials may be subject to quantum size effects and their behaviour cannot be described by classical mechanics. Decreasing to nano-dimensions can result in an increased ratio of surface area to volume which can have large effects on some systems, for example, nanosized materials are often more temperature sensitive than their bulk counterparts as less energy is required to overcome the binding of surface atoms. Metal nanoparticles can display features such as surface plasmon resonance and small changes in size at the nanoscale result in different observed colours. Some semiconductors such as silicon exhibit increased band gaps when present as small nanoparticles or nanowires. A famous example of how physical properties change at the nanoscale is the case of carbon nanotubes. Their design and atomic arrangement result in unique features such as tremendous tensile strength and changeable electric properties. These size dependent changes can result in the appearance of novel system properties when one or more dimensions reach the nanoscale. These properties cannot be extrapolated from those of the bulk materials and so require detailed study if these nanomaterials are to be used in technological applications.

1.2 Metal-Molecule-Metal Junctions.

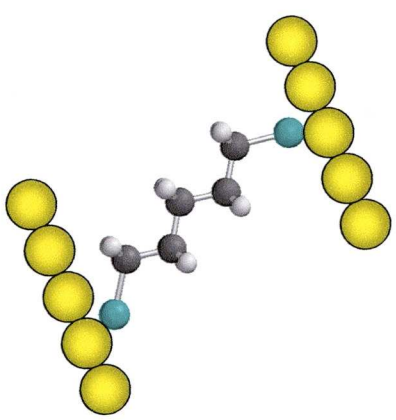

Figure 1.1. Single molecule (pentanedithiol) covalently attached to two gold contacts.

To produce devices incorporating organic molecules, a stable and reproducible contact between two metal electrodes must be formed as shown in the illustration in Figure 1.1. An electronic coupling across the junction is mediated by a molecular wire between the electrodes in a metal-molecule-metal junction, the strength of which can have an effect on the electron transport properties of the molecule.[27,28] Other factors that can have an effect include the chemical structure of the molecule in the junction,[29,30] the alignment of the molecular energy states of the molecule with the Fermi level of the electrodes, the geometry of the contact binding site,[28,29,31-33] the nature of the contacts and the nature of the terminal functional group of the molecule studied.[29,33] Also the environment and the presence of other molecules or components within the device can affect the properties of the molecule.[33] Although chemical synthesis is very advanced, if the purity of the molecules is not 100%, the distance between functional groups such as binding groups may vary due to the presence of small amounts of isomers or incorrectly synthesized molecules[34] Thermal stability[35,36] is also of great importance as increased temperatures may affect molecular conductance. This is a large number of variables to consider and tuning the junction properties only becomes viable once all of these factors are taken into consideration and the current flow through the molecule has been determined. Once these properties have been established, work can begin on designing suitable molecules for functional devices.

A wide variety of molecules have been considered for these applications for example, carbon nanotubes are exceptional structures that have been shown to have large application potentials within molecular electronics. They have metallic or semiconducting properties depending on their chirality and diameter.[37,38] Feldman *et al.*[37] demonstrated how single – walled carbon nanotubes can be used as molecule sized point contacts. They formed gaps in the nanotubes by oxygen plasma ion etching which resulted in carboxylic acid groups forming at the cut surfaces. They then introduced a variety of functionalised molecules, including DNA sequences, into the gap and produced "circuits" where the molecules could acts as molecular wires, sensors and switches.

1.3 Alkanedithiols

The electron transport properties of alkanedithiols have been extensively studied both in self-assembled monolayers and through single molecule experiments. Regardless of the fact that they are relatively insulating, the alkane series provides a test bed in which to study electron transport and contact effects. Their simple structure is well characterised and allows comparisons with other molecules and theoretical modelling in addition to providing a system with which to perfect techniques for measuring the conductance through single molecules. Monolayers can be prepared easily from the solution phase[31] with adsorption times seemingly independent of chain length.[39] The electron transport through alkanes proceeds via coherent non resonant tunnelling due to their large HOMO – LUMO gap of around 8 - 10eV and generally follows the equation:

$$G = A_N \exp(-\beta_N N) \quad (1)$$

Where G is the conductance, $\exp(-\beta_N N)$ is the tunnelling probability with β the decay constant, N the number of carbon atoms and A is a constant related to the metal-molecule coupling. In general the decay constant calculated for alkanes is around 1 per methylene group.[40-42] The exponential increase of chain resistance with chain length of alkanedithiols, together with weak temperature dependence supports this tunnelling mechanism and I-V curves for alkanedithiols are generally sigmoidal in nature.[42] The Simmons model is a way to describe the coherent non resonant tunnelling through a square potential barrier and assumes through bond tunnelling[43,44] and the current-voltage data for alkanedithiols can be fitted using this model. The case of alkanedithiols is discussed in more detail in Chapter 3.

Conjugated molecules exhibit more proficient electron transport capabilities due to the delocalisation of the electronic structure and their relatively small HOMO-LUMO gap as a result of lower lying unoccupied molecular orbitals.[25,43,45] They have been shown to exhibit large

conductance values compared to their saturated analogues[43] with a smaller decay factor of around 0.2 $Å^{-1}$.[45] The conductance of molecular wires incorporating phenyl derivatives has been reported to show a high dependence on the torsion angle between phenyl groups.[46]

1.4 Au Electrodes.

One of the most commonly used metals for surfaces in molecular conductance measurements is gold as it is reasonably inert, it does not corrode and is resistant to high acidity.[39] It is also very malleable and is the electrode material used throughout the following experiments. Studies have been performed on a wide range of electrode materials such as silver, palladium and platinum[36,42,47] where the work function of the different metals was shown to have an effect on the contact resistance, with higher work functions resulting in lower transport barriers. Hence the conductance of simple alkanedithiols bound to two Pt electrodes was found to be larger than corresponding experiments on gold by almost a factor of four. This highlights the influence of the molecule-metal contact within junctions. As gold will be the electrode material used here, the focus will be on comparable results using similar systems.

When deposited on glass, silicon or freshly cleaved mica, gold predominantly adopts the (111) crystallographic orientation,[39,48] which is a planar hexagonal close-packing arrangement. The most commonly studied metal-molecule binding motif is that of thiol on gold and the sulfur atom of a thiol group can adsorb in the hollow depressions between the triplet of gold atoms on the surface or at sites on top of atoms[36] according to the equation:

$$RSH + Au \rightarrow RS.Au + \tfrac{1}{2} H_2 \qquad (2)$$

After physisorption, the H atom is released resulting in the formation of a sulfur gold bond. Sulfur has a high affinity for gold and the bond is reasonably strong ~ 44 kcal/mol. Sulfur containing moieties are generally used as anchoring groups for this reason as the strength of the gold sulfur bond adsorbs preferentially over other terminal groups which

leads to controlled orientation of molecules in monolayers. Sulfur atoms can also form very strong bonds with many different types of metals including, gold, silver, copper and platinum.

1.5 Alternative Anchoring Groups

The nature of the contacts between the molecule and electrodes is strongly affected by the choice of anchoring group. Contacts differ in binding strength and can alter the state of energy level alignment. To investigate this effect, several groups have shown that carboxylate linkers can be used to create metal junction contacts[49,50] that show a higher contact resistance as a result of weak coupling with gold electrodes. Other terminal groups considered in single molecule measurements include isonitriles,[51] thiocyanates[36,45] and isocyanides. Pyridine groups have also been used as suitable contacts, with binding to electrodes also via the nitrogen lone pair.[18,41]

Amines are a popular alternative to sulfur as an anchoring group and have been shown to form reliable contacts to gold with weak covalent bonds[50,53] with a reported bond strength of ~ 8 kcal/mol. The measured conductance of amine terminated molecules is generally found to be lower than that of similar systems with thiol linkers as the amine gold bond shows a higher contact resistance then the S-Au bond. The amine bond in turn has a lower contact resistance then carboxylic terminated molecules. Venkataraman *et al.*[51] performed break junction measurements on 1,4-benzenediamine and a series of amine terminated alkanes. They found a very narrow range of conductance values as compared with thiol equivalents with a decay constant of around 0.9 per methylene group. They speculate that the amine groups bind to the gold by donating their two electrons to uncoordinated gold atoms. These well defined conductance values were investigated theoretically by Kristensen *et al.*[53] who used DFT calculations to deduce that amine groups show less variation in binding positions, generally forming contacts with gold through atop geometries. This is in contrast to sulfur groups that can

bind on top of gold atoms or in hollow sites and is due to the reduced available bonding sites on NH_2 as it is already bound to two hydrogens. Despite the well documented use of amine terminated molecules and SAMs on gold surfaces, their stability may be an issue. Lee *et al.*[48] completed a recent study using XPS and ToF-SIMS to show that the amine-Au contact degrades over time in ambient conditions as a result of oxidation of the amine.

1.6 Self-Assembly

Molecular layers are deposited on a surface in two main ways, Langmuir-Blodgett transfer and self-assembly. In the Langmuir-Blodgett preparation, monolayers are formed on the surface of a solution and then transferred onto solid substrates as films.[34,54] Self assembly meanwhile, relies on the intrinsic properties of certain molecules to anchor and orientate themselves onto a surface in an ordered fashion and therefore require a functional group to bind to a surface. Different substrates can result in different packing densities[55] and the degree of stability in the SAM is related to the chemical nature of the molecules.[35] However, only the case of SAMs on gold will be discussed here.

Self-assembled monolayers are attractive systems as they are highly ordered, easy to functionalise and can produce a variety of chemically tailored surfaces; they are capable of isolating a surface from its surroundings. Molecules that self assemble can address alignment issues within devices where difficulties are encountered in the positioning of nanometre scale features. However, there will always be a certain degree of defect sites owing to the difficulty in synthesising molecules with 100% purity[34] and the relative roughness of a surface can limit their long range order.[43] SAMs can be used for a variety of applications such as interface layers in biomedical systems between a metal surface and a solution[39] and self-assembly can be used to fabricate functionalised nanoparticles.[56] In alkanethiol and -dithiol SAMs the methylene groups are orientated and stabilised by van der Waals forces with reported tilt angles for alkanethiols on gold in the order of $\sim 30^0$.[39,43,55] In

monothiolated alkane layers adsorption stops at the monolayer level and multilayer formation is only observed after a long period of time,[39] these monolayers are reported to be stable up to temperatures of 110^0C[35] which is a desirable feature for electronic applications. Another aspect of alkanethiol monolayers is that they are densely packed and generally avoid contamination by water molecules due to their hydrophobicity.[57] This, coupled with their insulating nature means that they are often used as insulating matrices for the isolation and measurement of other, more conductive molecules.

There are a variety of methods available to characterise monolayers such as XPS, Infrared Spectroscopy and Ellipsometry. XPS allows the identification of different atoms within the monolayer and also gives an indication of their abundance. In infrared studies, the C-H stretching vibrations of the alkyl groups are sensitive to packing densities and defects allowing the quality of the monolayer to be investigated. Ellipsometry can be performed to measure the thickness of a monolayer and help to determine the tilt angles of the molecules within the layer.

Although the design and controlled orientation of SAMs has been studied extensively there is still the issue of the second contact. Methods of creating contacts at the free terminal end of a SAM include thermal evaporation[58] or nano-transfer printing, both of which can be used to deposit Au on the surface of the SAM. Hg drop methods[22] can also be used to create a second contact on films and the use of gold nanoparticles is common. The choice of top contact can have an effect on the conducting properties of the monolayer, for example, thermally evaporated contacts can exert pressure on the molecules or result in migration through the organic monolayer.[59] Efforts to prevent this migration have been reported, for example. Akkerman *et al.*[58] deposited a layer of highly conducting polymer on the top of an alkanedithiol SAM through spin coating. This provided a landing platform for the metal atoms and prevented them from entering into the SAM. The self-assembled monolayers presented in this study are contacted using a gold STM tip positioned at a set distance ensuring contact with the top of the monolayer with minimal intrusion into the monolayer structure.

1.7 STM

Scanning probe microscopy is a very powerful tool in nanoscale science which allows investigation into the structure and properties of molecules and surfaces with sub-nanometer resolution. The scanning tunnelling microscope (STM), was developed at IBM in 1981 by Binnig and Rohrer.[5] It was used to produce images of surfaces down to the atomic scale by scanning a sharp metal tip over a conducting sample at a distance sufficiently close to yield a measureable tunnelling current. Measuring the variation in height of the tip or the variation in tunnelling current results in the construction of a surface image. The development of the atomic force microscope (AFM) followed in 1986[60] and provided another way to image surfaces. It is based on a cantilever system that holds a sharp tip and measures the forces between tip and substrate or molecule, the measured forces are then used to create the image. In addition to topographic imaging, AFM also has a wide range of biological applications such as structural analysis of biomolecular assemblies and the binding of ligands and receptors [61] and, unlike STM, is not limited to conducting surfaces.

According to classical mechanics, electrons at the Fermi level do not have sufficient kinetic energy to overcome a vacuum barrier separating two closely packed metal electrodes. Tunnelling, however, is a quantum mechanical process that forms the fundamental basis for achieving charge flow between two closely placed electrodes and quantum mechanics can be used to rationalise the operation of an STM. When an STM tip is brought to within a certain distance of the substrate, typically 0.5 to 2 nm, electrons can tunnel through the gap upon application of a bias voltage as shown in Figure 1.2, which is an illustration of coherent tunnelling between two metals in a vacuum. The exponential distance dependence of this current allows precise control of the distance between tip and sample. The current is a result of the overlap of the wavefunctions of the two metal contacts and is in the order of nA (10^{-9} Ampere).[1] The probability of the transmission through this gap which acts as an insulating barrier decreases exponentially with the thickness of

the barrier, *d*, and the barrier height, φ. In UHV conditions, this tunnelling current is proportional to the applied voltage and an increase in *d* of even one Å results in a dramatic decrease in tunnelling current.[62]

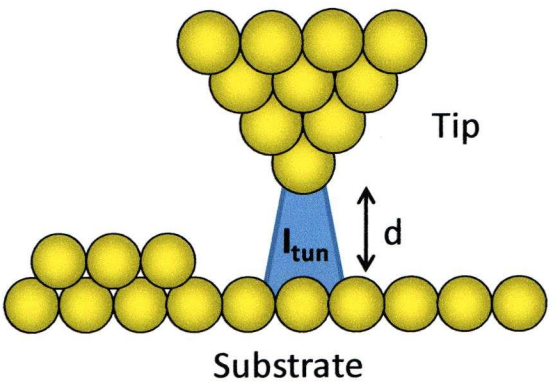

Figure 1.2. Illustration of the tunnelling current (I_{tun}) produced at sufficient tip sample separation (d).

In order for tunnelling to occur, one side of the junction must have unoccupied electronic states to accept electrons. Where the two metals are identical, their Fermi energies will be at the same level when the bias voltage is equal to zero as shown in Figure 1.3 (a). Application of a voltage across this junction means that the electronic energy of one of the metals is elevated with respect to the other with a subsequent shift in Fermi energies, electrons can then tunnel through the junction. For example, the application of a positive potential with respect to the sample results in a decrease in the energy level of the tip by a corresponding value (eV_b). This means that electrons from the filled sample states can tunnel into the unoccupied states of the tip as shown in Figure 1.3 (b). Altering the polarity of the bias voltage controls the direction of this tunnelling current with negative potentials producing an increase in the energy levels of the tip (Figure 1.3 (c)). For the majority of the following experiments, the STM will be used under ambient conditions: here the tip-sample gap can be occupied with water and other compounds

from the air which generally leads to lower barriers for electron tunnelling.

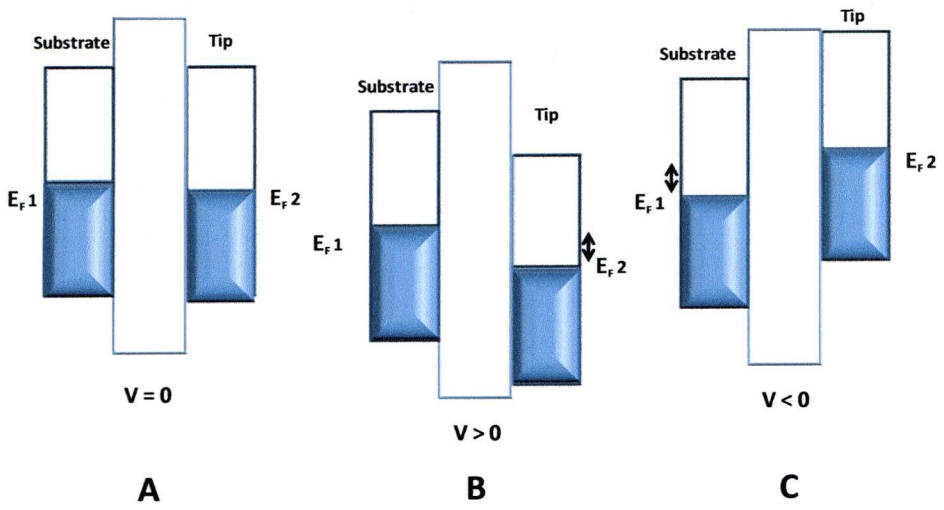

Figure 1.3. Relative alignment of energy bands between two metals in a vacuum at varying bias voltages, a) V = 0, b) V > 0 and c) V< 0.

1.7.1 Imaging

Atomic scale imaging using the STM is achieved by the application of a bias voltage between a sharp metallic tip and a conductive substrate. The tip is scanned over the surface either in a constant height or a constant current mode. In the constant height mode, the tip is kept at a fixed distance from the surface and the tunnelling current is recorded as a function of the lateral x – y position.[1,63] In the resultant image, the brightest areas correspond to the regions where the tunnelling current is greatest. In constant current mode, the vertical position of the tip can change in order to maintain a constant tunnelling current; here the feedback loop is crucial for the constant adjustment of the tip height. The Tersoff and Hamann approach,[64] assumes that tunnelling occurs through s-orbitals in the tip and using perturbation methods describes the tunnelling current as a function of the density of states of the surface at the Fermi energy at a distance r:

$$I \propto \rho(r, E_F) \qquad (3)$$

Image resolution is affected by several parameters; most significant is the structure of the tip apex. The sharper the tip, the more resolved the image will be, however, in most STM experiments the atomic scale structure of the tip apex is unknown. Also the electronic structure of the sample and external parameters such as vibrations and noise can limit the resolution.[1]

1.7.2 Components of the STM

The STM scanner contains piezoelectric components which are responsible for the sub Å precision movements of the STM tip. Piezomaterials are a group of compounds which are crystalline or ceramic in nature and possess a permanent dipole. A voltage applied to piezoelectric materials results in a change in shape of the material either through elongation or shrinkage in a variety of directions. In an STM, a piezo ceramic tube is used as an actuator and scans across the surface in a raster motion. The outside of the tube is divided into quadrants to which electrodes are attached; these electrodes are responsible for the lateral movement of the tube. They can produce bending of the tube proportional to the voltage applied to one or all of these x and y electrodes. There is also an electrode on the inside of the tube and when the voltage is applied to the inner and outer electrodes, the tube contracts or extends in the vertical direction, this results in three-dimensional tip movements. The STM also requires a vibration isolation system which in this case consists of a heavy based platform and suspension of the STM by ropes in a pendulum fashion. When a sample is introduced in to the STM, it is brought to within a few micrometers of the tip by manual positioning; a stepper motor is then used to close the gap between tip and substrate to a point where the scanner then takes over and controls the gap separation until a predetermined tunnelling current value is obtained. The electronic feedback then maintains a constant tip height or tunnelling current as described earlier.

The imaging capabilities of the STM are one of the principle reasons why it is such a powerful tool in molecular electronics. The potential to

image a surface before performing measurements is invaluable, as it allows identification and location of molecules on a substrate which can then be examined individually. It can also give data about the surface itself such as crystallographic orientation and the presence of defects. The STM also allows the study of systems in different environments such as liquids and UHV and at solid liquid interfaces. In 2003,[18] an STM was used to study single molecule conductance using a break junction method; since then many STM and AFM approaches have been developed with which to contact and measure current through molecules. It is this application of STM which is employed throughout the following work.

1.8 Quantum Conductance

When the tip sample distance is sufficiently decreased, the tip can make contact with the sample. The conductance measured when the contact between two metal electrodes is formed by a single atom is in the order of $2e^2/h$ where, e is the electron charge and h is Planck's constant and is equivalent to 77.4 μS. Experiments carried out using mechanically controlled break junctions with Na contacts and quantum point contact experiments with 2D gases showed a characteristic sequence of integer values of conductance in the conductance histogram.[18,65,66] These experiments confirmed the original Landauer expression[67] that related conductance to transmission, whereby:

$$G = \frac{2e^2}{h}\frac{t}{1-t}$$

Where t is the transmission probability and G is the conductance as a function of $2e^2/h$ and is equal to = 77.4 μS. These results have been realised experimentally in STM break junction techniques performed on gold,[18,40,41,51] where multiples of G, i.e. $_nG$ where n = 1, 2 or 3 are seen corresponding to n number of atomic gold chains. An STM tip is brought into contact with a gold surface and pulled apart, the conductance was seen to decrease in a stepwise fashion as the cross section of the contact was reduced down to a single chain of atoms.

1.9 Tunnelling Through a Molecule

When measuring the current through a single molecule such as an alkanedithiol connected to two electrodes, the Fermi level of the electrode is generally located between the HOMO and LUMO electronic states of the molecule as shown in Figure 1.4. For alkanedithiols this gap is sufficient to prevent resonant tunnelling through the molecular energy levels.

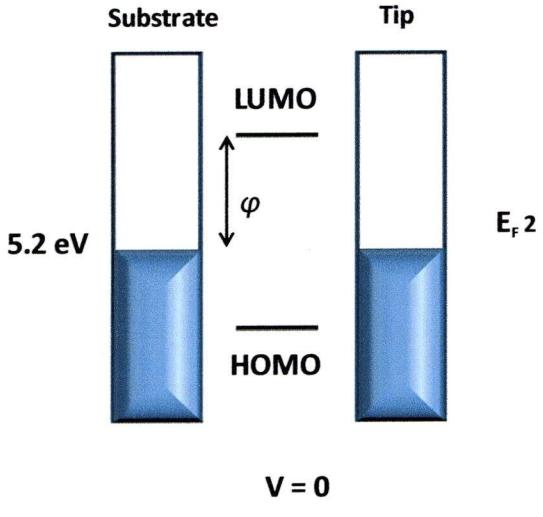

Figure 1. 4. Molecular orbitals of an insulating material relative to electrode Fermi level (in this case Au).

This is a simple representation of a one dimensional tunnelling barrier, where the metal contacts are separated by a relatively insulating material. The barrier has a potential barrier height, φ and the barrier thickness, d, is equivalent to the through bond length of the molecule in question. The barrier height is simply the difference in energy of the Fermi level of the metal and the frontier molecular orbital of the molecule that participates in the electron transport. An increase in the barrier height or barrier thickness results in a decrease in current. So for non resonant tunnelling, application of low voltages adjusts the energy of electrons in the metal meaning

electrons can tunnel through the HOMO or LUMO orbital of the molecule. As the applied potential is increased, the HOMO or LUMO orbital approaches the Fermi level of the electrode but the gap is sufficient that neither orbital will align with the Fermi energy. Resonant tunnelling will only occur if the bridging molecule has electronic states in resonance with the metal Fermi energy. The position of molecular energy levels is therefore a very important determining factor as to the mechanism of electron transport through a single molecule.

Double tunnelling barriers, also known as a quantum well or barrier indentations are generally associated with semiconductors. Examples include layers of GaAs separated by a layer of a semi conductor with a larger band gap. This essentially results in two single tunnelling barriers separated by a distance, d. The orbital energies of the compound in the gap are closer to the Fermi energies of the contacts which results in an enhanced conduction through the system. Double tunnel barriers can also be observed for single molecule junctions and can arise as a result of incorporating functional groups with different redox states between insulating structures such as the viologen compound described previously. The effect has also been observed for structures incorporating non redox active aromatic units.[68] The tunnelling mechanism becomes more efficient as the frontier orbitals of the indentation species are closer to the Fermi energy than the alkyl barriers. Double barrier models for hole transport have recently been produced by Hanss *et al.*[69] They studied the effects of methoxy substitution of tetra-*p*-xylene spacers between the donor acceptor structure of $Ru(bpy)_3^{3+}$ and phenothiazine. Photoexcitation triggered hole transfer for the substituted molecule resulted in significantly increased transfer rates in comparison to the unsubstituted molecule. This effect was attributed to the decreased barrier height of the bridging unit. A picture of a single molecule double tunnel barrier connected to gold electrodes is shown in Figure 1.5. Here a benzene group bridging two alkyl chains from reference[68] is used for illustrative purposes.

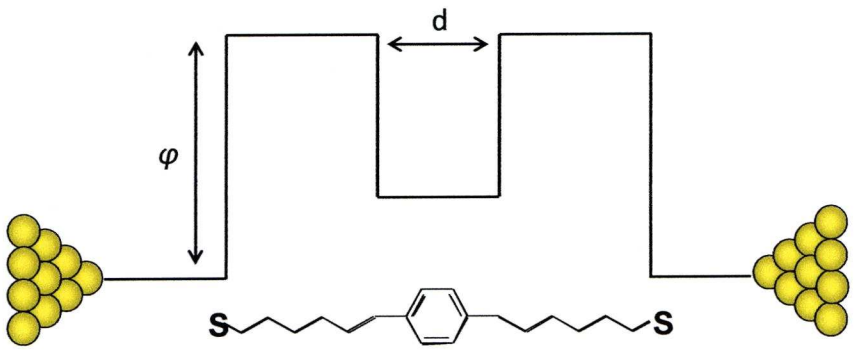

Figure 1.5. Illustration of a symmetric double tunnelling barrier with a barrier height of φ.

The current-voltage characteristics for double tunnelling barriers can vary and display features such as resonant tunnelling, rectification and negative differential resistance depending on the nature of the molecule, specifically the functional group providing the indentation.

1.10 Current Voltage Relationship.

Whilst the current voltage relationship of a number of molecules such as the alkanedithiols have been shown to exhibit ohmic behaviour, the current voltage characteristics for molecules can display alternative functions such as rectification or NDR (negative differential resistance). NDR is a phenomenon whereby the resistance of a molecule is not constant and a maximum peak is present in the current voltage relationship of the molecule. After this maximum, increasing the potential does not result in an increase in current, instead the current falls with increasing bias. This peak means that at certain values of current and voltage a negative value is obtained for the differential of the resistance as illustrated in Figure 1.6.

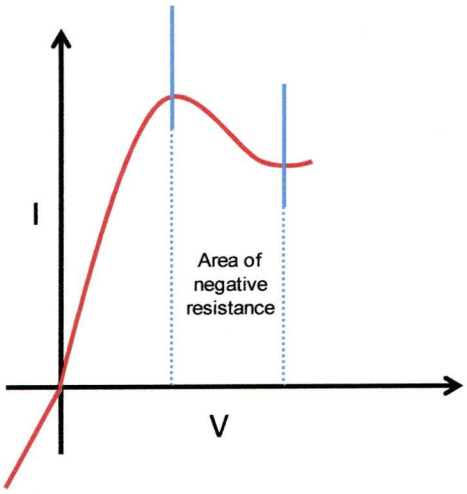

Figure 1.6. Current-voltage curve exhibiting negative differential resistance.

This is explained by the fact that at a certain potential, the molecular states of the molecule are aligned with the Fermi level of the metal and current is increased via a resonant tunnelling process. After this maximum, an increase in bias voltage moves the molecular orbitals out of alignment and the current drops accordingly producing a negative differential region. The NDR effect has been realised for compounds containing active redox centres such as nitroamine substituted ethynylphenyl derivatives[12] and nitro functionalised bipyridal molecules,[22] also alkanethiols with terminal ferrocene groups[16] where resonant tunnelling through the ferrocene was thought to be the cause of the observed NDR.

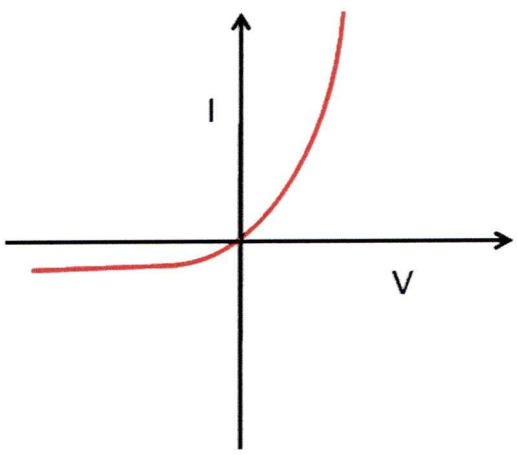

Figure 1.7. Illustration of current-voltage rectification behaviour.

Rectification is also a common feature of current voltage curves and occurs when the measured current at a bias voltage is larger than at a voltage of opposite sign resulting in asymmetric current response as shown in Figure 1.7. Rectification behaviour is often observed for molecules comprising a donor-acceptor structure as the orbitals of each species can be aligned in different ways relative to the Fermi level of the electrode thus favouring electron transport in one direction only. It has also been reported for molecules which simply have asymmetric geometry. Rectification effects are also observed for molecular wires that possess an inherent dipole such as the peptide sequences which will be presented later. This type of voltage dependent behaviour has important implications for molecular electronics with its possible application to memory and diodes.

1.11 Techniques overview

There are a number of key techniques that have been developed that enable reliable contacting of a single molecule between a pair of electrodes. Performing measurements using these methods permits the conductance through just one molecule to be quantified and excludes contributions from intermolecular interactions that can result from the measurements of groups of molecules or self-assembled monolayers.

1.11.1 STM -Break Junction Technique

The break-junction technique relies on the mechanical contact of an STM tip with a substrate in a solution of molecules. Withdrawal of the tip creates an atomic sized metallic wire which eventually breaks allowing molecules to bridge the gap between the ends of the chain. Many groups have adopted this method when measuring single molecule conductance.[41] Examples of this include the measurement of the length dependence of the conductance of oligothiophenes,[45] and conjugated polymers.[42] This technique has also been successfully applied to the measurement of very short peptide molecules[71] and double stranded DNA.[72] Break junction measurements performed in UHV conditions by

Suzuki *et al.*[40] on low coverage adlayers of hexane- and octanedithiol produced results consistent with those reported by Haiss.[73] UHV conditions were chosen to minimise the influence of environment and solvent effects on conductance.

Break junction techniques are not limited to STM, several groups have used mechanical controlled break junctions to measure the conductance of single molecules. For example the conjugated molecules oligo(phenylene vinylene) (OPV) and oligo(phenylene ethynylene) (OPE) were measured in solution by Huber *et al.*[74] who discovered that the OPV was more conductive than the OPE. Horiguchi *et al.*[21] also used MCBJ methods to study the conductance through benzenedithiol, a molecule that has been the subject of interest for other groups.[45] Break junction experiments can also be carried out using AFM methods.[75]

1.11.2 Matrix Isolation Technique

In 2001, Cui *et al*[20] reported a reliable method of measuring the conductance of single molecules and produced current vs. voltages curves for single octanedithiol molecules. They inserted octanedithiol molecules into a monolayer matrix of octanethiols on a Au(111) substrate; incubation of the monolayer with a suspension of gold nanoparticles resulted in the formation of gold-sulfur bonds between the dithiol and a gold nanoparticle. A gold-coated AFM tip was able to locate and contact individual gold nanoparticles which act as electrical contact pads and thereby create the circuit. Matrix isolation has many beneficial properties, for example, the molecules of interest can be immobilized with distance between them as the mole ratio of solution is the same as that on the SAM and the formation of islands can be avoided by controlling the deposition conditions. The target molecules are also adsorbed in an upright position due to the constraints of the surrounding matrix, however, this often corresponds to defect sites and step edges on the surface. This technique has been used by the group to produce I-V data for carotenedithiol molecules terminated by thiol groups at either end.[76] The conductance of these molecules was much higher than equivalent alkanedithiols as

expected due to their highly conjugated nature. Also molecules incorporating electroactive nitro functionality that produced negative differential resistance behaviour have been reported, where the I-V curve contains a region where current values decrease with increasing voltage.[77]

1.11.3 *I*(*s*) Technique

The *I*(*s*) technique is an STM based method in which the current through a molecular wire covalently bound to a gold substrate and a gold STM tip is measured. It is the primary technique that will be used throughout this thesis and is explained in detail in Chapter 2. Briefly, an STM tip is able to pick up molecules adsorbed at a low coverage on a substrate and tunnelling through a molecule appears as a plateau in the current decay as the tip is moved away from the sample. This *I*(*s*) approach has been successfully used to measure the conductance of alkanedithiols,[44] oligothiophenes,[78] alkylbenzene derivatives[68] and carboxylic acid terminated molecules.[50]

1.11.4 *I*(*t*) Technique

The *I*(*t*) technique relies on the spontaneous formation of molecular wires where molecules can 'jump' up and bridge the gap between an STM tip and a substrate. This occurs when an STM tip is positioned at a given distance from the Au surface and the feedback loop is disabled. A constant tip-sample separation is maintained and the difference in current values between the attachment and detachment of a molecule are measured. This approach minimizes through space tunnelling and general avoids the measurement of multiple molecules as normally just one molecule can bridge the distance between tip and sample at a time. The initial separation is chosen to reduce the effect of molecule tilt angles that can influence the measured currents due to unwanted electronic coupling between the backbone of the molecule and the gold surface.[4,36] This method has also been used by other groups, for example, to determine the conductance for a 7 nm long arylene-

ethynylene molecule, giving a value of around 1 nS.[79] It has also been used to measure the conductance of octanethiol adsorbed on Pt, although the resulting current values for this experiment were much larger than other reported values.[80]

Both the *I*(*s*) and *I*(*t*) technique have several advantages over other methods. Firstly they are non-intrusive as the STM tip does not make a contact with the substrate, this results in an improved consistency of contact geometry between molecule and substrate as it limits the defects on the surface caused by the pulling of atomic wires and also allows the tip to retain a steady structure throughout the measurements. This is particularly important when dealing with monolayer measurements as it also limits the destruction of the molecular film. Secondly, it favours the formation of a single molecule junction as opposed to some techniques such as nanopore experiments that trap multiple molecules where it is impossible to quantify exactly how many molecules are contacted within the junction. Low coverage surfaces have been shown to be stable over several days in ambient environments, also the processes are highly reproducible allowing large quantities of data to be collected and there is a good correlation between the *I*(*s*) and *I*(*t*) results for single-molecule conductance.[36]

1.11.5 Data Collection

As stated earlier, the structure of the tip apex is generally an unknown feature but has an important role in the electronic transport through molecules. Ideally the apex should constitute just a single atom, although this is difficult to achieve in reality. In the case of the *I*(*t*) approach, the electric field between the tip and sample is responsible for the formation of molecular bridges so there is a high probability that junctions form at the tip apex as this is the area with the highest field strength.

The geometry of the molecule metal binding site can have a large influence on observed current values, resulting in discrete conductance groups for the same molecule. The origin of these high and low conductance groups are rationalised in the next chapter. The net result of

these accumulated factors means that statistical analysis of large amounts of data is crucial for the calculation of a conductance value for a single molecular wire, as the events are subject to fluctuations and it is also possible to record events where more than one molecule is trapped in the junction.[81]

1.12 Single Molecule Conductance of Ethers

The three molecules studied in chapter four are *S*,*S*'-(oxybis(butane-4,1-diyl))diethanethioate, *S*,*S*'-((methylenebis(oxy))bis(ethane-2,1-diyl)) diethanethioate and *S*,*S*'-(thiobis(propane-3, 1-diyl))diethanethioate. They will be known throughout the rest of the thesis as DBE, TEG and DPTE respectively and their structures are shown below in Figure 1.8.

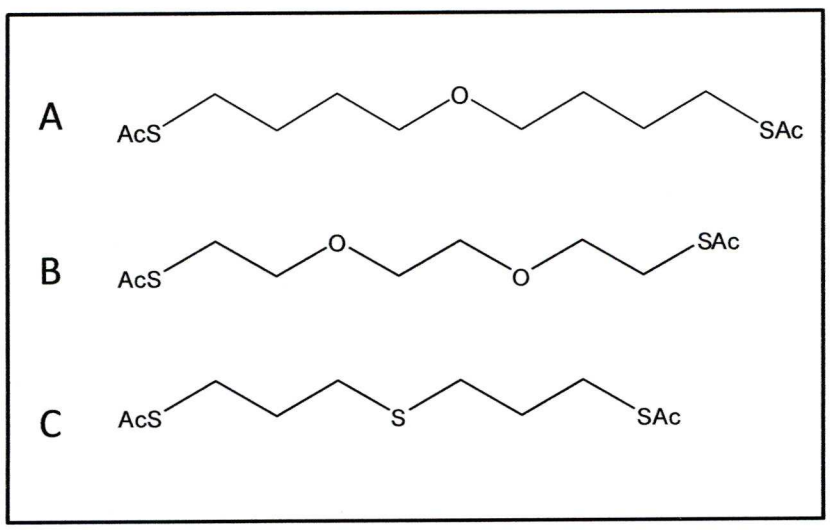

Figure 1.8. Structure of three molecules investgated, a) *S*,*S*'-(oxybis(butane-4,1-diyl))diethanethioate b) *S*,*S*'-((methylenebis(oxy))bis(ethane-2,1-diyl)) diethanethioate and c) *S*,*S*'-(thiobis(propane-3, 1-diyl))diethanethioate

The first two molecules are simple, thioacetate terminated ethers. The first has four carbons either side of the oxygen atom and the second has two oxygen bridges separated by three ethyl groups. The final molecule is a simple thioether with a central sulfur atom between two propyl

groups. They have been proposed for single molecule conductance measurements for two distinct reasons. Firstly, as discussed above, alkanedithiols have been extensively studied and can give reproducible conductance values. However, it will be valuable to see how the inclusion of the oxygen and sulfur within molecular bridges affects electron transport through such a simple system. Previous work has been carried out at Liverpool on molecules that feature a double tunnelling barrier junction such as the redox active α, ω-viologen dithiol mentioned earlier and alkane chains with various benzene derivatives in the centre. In all of these cases, it was found that the conductance of these molecules was significantly higher that the equivalent alkane chains due to the central units acting as tunnelling barrier indentations.[68,82] So, the results for the three molecules will be compared to their corresponding alkanedithiols, nonane-, octane- and heptanedithiol. This will give an indication as to the role of the oxygen or sulfur in the electron transfer mechanism. The molecular electrical properties will be determined using several different experimental techniques with the aim of determining an accurate value for the single molecule conductance. In this way the systematic variation of chemical structure can be studied directly.

The second reason for studying these molecules is to look at hydration effects. This will be achieved by carrying out the measurements in a number of different environments. Hydration effects have been studied previously by several groups, for example, microsphere molecular junctions were used by Long *et al.*[83] to study alkanedithiols. They concluded that such junctions are highly sensitive to hydration effects and that such effects occur predominantly at the gold-sulfur interface. Li *et al.*[84] used STM and AFM break junctions in various solvents to study alkanedithiols and found that the molecular conductance was not affected by the environment and gave evidence against hydration effects at the gold-sulfur interface. Obviously with two contradicting studies, further investigations are needed. The incorporation of the oxygen atom into the molecular wire should give a more defined approach to this issue.

1.13 Peptides

Peptides are composed from amino acid sequences and are the precursors of proteins. Peptides have many biological functions, for example, they can act as neurotransmitters and hormones and they are responsible for many natural electron transport processes required for operations such as respiration, photosynthesis and enzyme function.[85,86] There has been a great deal of interest in the possible application of peptide sequences in molecular electronics due to their predisposition to facilitate electron transfer.

Other biological molecules of interest in this field include DNA. The single molecule conductance of both single stranded[87] and double stranded[72] DNA has been reported and both show superior electron transport capabilities compared to similar length alkane chains. Double stranded DNA has a higher conductance than single stranded, indicating that the π-stacking and base pair interaction influence electron transport. However, the mechanism of charge transfer is still under debate. van Zalinge *et al.*[87] used the $I(t)$ method to measure the conductance of homopolymeric nucleotide sequences and found that guanine rich molecules were more conductive than nucleotides containing other DNA bases and that all the compounds studied displayed a linear current voltage dependence in the low bias region.

Charge transport through peptide systems can be very complex due to the various possible secondary structures and the many types of intermolecular interactions between sequences.[88] Experiments are often performed on peptide films with thiol functionalized peptides capable of self-assembly and there are also reports of single molecule conductance measurements. The amino acid cysteine is regularly used as a terminal peptide in a sequence, exploiting the thiol group to create covalent and stable links with a variety of metal substrates. Peptides with terminal cysteine residues are regularly used as capping ligands for the stabilisation or functionalization of nanoparticles.[89,90] Work carried out on the electron transport properties of helical peptide chains have shown them to be superior mediators of electron tunnelling than basic

hydrocarbon chains.[91,92] They show a marked change in tunnelling mechanism directly related to the peptide length. Shorter peptides tend to adopt a simple tunnelling mechanism, while longer peptides display a hopping mechanism,[91-93] this makes them attractive candidates for molecular wires due to their feasible long-range electron transfer. Indeed electron transfer has been observed in helical peptides more than 4 nm in length.[93] The peptide bond has partial double bond character which contributes to their electron transfer capabilities and peptides have an intrinsic dipole moment as a result of their polar amide bonds that results in directional electron transport.[91, 94-96]

Many groups have performed studies on peptides with the aim of developing peptide based nanocircuits.[91,97] One advantage of using peptides is that their sequence and their structures are tuneable and they can also be designed to be responsive to their environment, for example pH. It is relatively easy for a molecule with a specific chemical function to be attached to the peptide wire through amino acid side chains.[98,99] For example peptides can be made redox active by the incorporation of groups such as nitroaniline or ferrocene. Long *et al.*[88] used Fc-COOBt with solid and solution-phase peptide coupling to achieve a ferrocene labelled peptide that was easily immobilized onto gold. Kitagawa *et al.*[100-102] have also incorporated ferrocene groups into peptides immobilized on gold.

To employ biological molecules as components in devices their integration needs to be seamless which in the case of peptides means that several subjects need to be addressed. These include the orientation of a peptide within nanoelectronic circuits, appropriate surface binding motifs, precise surface patterning and the behaviour of the peptides on binding to a substrate compared to their behaviour in solution.[29,97,103] Much of the work done in the last few years to investigate the electron transport characteristics of short peptide chains has been undertaken by Sek *et al.* and Kimura *et al.* who have studied a wide range of peptide sequences, mainly present in self assembled monolayers. A review of this work is presented in Chapter 5.[91-93,104-107] A technique similar to the $I(s)$

method was developed by Sek *et al.* and it used in the work presented here for both peptides and ether molecules.

References

1. Castell, M. R. *Nanocharacterisation* 66-93. RSC (2007).
2. Moore, G. E. *Electronics*, **38** (8). (1965).
3. Wada, Y. *Ann. N. Y. Acad. Sci*, **960**, 39-61. (2002).
4. Haiss, W.: Wang, C.: Jitchati, R.; Grace, I.; Martin, S.; Batsanov, A.; Higgins, S. J.; Bryce, M.; Lambert, C.; Jensen, P and Nichols, R. J. *J. Phys. Condens. Matter*, **20**, 374119. (2008).
5. Binning, G.: Rohrer, H.: Gerber, C and Weibel, E. *Phys. Rev. Lett*, **49**, 57-61. (1985).
6. Eigler, D. M and Schweizer, E. K. *Nature*, **344**, 524-526. (1990).
7. Collier, C.; Mattersteig, G.; Wong, E.; Luo, Y.; Beverly, K.; Sampaio, J.; Raymo, F.; Stoddart, J and Heath, J. *Science*, **289**, 1172-1175. (2000).
8. Wasielewski, M and Lukas, A. Molecular Switches. Wiley. (2001).
9. Tans, S.; Verschueren, A and Dekker C. *Nature*, **393**, 49-52. (1998).
10. Aviram, A and Ratner, M. A. *Chem. Phys. Lett*, **29**, 277-283. (1974).
11. Haiss, W.; Nichols, R. J.; Higgins, S. J.; Bethell, D.; Hobenreich, H and Schiffrin, D. J. *Faraday. Discuss*, **125**, 179-194. (2004).
12. Chen, J.; Wang, W.; Reed, M. A.; Rawlett, A.; Price, D and Tour, J. M. *Appl. Phys. Lett*, **77** (8), 1224-1226. (2000).
13. Van der Molen, S. J.; Liao, J.; Kudernac, T.; Agustsson, J.; Bernard, L.; Calame, M.; van Wees, B.; Feringa, B and Schonenberger, C. *Nano Lett*, **9** (1), 76-80. (2009).
14. Diez-Perez, I.; Hihath, J.; Lee, Y.; Yu, L.; Adamska, L.; Kozhushner, M.; Oleynik, I and Tao, N. *Nature Chemistry*, **1**, 635-641. (2009).
15. Elbing, M.; Ochs, R.; Koentopp, M.; Fischer, M.; von Hanisch, C.; Weigend, F.; Evers, F.; Weber, H and Mayor, M. A. *Proc, Nat, Acad, Sci*, **102** (25), 8815-8820. (2005).
16. Gorman, C.; Carroll, R and Fuierer, R. *Langmuir*, **17**, 6923-6930. (2001).

17. Cardamone, D and Kirczenow, G. *Phys. Rev. B*, **77**, 165403. (2008).

18. Xu, B and Tao, N. J. *Science*, **301**, 1221-1223. (2003)

19. Seferos, D.; Trammell, S.; Bazan, G and Kushmerick, J. *Proc, Nat, Acad, Sci, USA*, **102** (25), 8821-8825. (2005).

20. Cui, X. D.; Primak, A.; Zarate, X.; Tomfohr, J.; Sankey, O. F.; Moore, A. L.; Gust, D.; Harris, G.; Lindsay, S. M. *Science*, **294**, 571-574. (2001)

21. Holmlin, R.; Haag, R.; Chabinyc, M.; Ismagilov, R.; Cohen, A.; Terfort, A.; Rampi, M and Whitesides, G. *J. Am. Chem. Soc*, **123**, 5075-5085. (2000).

22. Tran, E.; Grave, C.; Whitesides, G and Rampi, M. *Electrochimica, Acta*, **50**, 4850-4856. (2005).

23. Chen, J.; Wang, W.; Klemic, J.; Reed, M. Axelrod, B.; Kaschak, D.; Rawlett, A.; Price, D.; Dirk, S.; Tour, J. M.; Grubisha, D and Bennet, D. W. *Ann. N. Y. Acad. Sci*, **960**, 69-99. (2002).

24. Wang, W.; Lee, T and Reed, M. A. *Rep. Prog. Phys*, **68**, 523-544. (2005).

25. Majumdar, N.; Gergel, N.; Routenberg, D.; Bean, J.; Harriott, L.; Li, B.; Pu, L.; Yao, Y and Tour, J. M. *J. Vac. Sci. Technol*, **23** (4), 1417-1421. (2005).

26. Persson, S. H. M.; Olofsson, L.; Hedberg, L.; Sutherland, D and Olsson, E. *Ann. N. Y. Acad. Sci*, **852**, 188-196. (1998).

27. Moth-Poulsen, K and Bjornholm, T. *Nature Nanotechnology,* **4**, 551-556. (2009).

28. Yaliraki, S.; Kemp, M and Ratner, M. A. *J. Am. Chem. Soc*, **121**, 3428-3434. (1999).

29. Sek, S. *J. Phys. Chem. C*. **111**, 12860-12865. (2007)

30. Vonlanthen, D.; Mishchenko, A.; Elbing, M.; Neuburger, M.; Wandlowski, T and Mayor, M. *Angew, Chem, Int, Ed*, **48**, 8886-8890. (2009).

31. Jiang, W.; Zhitenev, N.; Bao, Z.; Meng, H.; Abusch-Magder, D, Tennent, D and Garfunkel, E. *Langmuir*, **21**, 8751-8757. (2005).

32. Fujihira, M.; Suzuki, M.; Fujii, S and Nishikawa, A. *Phys. Chem. Chem. Phys.* **8**, 3876-3884. (2006).

33. De Renzi, V. *Surface Science*, **603**, 1518-1525. (2009).

34. Lee, C.; Kang, Y.; Lee, K.; Kim, S. R.; Won, D.; Noh, J. S.; Shin, H. K.; Song, C. K.; Kwon, Y. S.; So, H.; Kim, J. *Current Applied Physics 2*, 39-45. (2002).

35. Chandekar, A.; Sengupta, S and Whitten, J. *Applied Surface Science*, **256**, 2742-2749. (2010).

36. Haiss, W.: Wang, C.: Grace, I.: Batsanov, A. S.: Schiffrin, D. J.: Higgins, S. J.: Bryce, M. R. Lambert, C. J.: Nichols, R. J. *Nature Materials*, **5**, 995-1002. (2006)

37. Feldman, A.; Steigerwald, M.; Guo, X and Nuckolls, C. *Accounts of Chemical Reaearch*, **41** (12), 1731-1741. (2008).

38. Ebbesen, T.; Lezec, H.; Hiura, H.; Bennett, J.; Ghaemi, H and Thio, T. *Nature*, **382**, 54-56. (1996).

39. Wink, Th.; van Zuilen, S. J.; Bult, A and van Bennekom, W. P. *Analyist*. **122**, 43-50. (1997).

40. Suzuki, M.; Fujii, S.; Fujihira, M. *Japanese Journal of Applied Physics*, **45** (3B), 2041-2044. (2006).

41. Zhou, X-S.; Chen, Z-B.; Liu, S-H.; Jin, S.; Liu, L.; Zhang, H-M, Xie, Z-X, Jiang, Y-B and Mao, B-W. *J. Phys. Chem. C*, **112** (10), 3935-3940. (2008).

42. Engelkes, V.; Beebe, J and Frisbie, C. D. *J. Am. Chem. Soc*, **126**, 14287-14296. (2004).

43. Mativetsky, J.; Palma, M.; Samori, P. *Top. Curr. Chem*, **285**, 157-202. (2008).

44. Haiss, W.; Martin, S.; Scullion, L. E.; Bouffier, L.; Higgins, S. J and Nichols, R. J. *Phys. Chem. Chem. Phys*, **11**(46), 10831-10838. (2009).

45. Yamada, R.; Kumaza, H.; Noutoshi, T.; Tanaka, S and Tada, H. *Nano Lett*, **8** (4), 1237-1240. (2008).

46. Mischenko, A.; Vonlanthen, D.; Meded, V.; Burkle, M.; Li, C.; Pobelov, I.; Bagrets, A.; Viljas, J.; Pauly, F.; Evers, F.; Mayor, M and Wandlowski, T. *Nano. Lett*, **10**, 156-163. (2010).

47. Beebe, J.; Engelkes, V.; Miller, L and Frisbie, C. D. *J. Am. Chem. Soc*, **124**, 11268-11269. (2002).

48. Lee, S.; Lin, W.; Kuo, C.; Karakachian, M.; Lin, Y.; Yu, B and Shyue, J. *J. Phys. Chem. C.* **114**, 10512-10519. (2010).

49. Chen, F.; Li, X.; Hihath, J.; Huang, Z and Tao, N. *J. Am. Chem. Soc*, **128**, 15874-15881. (2006).

50. Martin, S.; Haiss, W.; Higgins, S.; Cea, P.; Carmen Lopez, M and Nichols, R. J. *J. Phys. Chem. C.* **112**, 3941-3948. (2008).

51. Venkataraman, K.; Klare, J.; Tam, I.; Nuckolls, C.; Hybertsen, M and Steigerwald, M. *Nano. Lett*, **6** (3), 458-462. (2006).

52. Kiguchi, M.; Miura, S.; Takahashi, T.; Hara, K.; Sawamura, M and Murakoshi, K. *J. Phys. Chem. C*, **112** (35), 13349-13352. (2008).

53. Kristensen, I.; Mowbray, D.; Thygesen, K and Jacobsen, K. W. *J. Phys. Condens. Matter*, **20**, 374101. (2008).

54. Roberts, G. G. *Sensors and Actuators*. **4**, 131-145. (1983).

55. Zharnikov, M.; Frey, S.; Rong, H.; Yang, Y.; Heister, K.; Buck, M and Grunze, M. *Phys. Chem. Chem. Phys*, **2**, 3359-3362. (2000).

56. Higashi, N.; Kawahara, J and Niwa, M. *J. Coll. Inter. Sci.* **288**, 83-87. (2005).

57. Sek, S.; Moszynski, R.; Sepiol, A.; Misicka, A and Bilewicz, R. *Journal of Electroanalytical Chemistry*. **550**, 359-364. (2003).

58. Akkerman, H.; Naber, R.; Jongbloed, B.; van Hal, P.; Blom, P.; Leeuw, D and de Boer, B. *Proc, Nat, Acad, Sci*, **104** (27), 11161-11166. (2007).

59. Prokopuk, N and Son, K-A. *J Phys. Condens. Matt*, **20** (37) 374116. (2008).

60. Binnig, G.; Quate, C. F and Gerber, C. *Phys. Rev. Lett*, **56**, 930-933. (1986).

61. Ebner, A.; Wildling, L.; Zhu, R.; Rankl, C.; Haselgrubler, T.; Hinterdorfer, P and Gruber, H. J. *Top. Curr. Chem*, **285**, 29-76. (2008).

62. Binnig, G.; Rohrer, H.; Gerber, C and Weibel, E. *Appl. Phys. Lett*, **40** (2), 178-180. (1982).

63. Lei, S and De Feyter, S. *Top. Curr. Chem*, **285**, 269-321. (2008).

64. Tersoff, J and Hamann, D. R. *Phys. Rev. B*, **31**(2), 805-813. (1985).

65. Krans, J. M.; van Rultenbeek, J.; Flsun, V.; Yanson, I and de Jongh, L. J. *Nature*, **375**, 767-769. (1995).

66. van Houten, H and Beenakker, C. *Physics Today*, **49** (7), 22-27. (1996).

67. Landauer, R. *IBM J. Res. Dev*, **1**, 223-231. (1957).

68. Leary, E.; Higgins, S. J.; Van Zalinge, H.; Haiss, W and Nichols, R. J. *Chem. Commun*, **38**, 3939-3941 (2007).

69. Hanss, D.; Walther, M. E and Wenger, O. *Chem. Comm*, **46**, 7034-7036. (2010).

70. Lafferentz, L.; Ample, F.; Yu, H.; Hecht, S.; Joachim, C and Grill, L. *Science*, **323**, 1193-1197. (2009).

71. Xiao, X, Xu, B and Tao, N. *Angew. Chem. Int. Ed.* **43**, 6148-6152. (2004).

72. Xu, B.; Zhang, P.; Li, X and Tao, N. *Nano, Lett*, **4** (6), 1105-1108. (2004).

73. Haiss, W.; Nichols, R.; Zalinge, H. V.; Higgins, S. J.; Bethell, D.; Schiffrin, D.J. *Phys. Chem. Chem. Phys*, **6**, 4330-4337. (2004).

74. Huber, R; Gonzalez, M.; Wu, S.; Langer, M.; Grunder, S.; Horhoiu, V.; Mayor, M.; Bryce, M.; Wang, C.; Jitchati, R.; Schonenberger, C and Calame, M. *J. Am. Chem. Soc*, **130**, 1080-1084. (2008).

75. Li, X.; He, J.; Hihath, J.; Xu, B.; Lindsay, S. M and Tao, N. *J. Am. Chem. Soc*, **128**, 2135-2141. (2006).

76. Ramachandran, G.; Tomfohr, J.; Li, J.; Sankey, O.; Zarate, X.; Primak, A.; Terazono, Y.; Moore, T.; Moore, A.; Gust, D.; Nagahara, L and Lindsay, S. *J. Phys. Chem. B*, **107**, 6162-6169. (2003).

77. Rawlett, A.; Hopson, T.; Nagahara, L.; Tsiu, R.; Ranachandran, G and Lindsay, S. *Appl. Phys. Lett.* **81** (16), 3043-3045. (2002).

78. Leary, E.; Hobenreich, H.; van Zalinge, H.; Haiss, W.; Nichols, R. J.; Finch, C. M.; Grace, I.; Lambert, C. J.; McGrath, R and Smerdon, J. *Phys. Rev. Lett*, **102**, 086801. (2009).

79. Ashwell, G.; Urasinska, B.; Wang, C.; Bryce, M.; Grace, I and Lambert, C. J. *Chem. Commun*, **45**, 4706-4708. (2006).

80. Kockmann, D.; Poelsema, B and Zandvliet, H. *Nano. Lett*, **9** (3), 1147-1151. (2009).

81. Jang, S.: Reddy, P.: Majumdar, A.: Segalman, R. A. *Nano Letters*, **6** (10), 2362-2367. (2006).

82. Haiss, W.; van Zalinge, H.; Höbenreich, H.; Bethell, D.; Schiffrin, D. J.; Higgins, S. J and Nichols, R.J. *Langmuir*, **20**, 7694-7702. (2004).

83. Long, D. P.; Lazorcik, J. L.; Mantooth, B. A.; Moore, M. H.; Ratner, M. A.; Troisi, A.; Yao, Y.; Ciszek, J. W.; Tour, J. M and Shashidhar, R. *Nature Materials*, **5**, 901-908. (2006).

84. Xiulan, Li.; He, J.; Hihath, J.; Xu, B.; Lindsay, S. M and Tao, N. *J. Am. Chem. Soc*, **128**, 2135-2141. (2006).

85. Cordes, M and Giese, B. *Chem. Soc. Rev.* **38** 892-901. (2009).

86. Samori, P. *Topics in Current Chemistry*, **285**. Springer. (2008).

87. van Zalinge, H.; Schiffrin, D.; Bates, A.; Haiss, W.; Ulstrup, J and Nichols, R. J. *ChemPhysChem*, **7** (1), 94-98. (2006).

88. Long, Y.; Abu-Irhayem, E.; Kraatz, H. *Chem. Eur. J*, **11**, 5186-5194. (2005)

89. Higuchi, M.; Ushiba, K and Kawaguchi, M. *J. Coll. Intf. Sci.* **308**, 356-363. (2007).

90. Levy, R.; Thanh, N.; Doty, C.; Hussain, I.; Nichols, R. J.; Schiffrin, D. J.; Brust, M and Fernig, D. G. *J. Am. Chem. Soc.* **126**, 10076-10084. (2004).

91. Okamoto, S.; Morita, T and Kimura, S. *Langmuir*, **25**. 3297-3304. (2009).

92. Sek, S.; Swiatek, K.; Misicka, A. *J. Phys. Chem. B*, **109** (49), 23121-23124. (2005)

93. Watanabe, J.; Morita, T and Kimura, S. *J. Phys. Chem. B.* **109**, 14416-14425. (2005).

94. Grant, G. A. Synthetic Peptides. W. H. Freeman and Company. (1992).

95. Cristancho, D and Seminario, J. M. *J. Chem. Phys.* **132**, 065102. (2010).

96. Doonan S. Peptides and Proteins. Cambridge : Royal Society of Chemistry, (2002).

97. Pepe-Mooney, B and Fairman, R. *Current Opinion in Structural Biology.* **19**, 483-494. (2009).

98. Pace, G.; Venanzi, M.; Castrucci, P.; Scarselli, M.; De Crescenzi, M.; Palleschi, A.; Stella, L.; Formaggio, F.: Toniolo, C.; Marletta, G. *Materials Science and Engineering* (2005)

99. Venanzi, M.; Pace, G.; Palleschi, A.; Stella, L.; Castrucci, P.; Scarselli, M.; De Crescenzi, M.; Formaggio, F.; Toniolo, C.; Marletta, G. *Surface Science*, **600** (2), 409-416. (2006).

100. Kitagawa, K.; Morita, T.; Kawasaki, M.; Kimura, S. *J. Polymer Science. A.* **41** (22). 3493-3500. (2003).

101. Kitagawa, K.; Morita, T and Kimura, S. *J. Phys. Chem. B.* **109**, 13906-13911. (2005).

102. Kai, M.; Takeda, K.; Morita, T and Kimura, S. *J. Pep. Sci.* **14**, 192-202. (2008).

103. Zimmermann, R.; Osaki, T.; Kratzmuller, T.; Gauglitz, G.; Dukhin, S and Werner, C. *Anal. Chem.* **78**, 5851-5857. (2006).

104. Sek, S.; Tolak, A.; Misicka, A.; Palys, B.; Bilewicz, R. *J. Phys. Chem. B*, **109** (39), 18433-18438. (2005).

105. Arikuma, Y.; Takeda, K.; Morita, T.; Ohmae, M and Kimura, S. *J. Phys. Chem. B.* **113**, 6256-6266. (2009).

106. Sek, S.; Misicka, A.; Swiatek, K and Maicka, E. *J. Phys. Chem. B.* **110.** 19671-19677. (2006).

107. Takeda, K.; Morita, T and Kimura, S. *J. Phys. Chem. B.* **112**, 12840-12850. (2008).

Chapter 2. Experimental Methods

2.1 Introduction

This chapter presents the main techniques used to measure single molecule conductance throughout this thesis. A PicoScan™ 2500 (Molecular Imaging) STM was used throughout. Gold on glass slides were purchased from Arrandee® and flame annealed with a Bunsen burner before use. 0.25mm (99.99%) gold wire purchased from Goodfellow® was used to make STM tips. Generally cut gold tips were used but for some imaging the tips were etched in a 50:50 HCl/ethanol solution. The tip was coated with Apiezon® wax for measurements in solution, ensuring only the tip apex was exposed.

2.2 The *I*(*s*) Technique

This technique involves the formation of a molecular wire between a gold STM tip and a gold substrate and was first used to measure the single molecule conductance of a redox active viologen molecule in 2003.[1] A gold on glass substrate is immersed into a solution of the molecule of interest, often a dithiol molecule, for a short period of time to produce a low coverage of flat lying molecules. The substrate is then mounted onto a sample plate and the tip is brought to within tunnelling distance of the surface. The tip is then placed at a certain height defined by the set point current I_0. When the distance between tip and substrate is sufficiently small, molecules are able to span the gap between them. A bias voltage is applied and the tip is lifted whilst maintaining a constant $x - y$ position as shown in Figure 2.1. It is possible for the STM to chemically bind to one terminus of the molecule and effectively lift it.

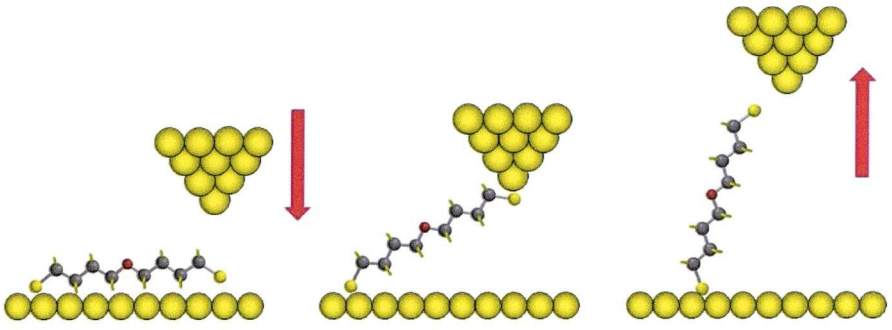

Figure 2.1. Illustration of the *I*(*s*) technique on a gold surface.

Normally on a bare gold substrate when the tip is retracted, the tunnelling current decays to zero in an exponential fashion. When molecules are adsorbed on the surface they can form a bridge and a plateau can be seen in the tunnelling current attributed to conduction through a single molecule or multiple molecules. These plateaus appear at a characteristic current value for different molecules. As the tip is retracted further, the molecule disengages and the current drops down to zero. Figure 2.2 shows an example of one of the *I*(*s*) scans obtained during experiments on the *S*,*S*'-((methylenebis(oxy))bis(ethane-2,1-diyl)) diethanethioate (TEG) molecule. The plateau is very well defined with a sharp drop in current as the tip is retracted.

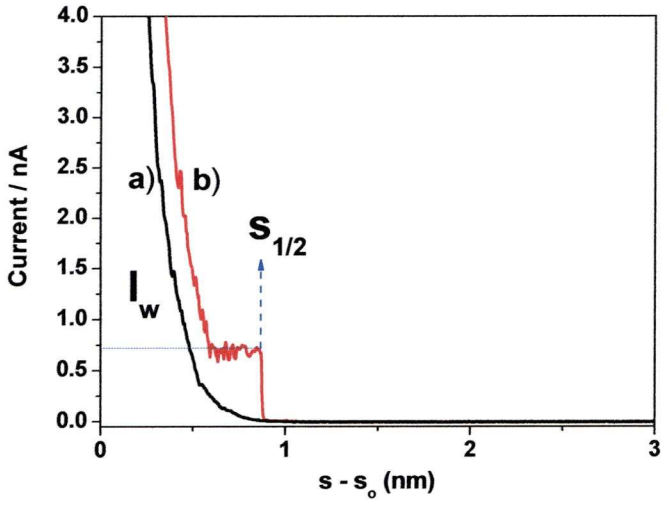

Figure 2.2. Example of an *I*(*s*) measurement. Curve a) is a typical baseline curve with a fast exponential decay due to tunnelling between the tip and the bare metal. b) curve displaying a plateau attributed to conduction through a molecular wire.

The current values, termed I_w, from the $I(s)$ scans are then added together to form a current histogram like the one shown in Figure 2.3. Generally at least 100 scans are needed to produce a high quality analysis. The histogram is constructed from 120 scans from measurements on the molecule TEG at a bias voltage of 0.6 V.

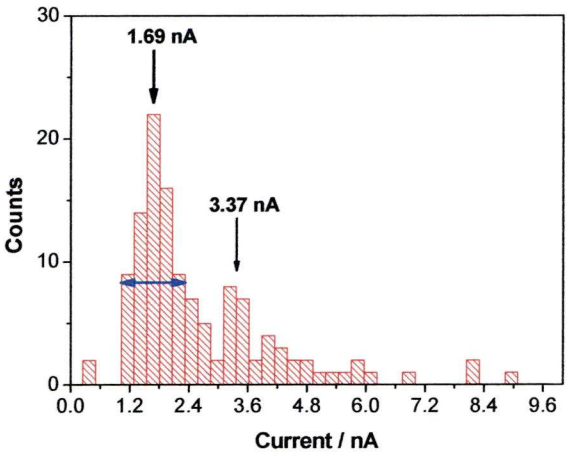

Figure 2.3. Histogram showing current values for TEG at 0.6 V, I_0 = 40nA.

The resulting histograms show well defined peaks that appear at integer multiples of a fundamental value. These peaks correspond to one, two or even three molecules in the junction. The major peak seen in Figure 2.3 appears at 1.69 nA, this is taken as the current value for just one molecule as no smaller current values are observed, this peak is termed A_1 for reasons that will be discussed later. There is a second smaller peak at 3.37 nA which is roughly double the value of the first, this peak is due to two molecules in the junction and is termed A_2. Occasionally peaks due to three or four molecules between tip and substrate can be observed. Once the value of the current for each molecule has been determined experimentally, Equation 1 can be used to calculate the conductance through the molecule.

$$\sigma\,(\text{nS}) = \text{I}\,(\text{nA}) / \text{V} \qquad (1)$$

Equation 1. Relationship between current, voltage and conductance

Therefore, the conductance calculated from the two peaks in Figure 2.3 are: 2.82 nS and 5.61 nS respectively. Throughout this thesis, conductance values will be quoted in both nS and as a function of the conductance quantum G_0, where G_0 corresponds to the conductance through a single chain of metallic atoms as described in Chapter 1. For comparison purposes, the values in nS will be used.

Experiments are performed over a range of bias voltages, usually between 0.6 and -0.6 V with intervals of 0.2 V. Current values extracted from each histogram are plotted against the varying potentials to produce current voltage graphs that can be used to determine the single molecule conductance.

2.2.1 Distance measurements

A useful feature of the *I*(*s*) technique is the ability to quantify the distance at which the molecule detaches from the tip. In most cases, especially for rigid molecules, as the tip is retracted the molecule is lifted vertically to full extension before the current drops to zero. This distance moved by the tip added to the initial tip sample separation (S_0) should therefore correspond to the molecular length of the molecule.[7,8,9,11] As shown in Figure 2.2, the point at which the molecule detaches and the current drops to zero is termed $S_{1/2}$. To determine S_0, *I*(*s*) scans displaying no current plateau were recorded during every experiment as shown in Figure 2.4 (a) for the TEG molecule at -0.2 V and I_0 = 20 nA. Linear regression was then used to determine the slope of $ln(I_0)$, where I_0 is the initial set point current as shown in Figure 2.4 (b).

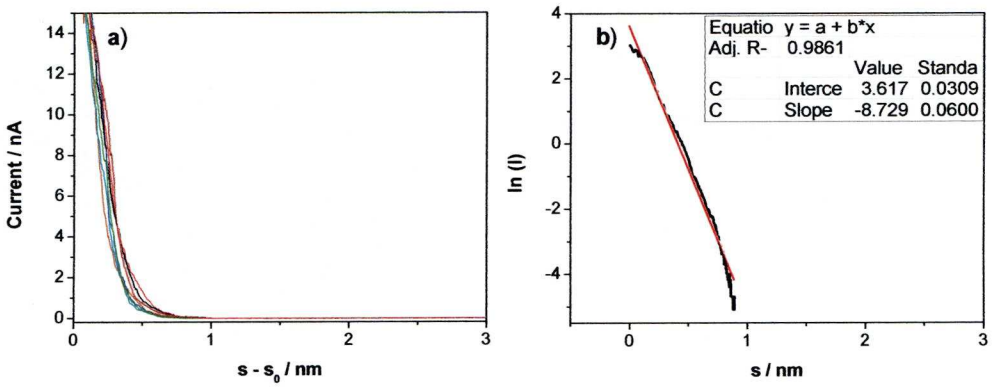

Figure 2.4, a) tunnelling decay curves showing no molecules present in the gap, b) linear regression of *ln*(I) against distance, *s*. This example gives parameters of; slope = -8.729, intercept = 3.617, with Adj R^2 = 0.986.

For each bias voltage, at least five of these current-distance curves were recorded and the slopes of the linear regression (inset Figure 2.4 b)) were averaged to give a value of 8.89 nm^{-1}. This value was then extrapolated to the point contact conductance allowing calibration of the gap separation using Equation 2.

$$s(I) = \frac{\ln(G_0 \times U_o/I)}{d\ln(I)/ds} \qquad (2)$$

In the example shown in Figure 2.4, d ln(I)/ds is calculated as (8.89 ± 0.8) nm^{-1} , giving an S_0 value of 0.74 nm. This can then be added to the experimentally determined break off distance which is obtained from a histogram of all the measured $S_{1/2}$ values as shown in Figure 2.5. Here the value of the peak is (0.78 ± 0.1) nm, so S + S_0 is (1.52 ± 0.9) nm. Once these values have been calculated they can be compared to theoretical S-S distances which will be calculated using the SPARTAN® molecular modelling program.

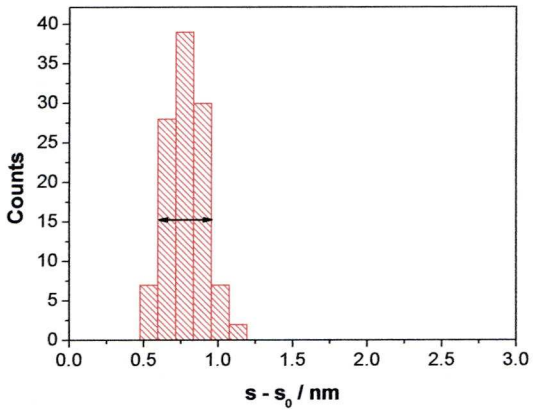

Figure 2.5. Histogram of break off distances for TEG at 0.2 V.

2.3 The *I*(*t*) Technique

A complementary technique to the *I*(*s*) method is the *I*(*t*) method developed in 2004.[2] Here contact events are measured in the time domain as shown in Figure 2.6. Once the STM tip is in position, the feedback loop is disabled and the spontaneous formation of bridges can occur. This is observed through sudden current jumps seen in Figure 2.7.

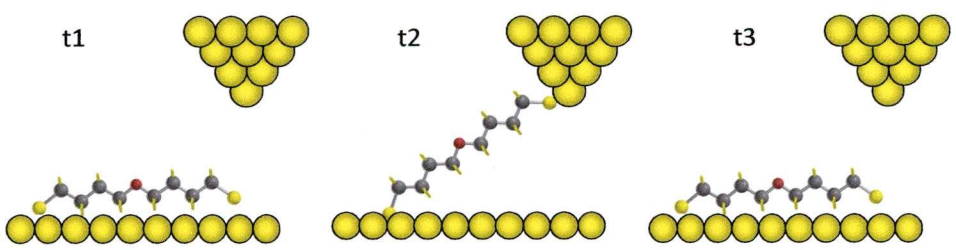

Figure 2.6. At t_1 and t_3, the molecule is in a flat-lying phase on the substrate and is not attached to the tip. At t_2 it forms a molecular bridge between the tip and the substrate.

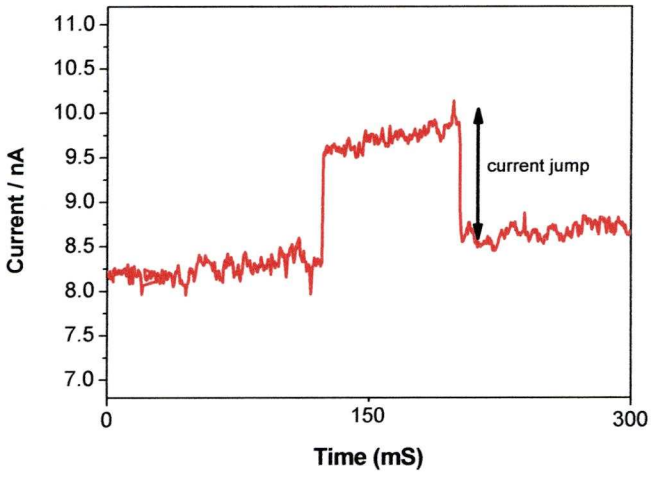

Figure 2.7. Example of an *I*(*t*) jump recorded for HDTA at -0.2 V, I_0 = 8 nA.

Only jumps with fairly level plateaus either side are used to construct histograms. The absolute values between the top and bottom of the jump are collected and used in data analysis.

2.4 Sek Technique

An important technique that was used throughout the following experiments is that developed by Sek *et al.*[3] in 2005. They use a very similar method to the *I*(*s*) technique but instead of adsorbing molecules to form a low coverage, a self assembled monolayer is prepared. This is usually accomplished by the immersion of a gold substrate in a 0.5 mM solution of the desired molecule for 24 hours. An illustration of this is shown in Figure 2.8.

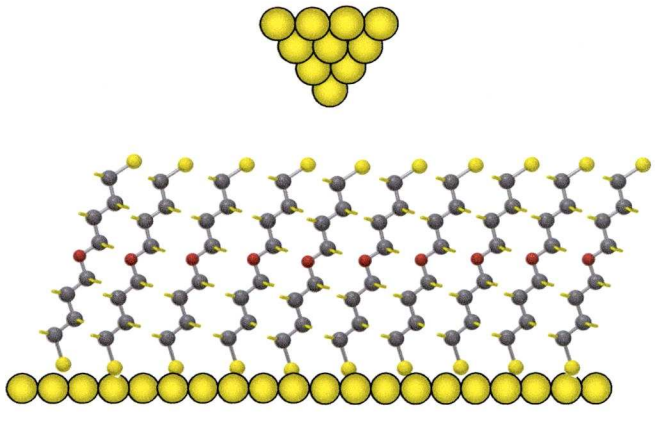

Figure 2.8. Self assembled monolayer of *S*,*S*'-(oxybis(butane-4,1-diyl))diethanethioate (DBE) used in the Sek technique.

These experiments were initially performed on a self assembled monolayer formed from an α-helical peptide. The peptide sequence was composed of 14 residues, including alanine, lysine and glutamic acid. The peptide was designed with two terminal thiol groups to enable self assembly on the gold substrate and to allow the formation of junctions with an STM tip.

The gold STM tip was located on the surface of the monolayer at a predetermined distance corresponding to a set point of between 0.05 and 0.5 nA. The tip was then lifted in the same way as the *I*(*s*) technique whilst keeping a constant *x*-*y* position. Similar current plateaus were observed and the experiments were performed many times and the current values statistically analysed. Resulting histograms again show multiples of an integer value corresponding to one or two molecules in the junction.

2.5 Break Junction

The break junction technique was developed by Tao and colleagues in 2003[5] and was first used to measure the single molecule conductance of a 4,4′ bipyridine molecule and a sequence of *N*-alkanedithiols where N = 6, 8 and 10. Using a gold STM tip and substrate they formed molecular junctions by driving the tip into the surface in the presence of a solution of molecules. As the tip was retracted, it pulled out a chain of atomic gold atoms. When this chain was broken, molecules were able to bridge the gap and form junctions (Figure 2.9), indicated by steps in the conductance curve. Compilation of thousands of these curves produced a conductance histogram, much like the current histogram used in the *I*(*s*) *and I*(*t*) techniques.

An analogue of the break junction technique will be used throughout the following experiments. As opposed to using the method in a solution of molecules, molecules will first be adsorbed onto a gold surface to form a low coverage. The z displacement of the STM is then set to a specific value, usually -2 to -6 nm to ensure contact with the substrate. This method has been shown to give equally valid results.[7,12]

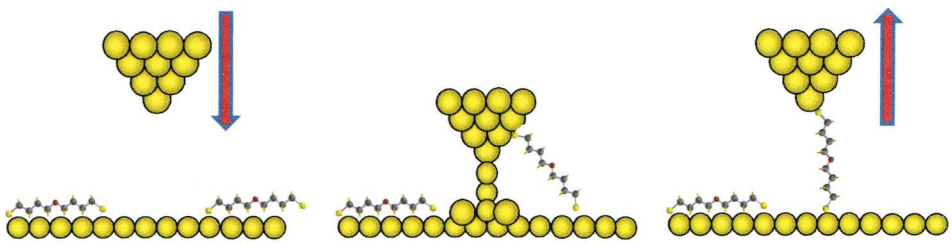

Figure 2.9. Illustration of STM break junction method.

For the case of alkanedithiols, the break junction technique initially appeared to give a higher conductance than the *I*(*s*) and *I*(*t*) methods by around a factor of twenty.[5] In more recent experiments, this apparent disparity decreased to a factor of four.[10] The reason for this higher conductance value is thought to be down to the contact morphology of either of the terminal sulphur groups with the gold substrate or tip.[6,7] The way in which the molecule is bound in the junction can be related to surface roughness. Haiss *et al.*[7] performed measurements on octanedithiol using four different techniques, the *I*(*s*) and *I*(*t*) techniques and also matrix isolation and break junction methods. An illustration of this is shown in Figure 2.10.

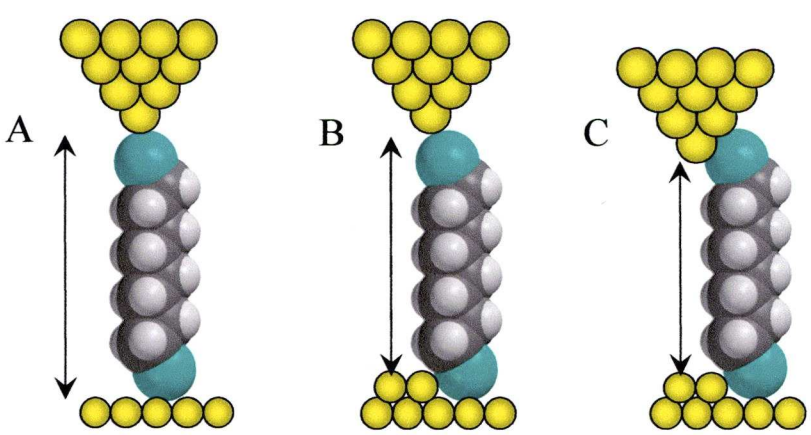

Figure 2.10. Three different contact morphologies for an alkanedithiol on gold.

Group A events, which are labelled as the low conductance group, occur when molecules are adsorbed on flat areas of the sample The group B conductance is generally for alkanedithiols a factor of four larger than the A group due to one of the contacts being bound on a step edge of the Au(111) substrate. This effectively decreases the tunnelling distance between tip and substrate. The group C conductance arises from both contacts anchored in defect sites and is significantly larger than the B group by a factor of around 15-17. All three conductance groups can be seen when using the break junction technique as this method involves physical contact with the surface and can result in modified surfaces features due to the pulling of atomic gold wires. It is possible to see group A and to a lesser extent group B conductance groups in the $I(s)$ method, although it is rare to encounter group C events.

2.6 Sample Preparation

A 0.1 mM solution of each target molecule was prepared, for the ether and thioether molecules dichloromethane was used as a solvent. For peptides solutions the solvent varied depending on the specific peptide sequence used. The gold substrates were immersed in these solutions for an average of one minute. Immersion times were altered occasionally if no current jumps were recorded after a set period of time, this was often the case for molecules containing only one terminal thiol moiety. These short immersion times have been shown to produce a low coverage of flat lying molecules on the surface of the gold substrate[4] and this was confirmed with XPS measurements. High coverage surfaces were obtained by increasing the immersion time to 24 hours. The substrates were then removed from the solutions and washed with dichloromethane or the respective solvent. Nitrogen was used to dry the samples thoroughly before they were positioned in the STM. Deionised water was obtained using a Milli-Q® plus 185 system. Environmental experiments were carried out in the appropriate solution using the STM Teflon cell. For each experiment the cell was cleaned with a hot

(H_2O_2/H_2SO_4) piranha solution followed by sonication in Milli-Q® water and dried prior to use.

2.7 XPS

X-ray photoelectron spectroscopy is a powerful surface analytical technique that can be used to study the composition and chemical state of molecules on a solid surface with a depth of up to 10 nm. An XPS instrument has a source of x-rays, in this case Mg K α (1253.6 eV), an analyser to measure the kinetic energy of the emitted electrons and an electron detector. XPS spectroscopy is performed under UHV conditions. These monochromatic soft x-rays are used to irradiate the sample which results in the emission of core level electrons. These core electrons have a characteristic binding energy which can be used to identify the element. These binding energies are dependent on the chemically environment surrounding the atom meaning that details of their chemical state can be obtained. Varying the x-ray take off angle alters the depth to which the x-rays penetrate the surface. This makes the technique very useful as decreasing this angle makes the technique more surface sensitive. XPS spectra acquired here were performed at Daresbury Laboratory, UK using a Scienta ESCA 300 spectrometer and 10^0 and 90^0 take off angles. For all measurements, gold on glass substrates were flame annealed immediately prior to use and molecules adsorbed as described above.

2.8 Imaging

Prior to each experiment, STM images were taken of the gold surface. Most images were taken using a cut gold tip. Images were obtained that show flat Au(111) terraces as a result of surface reconstruction as shown in Figure 2.11 (crossed lines). Imaging for gold was generally carried out at a bias voltage of between -0.05 and 0.2 V and a set point current of 0.2 to 0.5 nA on areas between 50nm^2 and 400 nm^2. Molecular

structure would not be seen at this magnification and in any case the low adsorption times and relatively low solution concentrations are not expected to yield ordered ad-layers.[2] Molecular level resolution was not a focus of the studies in the thesis.

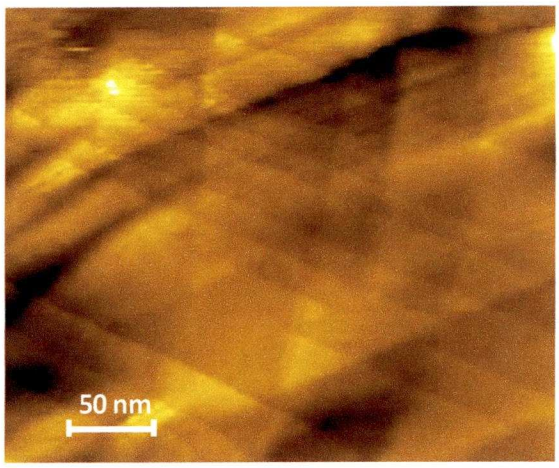

Figure 2.11. Image of low coverage DBE on gold under argon. Bias 0.1 V and I_0 = 0.5 nA.

2.9. Data Analysis

The way in which data is analysed has important implications for the reported conductance. As described in Chapter 1, the difficulty in creating identical junctions means that very large amounts of data must be collected in order to perform a statistical analysis. It is common practice for groups carrying out these types of experiments to pre-select data for their conductance histograms and there are several justifications for the practice. Firstly, although the STM allows a degree of automation for the *I*(*s*) technique, the probability of creating molecular junctions can sometimes be very low. Automatically collected data would then produce many thousands of scans which can be difficult to process using programs such as Origin™ and often produce little results if the tip is not moved to different locations on the sample. Secondly, due to the sensitivity of the STM, scans are often observed that show large amounts of noise due to external vibrations or instability of the

molecule in the junction. Inclusion of such scans in the data set can produce erroneous results. These are the main reasons why only scans displaying a well defined plateau are carried over for data analysis.

Initially, all the data analysis for the $I(s)$ and $I(t)$ methods was done by hand. For the $I(s)$ technique, a point was chosen by eye on the plateau of the scan that best represented the average value of the plateau current. These values were then compiled and Origin™ used to construct a conductance histogram. An example of this for TEG is shown in Figure 2.12 (a). A clear peak is obtained and the conductance and its associated error can be calculated. This method of analysis is very time consuming and more importantly there is a degree of human error involved in selecting the value for each scan.

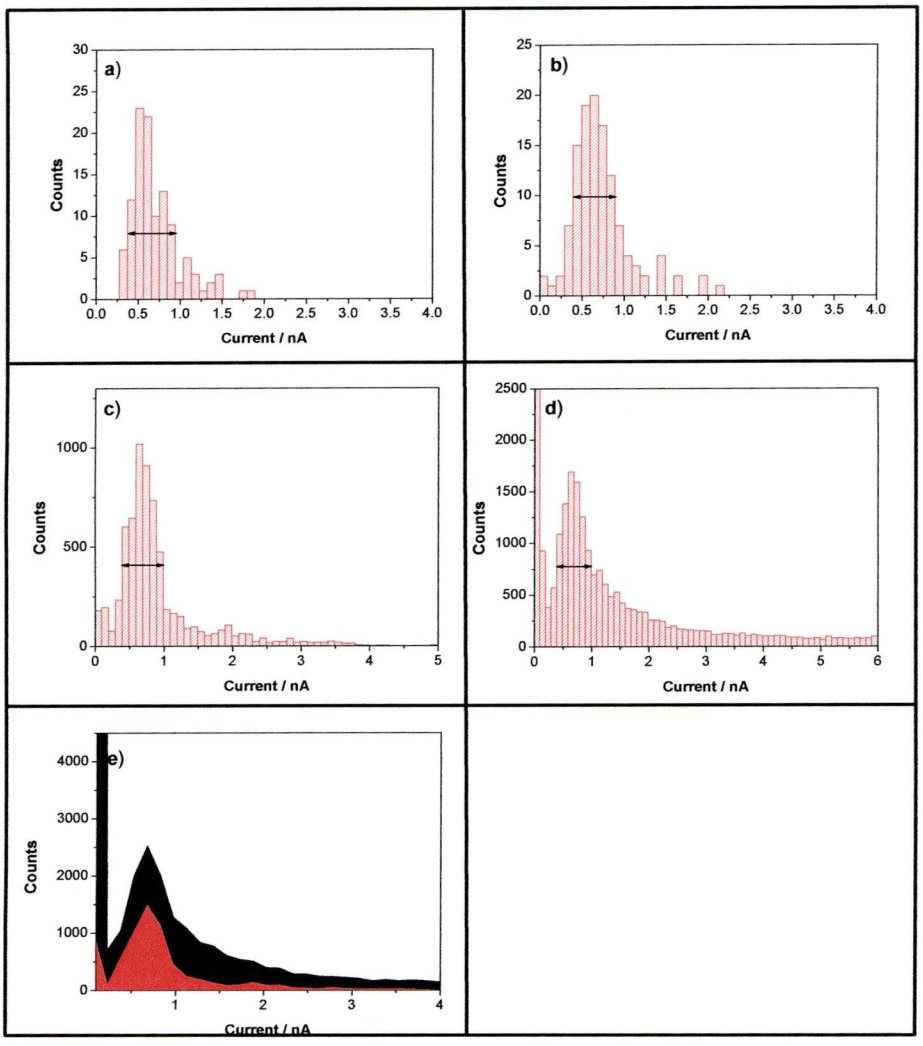

Figure 2.12. a) hand analysed data for TEG, at 0.2 V, I_0 = 20nA, b) data analysed with a single point assigned per given plateau, c) all data plateau histogram, d) all data histogram and e) Line graph, all data (black) and plateau data (red).

In recent years a LabVIEW^{TM} program was developed by the Nichols group to enable automated data analysis. Early use of this technique produced very similar histograms to the hand analysed data, however the single point of the plateau was chosen by the program (Figure 2.12 (b)). As the program developed, histograms displaying every data point of the *I*(*s*) curve could be constructed. Figure 2.12 (c) shows the compilation of every data point in just the plateau for 120 scans, Figure 2.12 (d) is a histogram of all the data. The final histogram, (e), is a line graph representing the initial output from the program. This line can be altered

by controlling the bin size of the data. The conductance values in nS obtained from the different methods of data analysis are as follows:

a) Hand analysed = (3.14 ± 0.77) nS.
b) Data analysed single plateau point = (3.22 ± 0.70) nS
c) All data plateau (3.46 ± 0.78)
d) All data (3.47 ± 0.79) nS
e) Original line graph (3.39 ± 1.20) nS

All of the values are well within error limits with a conductance range of 3.14-3.47 nS. The histograms that include all data points, either all the plateau data or all the current data have slightly higher conductance values than the others. This difference arises because when a molecule bridges the gap, the transition is not often sharp between the current decay and the onset of the plateau as illustrated in Figure 2.13.

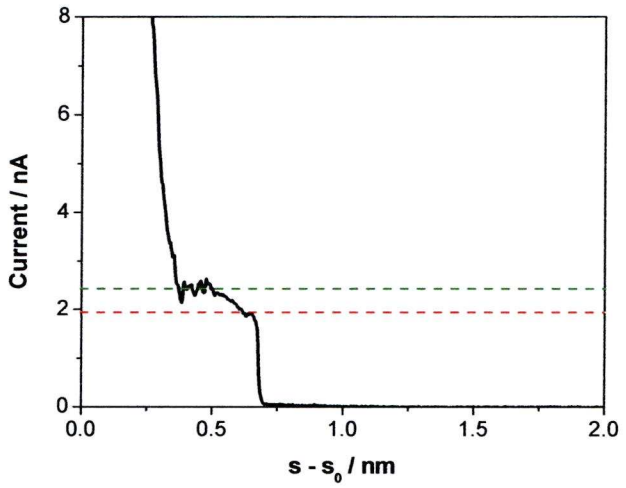

Figure 2.13 Example of *I*(*s*) curve for TEG in H_2O at 0.6 V, I_0 = 40 nA.

As shown in Figure 2.13 acceptable plateaus are not always level, here the beginning and end of the plateau vary by almost 0.5 nA. When every data point is included, the slightly higher conductance values (green line) contribute towards the current peak in the histogram. Inspection of many *I*(*s*) scans indicates that the additional higher current values slightly outweigh the lower (red line). When selecting data by hand, the value picked is the one that best represents the current plateau and

usually corresponds to the most level part. The final graph in Figure 2.12 e) shows the line graph generated by the LabVIEW™ program. The first peak (black) is the line graph for all the data and the second, red peak is the line representing just the plateau data. An advantage to displaying current values in this fashion is that LabVIEW™ enables the user to control several variables that further select the data. For example, the deviation on the plateau current, the signal to noise ratio and the length of the plateau can all be modified to desired values. As a standard throughout the following experiments, the all data current histogram, Figure 2.12 d), will be utilised. Although this method overestimates the current very slightly, using all the data gives the clearest picture and eliminates any further selection issues. It also incorporates every data point present in long plateaus which are indicative of the more stable molecular events. Screenshots of the Labview™ program used alongside definitions of the parameters are given in Appendix 1 to guide the reader through the analysis procedure.

References

1. Haiss, W.; van Zalinge, H.; Higgins, S. J.; Bethell, D.; Höbenreich, H.; Schiffrin, D.J.; Nichols, R. *J. Am. Chem. Soc,* **125**, 15294-15295. (2003).
2. Haiss, W.; Nichols, R.; Zalinge, H. V.; Higgins, S. J.; Bethell, D.; Schiffrin, D.J. *Phys. Chem. Chem. Phys*, **6**, 4330-4337. (2004).
3. Sek, S.; Swiatek, K.; Misicka, A. *J. Phys. Chem. B,* **109** (49), 23121-23124. (2005).
4. Haiss. W.; Zalinge, H. V.; Höbenreich.; Bethell, D.; Schiffrin, D.J.; Higgins, S. J and Nichols, R. J. *Langmuir*, **20**, 7694-7702. (2004).
5. Xu, B and Tao, N. J. *Science*, **301**, 1221-1223. (2003).
6. Nichols, R. J.; Haiss, W.; Higgins, S. J.; Leary, E.; Martin, S and Bethell, D. *Phys. Chem. Chem. Phys*, **12**, 2810-2815. (2010).
7. Haiss, W.; Martin, S.; Leary, E.; van Zalinge, H.; Higgins, S. J.; Bouffier. L and Nichols, R. J. *J. Phys. Chem. C.* **113**, 5823-5833. (2009).
8. Haiss, W.; Wang, C.; Grace, I.; Batsanov, A.; Schiffrin, D. J.; Higgins, S. J.; Bryce, M. R.; Lambert, C. J and Nichols, R. J. *Nature Materials*, **5**, 995-1002. (2006).
9. Martin, S.; Manrique, D. Z.; Garcia-Suarez, V. Haiss, W.; Higgins, S.; Lambert, C. J and Nichols, R. J. *Nanotechnology*. **20**, 125203. (2009).
10. Li, X.; He, J.; Hihath, J.; Xu, B.; Lindsay, S. M and Tao, N. *J. Am. Chem. Soc*, **128**, 2135-2141. (2006).
11. Martin, S.; Giustiniano, F.; Haiss, W.; Higgins, S. J.; Whitby, R, J and Nichols, R. J. *J. Phys. Chem. C*, **113**, 18884-18890. (2009).

12. Haiss, W.; Martin, S.; Scullion, L. E.; Bouffier, L.; Higgins, S. J and Nichols, R. J. *Phys. Chem. Chem. Phys*, **11**(46), 10831-10838. (2009).

Chapter 3. Alkanedithiols: Measurements and Voltage Dependence.

3.1 Introduction

Alkanes are simple non-branching chains of sp^3 hybridized carbon atoms and are considered as the simplest system with which to study single molecule conductance. Dithiolated alkanes possess thiol groups in the α-ω positions which enable molecules to form contacts between two electrodes. They have been extensively studied as they form well ordered monolayers on gold. This is due to the ease of chemisorption from solution through the S-Au bond which results in a crystalline *all-trans* structure as a result of the packing process. Alkanedithiols are produced from simple synthetic methods which allow for the introduction of functional terminal groups with which to study the effects of contacts within metal-molecule-metal junctions.[1,2] Their simple structure allows experimental and theoretical investigations into length dependence and electromechanical properties.[3] This has resulted in numerous techniques being developed and applied to the study of charge transport through these simple systems as described in the first two chapters.

Despite their extensive use in basic molecular electronics research, they have little potential for real application in molecular electronics for applications such as switches or charge conduits, for example. This is since they exhibit high resistance due to their large HOMO-LUMO gap which is generally considered to be around 8-10 eV, with the Fermi energy of metal contacts generally lying within this gap. They allow conductance characteristics such as length dependence to be studied as the sulfur linkers provide a stable attachment to the gold but do not drastically alter the original energies and shapes of the alkane molecular orbitals.[4] The conductance of these molecules therefore decreases exponentially with increasing number of methylene units. The aim is simply to investigate charge transport through a simple family of molecules through both experimental methods and theoretical

calculations. This then provides a standard to which other molecules can be compared and their electrical behaviour rationalised.

Many experimentally and theoretically determined conductance values have been reported, even for identical alkanedithiols with the seemingly same metal electrode contacts. As mentioned earlier, the nature and geometry of the contacts, even for covalently bound electrodes can have an effect on the measured conductance through a molecule. These contact geometries have been addressed by several groups to provide explanations for the variation in experimental data. The general consensus is that multiple conductance groups are a generic feature of the alkanedithiols with certain techniques favouring specific groups. Table 1 shows a summary of the experimental conductance measured in nS from several different groups for the octanedithiol molecule. This particular molecule is the most widely studied due to its symmetry and ease of synthesis. It is also available to purchase commercially and has a length of around 1 nm. The STM-break junction results represent the reported values of the Tao group, although other groups have used this approach also. The L, M and H conductance values are the low, medium and high values respectively.

	Low	Medium	High
STM-BJ	1[5]	4[6]	18.5[7]
AFM-MI	0.99[8]	5.6[9]	16.1[9]
I(s)	1[10]	3.7[10]	17[10]
I(t)	0.99[11]		
UHV - BJ	1.01[12]		

Table 1. Summary of reported conductance values in nS for ODT using break junction, matrix isolation, *I*(*s*) and *I*(*t*) techniques.

Results derived from STM break junction experiments[7] generally assign the value of 4 nS to the low conductance group for ODT, however, peaks in the current histograms corresponding to a conductance value of ~1 nS have since been observed which correlate well with the values determined by *I*(*s*) and *I*(*t*) methods.[5,13] The medium and high

conductance values obtained using the C-AFM matrix isolation method are the result of repeated experiments using large nanoparticles of around 5.4 nm as opposed to the smaller nanoparticles ~1.5 nm used in the original study that produced the low conductance group value. The differences in conductance values were attributed to a decreased contact resistance between the AFM probe and the larger nanoparticles thus presenting a smaller Coulomb blockade barrier.[8,9] The conductance through single molecules or SAMs of alkanedithiols has now become the standard to which other molecules of interest are compared and allows for predictions of electron transport through different systems. The conduction mechanism in alkanes is dominated by direct tunnelling via the C-C bonds along the alkane chains and studies have shown that electron transport through alkanedithiols is temperature independent, at least when they are rigidly packed in self assembled monolayers.[6,14] This is not the case for single molecules where the temperature dependent partitioning between differ conformers produces a substantial temperature dependence, due to differing conductance for different conformers.[10]

Although the conductance of *n*-alkanedithiols has been well studied, *n* is usually restricted to 6, 8, 10 and 12. Studies have been carried out on pentane and nonanedithiol, however, experiments so far have not included conductance values of heptanedithiol. For this reason α-ω heptanedithioacetate was synthesized and its conductance measured using the $I(s)$ and $I(t)$ techniques. The synthesis can be found at the end of this chapter. The terminal acetate groups were not removed from the molecule prior to adsorption on the gold surface as the results of XPS experiments presented in the next chapter demonstrate the formation of the sulfur-gold bond without the need for deprotection. There are several examples of the direct self assembly of thioacetate terminated molecules in the literature. For example Kang *et al*[15] studied the adsorption rates of dodecanethiol and dodecanthioacetate using electrochemical QCM and spectroscopic ellipsometry. They discovered that although the rate of adsorption for the thioacetylated molecules was slower than their thiolated analogues, they still formed ordered monolayers on the gold

surface. More recently Singh *et al*[16] carried out ^{1}H NMR and STM imaging experiments on the formation of monolayers of decanethioacetate on gold substrates. They discovered that deprotection of thioacetate groups produced more ordered, crystalline monolayers of the molecules on the gold than the untreated thioacetates. They found that SAM's were able to form also from untreated molecules and attribute the growth of the monolayers to presence of thiol or disulfide impurities. Both groups propose advantages of using thioacetates over thiols which include a decreased risk of oxidation form the air as sometimes encountered when using thiols, also the use of thioacetates can decrease the formation of aggregates or disulfides within the monolayer. For the purposes of $I(s)$ and $I(t)$ measurements, only a low coverage of flat lying molecules are necessary, therefore the formation of ordered monolayers is not a priority.

The resulting conductance value of the heptane molecule was compared to the conductance values of the n-alkane series from n=5 to n=12. The molecule and its subsequent conductance values were then used as part of a more detailed study into the length and voltage dependence of *n*-alkanedithiols. It was then shown that the non-resonant tunnelling properties of the alkanedithiols can be fitting using the Simmons equation which calculates the current density based on the I-V properties of a given molecule.

3.2 Results

3.2.1 Heptanedithioacetate.

The α-ω dithioacetate was synthesized according to the scheme in Figure 3.1. 1, 7 dibromoheptane was refluxed with potassium thioacetate to produce the 1, 7 heptanethioacetate (HDTA).

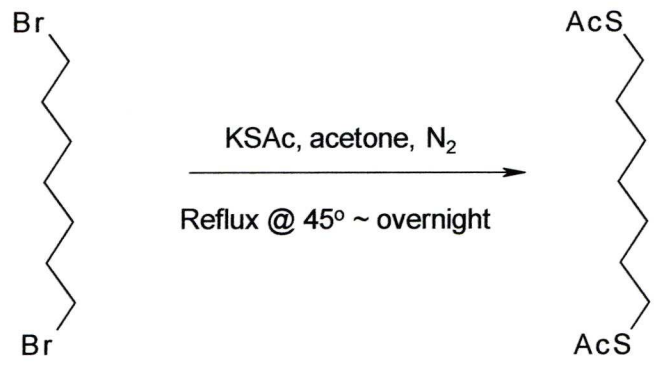

Figure 3.1. Synthesis of 1,7 heptanedithioacetate from 1,7 di-bromoheptane.

3.2.2 *I*(*t*) and *I*(*s*) Results

Imaging was carried out prior to each measurement to ensure the presence of flat Au(111) terraces on the substrate. Figure 3.2 shows an example of such an STM image of the heptanedithioacetate adsorbed on a gold substrate, the terraces are clearly visible within the image.

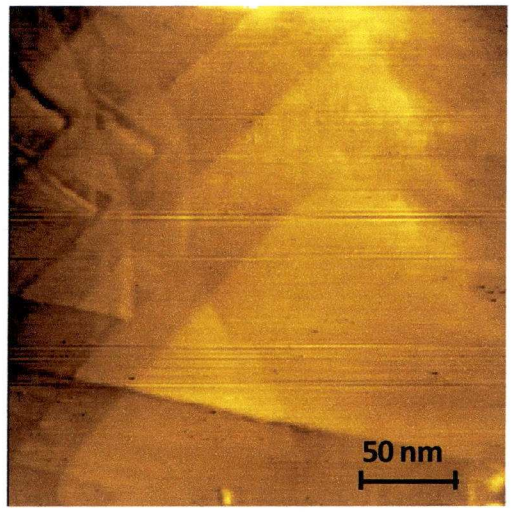

Figure 3.2. STM image of 1,7 heptanedithioacetate on Au substrate at 0.2 V, I_0 = 0.5 nA.

I(*t*) measurements were carried out between bias voltages of 0.6 to -0.6 V on Au(111) substrates with a low coverage of molecules. Adsorption times were between 30 seconds and one minute. Figure 3.3 shows examples of *I*(*t*) jumps recorded for HDTA at -0.2 V with a current set point of 2 nA

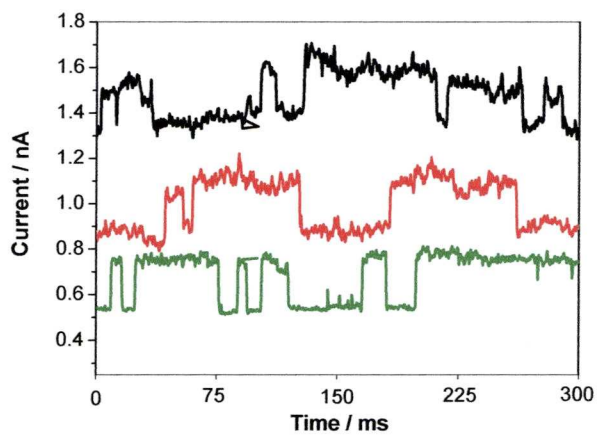

Figure 3.3 *I*(*t*) jumps recorded for HDTA at -0.2 V, I_0 = 2 nA.

Figure 3.4 shows the resulting current histograms from measurements performed at -0.2 and -0.4 V, where each histogram is constructed from over 90 *I*(*t*) jumps. The initial set point current used was 2 nA and this value was increased linearly with increasing voltage.

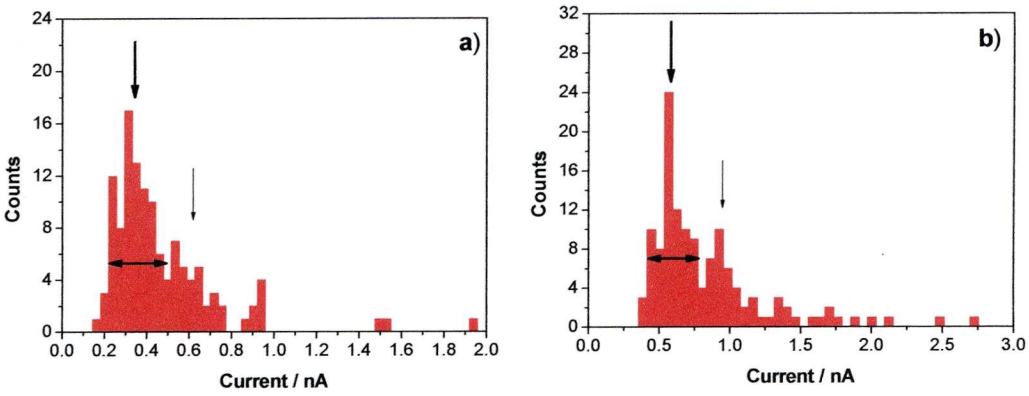

Figure 3.4 Current histograms for *I*(*t*) measurements of HDTA, a) -0.2 V, I_0 = 2nA, b) -0.4 V, I_0 = 4nA.

The main histogram peaks at the two bias voltages shown are clear and can be attributed to just one molecule present in the junction. Smaller peaks can also be observed that have an average current value that is approximately double that of the first peak and thus correspond to two molecules measured simultaneously. At -0.2 V, Figure 3.4 a), the current peak corresponds to a single molecule conductance value of (1.71 ± 0.33) nS or (2.21 x 10^{-5}) G_0 and is termed A_1 accordingly. The second peak (A_2) gives a conductance of (3.03 ± 0.32) nS. The histogram produced from experiments at -0.4 V, Figure 3.4 b), gives a conductance value of (1.48 ± 0.24) nS or (1.9 x 10^{-5}) G_0 with an A_2 value of (2.36 ± 0.15) nS.

To complement the *I*(*t*) results the HDTA molecule was also measured using the *I*(s) technique. Examples of *I*(*s*) scans recorded at a bias voltage of -0.2 V and a set point of 20 nA are shown in Figure 3.5 b)

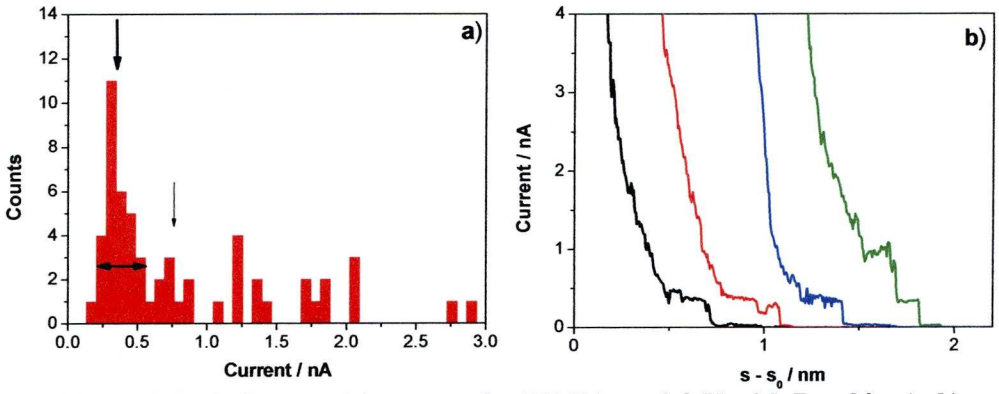

Figure 3.5. a) Current histogram for HDTA at -0.2 V with I_0 = 20 nA. b) Example *I*(*s*) scans.

The main peak from the current histogram in Figure 3.5 a) gives a conductance value of (1.81 ± 0.42) nS or (1.52 x 10^{-5}) G_0. The smaller peak indicated by the arrow is the A_2 conductance group that has a value which is around double that of the first peak and gives a conductance of (3.94 ± 0.69) nS. The *I*(*s*) traces in Figure 3.5 b) show clear plateaus attributed to conduction through the molecule. The *I*(*t*) experiments at this bias voltage give a conductance value of (1.71 ± 0.33) nS which correlates well with the *I*(*s*) results illustrating the complementary nature of these two experimental approaches. The current values from the *I*(*t*) histograms were plotted against their respective bias voltage values to give an I-V plot. This is shown in Figure 3.6. The linear fit to the data is very good with an Adj.R-square of 0.99268.

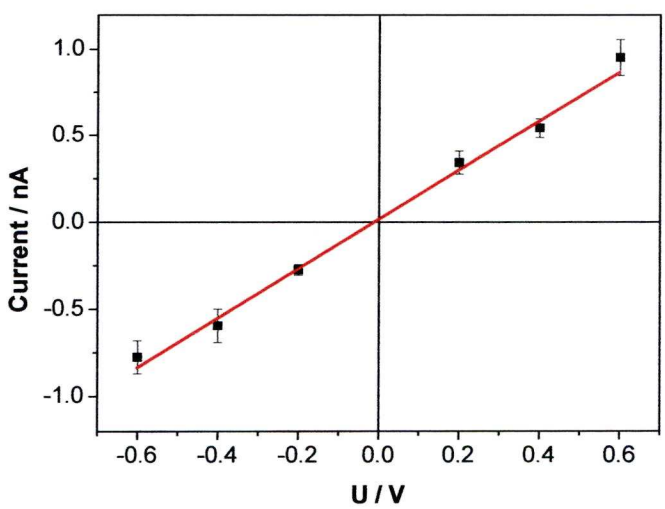

Figure 3.6. I-V plot for HDTA using the *I*(*t*) technique from 0.6 to -0.6 V.

The overall conductance calculated from the linear fitting is (1.42 ± 0.05) nS or (1.83 x 10^{-5}) G_0. This is higher than the conductance reported for octanedithiol (0.99 ± 0.07) nS[11] and lower than that reported for hexanedithol (2.54 ± 0.02) nS[17] using the same techniques. This new value for heptanedithioacetate can be plotted in relation to these values and to the reported values of n=5, n=9 and n=12, as shown in Figure 3.7. The values of these other alkanedithiols are taken from reported *I*(*s*) results from the Haiss group.

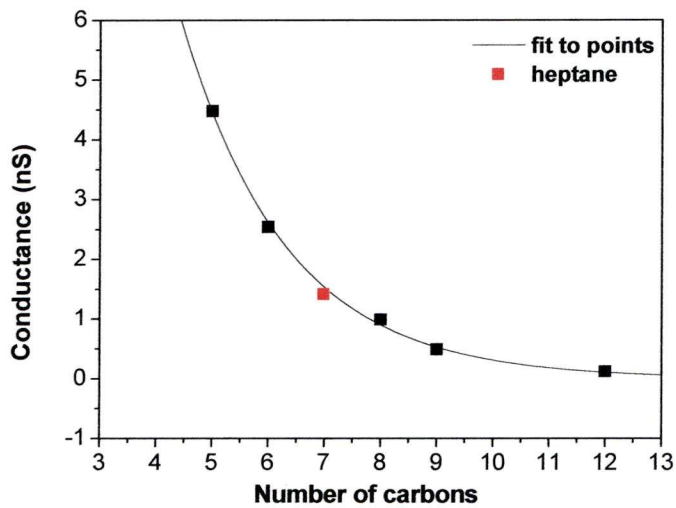

Figure 3.7 Relative conductance value of a series of *n*-alkanedithiols from n = 5 to n = 12[10,11,17,18]

This rough fitting to the points shown in Figure 3.7 indicates that the measured conductance for HDTA is in the correct order of magnitude and initially fits well with the values of the alkane series. The measurements for HDTA were then used in a detailed study to investigate the length dependence of alkanedithiols.[19] It was found that alkanedithiols with less than eight methylene units showed anomalous length and voltage dependence. The whole range from n=3 to n=12 (with the exception of n = 11) was studied using *I*(*s*) and break junction methods. The A_1 group values were found to be in good agreement using both techniques and the B_1 group for the HDTA molecule was found to be around 9.2 nS. Figure 3.8 shows the log values of the A_1, B_1 and C_1 conductance groups for all the molecules measured.

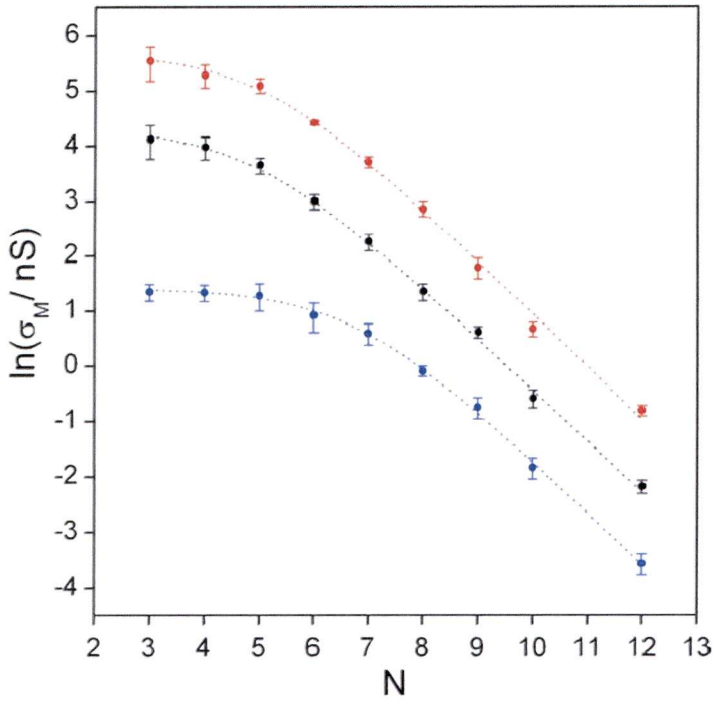

Figure 3.8. Single molecule conductance displayed on a logarithmic scale for *n*-alkanedithiols between *n*=3 and *n* = 12 at 0.6 V. A conductance group (blue), B group (black) and C group (red).

At this stage it was noted that when *n* was above 7, the exponential conductance decay (0.89 ± 0.03) per CH_2 for both A and B events were consistent with previously reported values.[7,20] For molecules less than eight carbons in length, however, the decay does not follow this pattern; instead it becomes less pronounced and for molecules with less than 5 carbons seems to be independent of length.

3. 3 Simmons Model

To investigate this phenomenon further, the voltage dependence of ODT and BDT were studied and fitted using a modified Simmons equation shown as equation 1.

$$J = \frac{e}{4\pi^2 \hbar d^2} \left\{ \begin{array}{l} \left(\phi_b - \frac{eV}{2}\right) exp\left[-\frac{2(2m)^{1/2}}{\hbar} \alpha \left(\phi_b - \frac{eV}{2}\right)^{1/2} d \right] \\ -\left(\phi_b - \frac{eV}{2}\right) exp\left[-\frac{2(2m)^{1/2}}{\hbar} \alpha \left(\phi_b + \frac{eV}{2}\right)^{1/2} d \right] \end{array} \right\} \quad (1)$$

The Simmons equation[21] expresses the current density, *J*, through a one dimensional barrier in the tunnelling regime of $V < \phi_b$[22] and can be used to produce I-V characteristics for a given barrier height or to fit experimental results. The term ϕ_b represents the barrier height and V is the applied bias. *m* is the mass of an electron and *e* is the charge of an electron. α is a dimensionless adjustable parameter that is introduced to the Simmons equation and is related to the effective mass (m_{eff}) of the tunnelling electron (or hole) through the junction. Here m_{eff} is equal to the effective mass multiplied by α^2. α can also be altered to account for the application of the tunnelling model to a non rectangular barrier.[4,6,14,22,23]

Finally *d* is the barrier width, which in this case is the through bond length of the alkanedithiols calculated using the SPARTAN® program. A value of 0.217 nm^2 was used as the surface area occupied by a single alkanedithiol molecule. This is equivalent to the area occupied by a single molecule in a ($\sqrt{3}$ x $\sqrt{3}$) $R30^0$ structure on Au(111).

3.3.1 Effective Barrier Height

To estimate the effective barrier height, the energetic positions of the molecular orbitals were estimated using a SPARTAN® implementation of DFT. This involved a B3LYP hybrid exchange correlation function in conjunction with G31-G* basis sets. The molecules had a single gold atom attached to either terminal and pseudopotentials were used to represent the gold core orbitals. For the alkanes, the LUMO orbitals are located exclusively at the sulfur gold contacts while the HOMOs are responsible for charge transport. The HOMO-2 and the HOMO-4 levels

are located on the alkane chain and the difference then between the frontier orbital and the gold Fermi level is calculated as 2 eV. This value was then corrected to account for image potential effects as described below.

3.3.2 Image Potentials

Image potential effects are created when a charge (for instance a tunnelling electron or hole) is close to a conducting surface. They can diminish the height and width of the effective tunnelling barriers and this is particularly important for short molecules.[24] Metals such as gold are effective at screening charge in their immediate proximity since the electron plasma can respond very quickly to polarisations due to the high plasma frequency of gold (1.36×10^{16} s^{-1})[25] The influence of this image charge can be quantified and it results in a reduction of the barrier determined from the DFT calculations. The barrier height for the static image potential effects, is represented by $\Delta\phi(x, s_0)$ in Figure 3.9. Replacement by an effective rectangular barrier gives an image potential corrected barrier height according to equation 2.

$$\phi_i = \phi_0 - \frac{2\phi_0 c}{\Delta s} ln\left(\frac{s_0+\Delta s}{s_0-\Delta s}\right) \qquad (2)$$

Here, ϕ_0 is the height of the uncorrected barrier, s_0 is the original width, Δs is the reduction of the barrier width and c is a constant which can be calculated from equation 3 and is approximately equal to $0.288/\phi_0\varepsilon_r$ when considering units of nm and eV. The dielectric constant ε_r used here has been calculated as 2.1[24] and Δs can be calculated using equation 4 shown below:

$$c = \frac{1.15e^2 ln2}{16\pi\varepsilon_r\varepsilon_0\phi_0} \qquad (3)$$

$$\Delta s = s_0\left(1 - {}^{4c}/_{s_0}\right)^{1/2} \qquad (4)$$

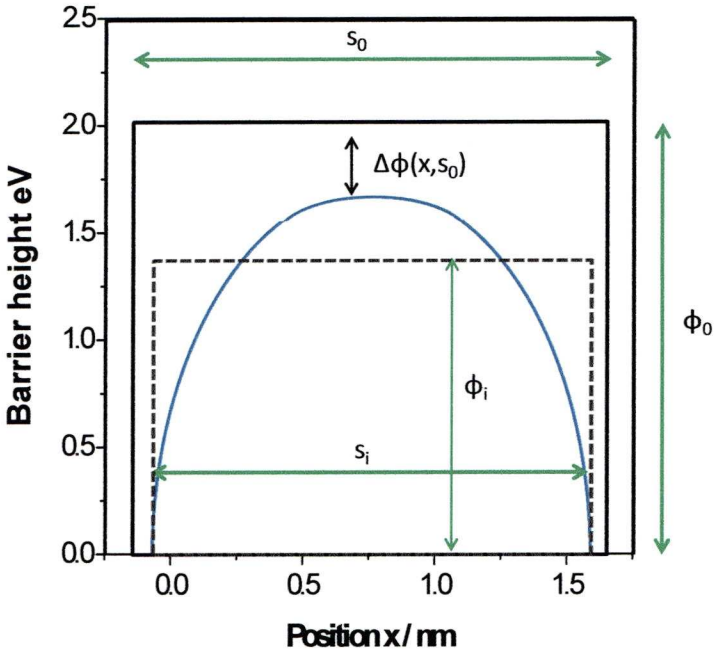

Figure 3.9. Image potential correction. S_0 = original barrier width, S_i – new barrier width. Dashed line = effective rectangular barrier with ϕ_i = reduced barrier height.

Figure 3.9 demonstrates how the potential barrier is affected when image charge corrections are implemented. The potential barrier (blue) appears lower and more rounded than the original rectangular barrier and the total area under the new effective potential barrier (dashed line) is now much less than the original. For ODT this results in a reduction of the barrier height from 2 eV to 1.36 eV. The reduced barrier height in Figure 3.9 is shown by ϕ_i and the reduced barrier width as S_i

This corrected barrier height value was then used to calculate the current through single ODT and butanedithiol (BDT) molecules as a function of the applied voltage using equation (1). Figure 3.10 shows the results of these calculations. The current values for the ODT in Figure 3.10 a) produce an excellent fit with the experimentally measured values for the A_1 conductance group from $I(s)$ measurements and also the B_1 conductance group values determined from break junction experiments.

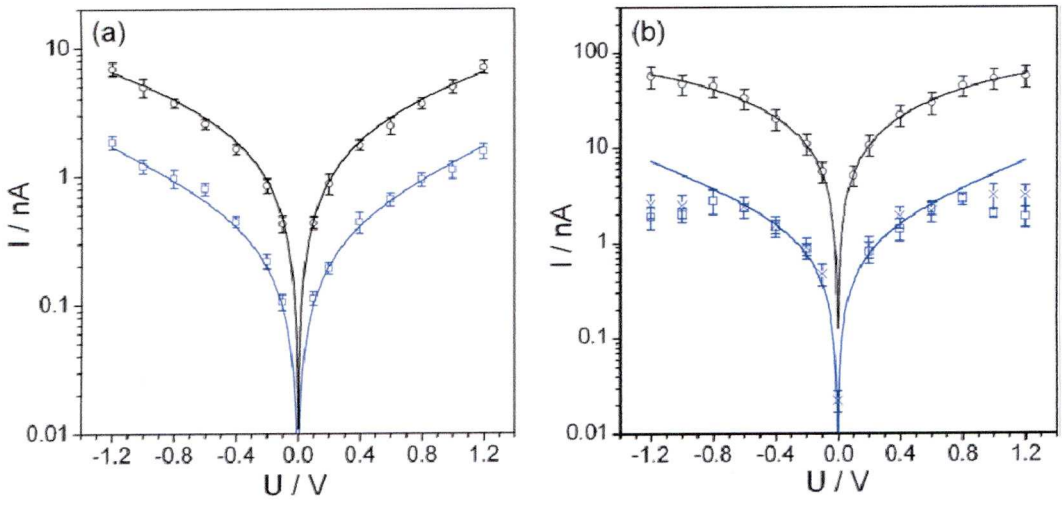

Figure 3.10. Simmons equation fitting for a) ODT and b) BDT including image charge effects. A_1 conductance group is shown in blue (squares I(s), crosses BJ) and the B_1 conductance group is shown in black.

The ODT fitting resulted in an α value of 0.53 which was compared to reported values of the predicted effective hole mass for ODT (0.28 x m_e)[26] and (0.30 x m_e)[27] and the effective electron mass for extended alkane chains (3.03 x m_e)[27] Using (m_e x α^2 = m_{eff}) ,the similarity of the α value with the effective hole mass values reported in the literature supports the involvement of the HOMO orbitals in the charge transport of alkane chains.

The resulting fit for BDT (Figure 3.10 b)) proved less straightforward. As already observed, experimental I-V current values for *n*-alkanedithiols with n < 7 are almost length independent. Using an α value of 0.5 and ϕ_0 as 2 eV, the current values for BDT were plotted as a function of the barrier width, S_0, with and without image potential corrections (Figure 3.11). Taking image charge into account, the A_1 data (blue crosses) fit well from n = 7 to n = 12 but n values below this cannot be rationalised by image potential effects.

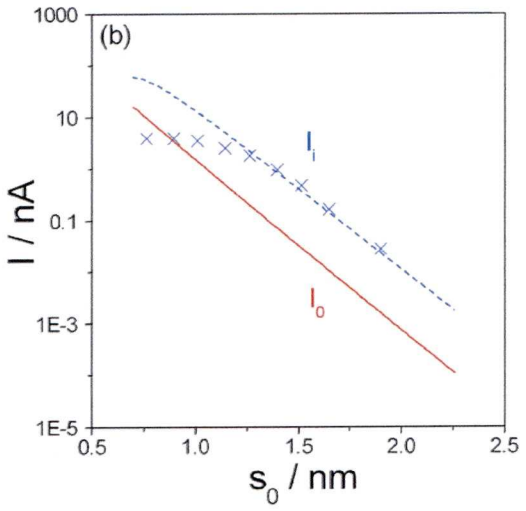

Figure 3.11. Tunnelling current versus barrier width calculated using the Simmons equation with image potential correction (blue line) and without (red line).

The calculated Simmons current was also plotted for n = 3 to n = 12 as a function of α between α = 0 and α = 12 to deduce that large values of α are required to fit the length dependence for the single molecule conductance of short molecules. As α approaches 1, this correlates to the effective mass of the tunnelling hole approaching unity for short molecules. Following these results, an α value of 0.94 (with ϕ_0 as 2 eV) was used to fit the A_1 conductance data for BDT as shown in Figure 3.10 b). The resulting fit agrees well with both the experimentally determined $I(s)$ and break junction values for the voltage range of 0.6 to -0.6 V. However, this model does not hold for the currents measured at higher voltages.

3.4 Discussion

The anomalous voltage dependence of short alkanedithiols cannot be explained by image charge effects or an independent α value. For longer molecules, n > 7, the Simmons equation results in a good fit to experimental data using a range of techniques. The image charge corrected barrier height for ODT was found to be 1.36 eV with an α value of 0.53. These values also correlate well with other values reported in the literature for ODT in similar systems. The barrier height and α

value reported by Wang *et al.*[14] for ODT SAMs was (1.2 ± 0.03) eV and α = (0.59 ± 0.01). This group formed monolayers of octanedithiol sandwiched between two metal contacts within a nanopore which had been filled with thermally evaporated gold. The nanopore was created by e-beam lithography and reactive ion etching of a Si_3N_4 film suspended over a silicon wafer. The ϕ_b and α values were the result of systematic variation to produce the best fit for their measured I-V data.

Simmons fitting was used by Majumdar *et al.*[22] to determine the effective barrier height for ODT. They used experimental I-V data to determine a curve of best fit for the Simmons equation. The I-V data was obtained from ODT molecules in a self-assembled monolayer present in a nanowell device with a gold base, with a top contact consisting of electron beam deposited Ti and Au. The resulting barrier height was found to be (2.05 ± 0.15) eV with an α value of (0.72 ± 0.04). This result is similar to the estimated barrier height found here of 2 eV before image charge corrections are applied. Engelkes *et al.*[28] have also produced I-V traces for ODT molecules as part of their work on alternative metal electrodes using CF-AFM. The barrier height calculated from the Simmons equation for ODT was 2.5 eV which is higher than the values reported here. This may be a result of the much higher α value they used of 1. Li *et al.*[6] also demonstrated the sensitivity of the fitting parameters ϕ_0 and α to the I-V behaviour of octanedithiol measured using the STM-break junction technique. They determined that the measured current values gave the best fit to the Simmons model with values of ϕ_0 = 1.83 and α = 0.61 which are both higher than the results presented here.

The Simmons model has also been applied to a series of aromatic single molecules to rationalise the observed difference in conduction values for single and double thiol linkers.[23] A conducting probe AFM was employed to produce I-V characteristics for biphenyl-4,4′-dithiol and biphenyl-4,4′-dicarbodithioic acid. The best fit parameters for the single thiol linker molecules were calculated as ϕ_b = 1.35 eV and α = 0.59, whereas the molecule with double thiol linkers was found to fit well with

parameters of $\phi_b = 0.59$ eV and $\alpha = 0.66$. These values were found to be lower than those of alkanedithiols of similar lengths due to the enhanced electron transport through the conjugated systems. The lower barrier for the second molecule was attributed to enhanced overlap of the electronic wavefunctions of the double thiol linkers between the molecule and the gold substrate.

3.5 Conclusions.

Heptanedithioacetate has been synthesised and characterised using NMR techniques. $I(t)$ and $I(s)$ techniques have been used to determine the single molecule conductance of this molecule between a gold substrate and an STM tip. Good agreement between the values measured with the two different techniques was observed. The anomalous length dependence of a series of alkanedithiols was investigated experimentally and with DFT calculations. The Simmons model was found to fit the experimental data for longer molecules well. However, in order to fit the conductance observed for shorter molecules with the Simmons model a length dependent α value has to be introduced. Such a length dependent α value has a certain literature basis, although it is clear that more sophisticated theoretical models are needed which go far beyond the Simmons model to understand the influence of image charge and the molecule-metal interface and also to rationalise tunnelling through very narrow barriers with close separation between the metal leads.

3.6 Synthesis of 1,7 heptanedithioacetate

Dibromoheptane and potassium dithioacetate were purchased from Sigma Aldrich and used as received.

To a solution of dibromoheptane in acetone 2.5 equivalents of potassium thioacetate were added. The resulting mixture was stirred at reflux for approximately 12 hours under N_2. The mixture was then allowed to cool

to room temperature at which point water was added followed by extraction with ethyl acetate. The combined organic extracts were washed with brine and then dried over $MgSO_4$ and filtered. After removal of the solvent, the dithioacetate was purified by column chromatography (hexane/ CH2Cl2 8/2) to provide the heptanedithioacetate (64% yield). The presence of the compound was confirmed by ^{1}H NMR (CDCl3) δ 2.85 (t, 4H) 2.32 (s, 6H) 1.52- 1.60 (m, 4H) 1.31-1.39 (m, 4H) 1.19-1.21 (m, 2H). ^{13}C NMR (CDCl3) δ 196.3, 31.0, 30.1, 29.8, 29.4, 28.9. The original NMRs with Mass Spec data are shown in Appendix 2.

References

1. Chen, F.; Li, X.; Hihath, J.; Huang, Z and Tao, N. *J. Am. Chem. Soc*, **128**, 15874-15881. (2006).
2. Martin, S.; Haiss, W.; Higgins, S.; Cea, P.; Carmen Lopez, M and Nichols, R. J. *J. Phys. Chem. C.* **112**, 3941-3948. (2008).
3. Xu, B.; Xiao, X and Tao, N. *J. Am. Chem. Soc*, **125**, 16164-16165. (2003).
4. Seminario, J. M and Yan, L. *Int. J. Quant. Chem*, **102**, 711-723. (2005).
5. He, J.; Sankey, O.; Lee, M.; Tao, N.; Li, X and Lindsay S. *Faraday Discuss*, **131**, 145-154. (2006).
6. Xiulan, Li.; He, J.; Hihath, J.; Xu, B.; Lindsay, S. M and Tao, N. *J. Am. Chem. Soc*, **128**, 2135-2141. (2006).
7. Xu, B and Tao, N. J. *Science*, **301**, 1221-1223. (2003)
8. Cui, X. D.; Primak, A.; Zarate, X.; Tomfohr, J.; Sankey, O. F.; Moore, A. L.; Gust, D.; Harris, G.; Lindsay, S. M. *Science*, **294**, 571-574. (2001)
9. Morita, T and Lindsay S. *J. Am. Chem. Soc*, **129**, 7262-7263. (2007).
10. Haiss, W.; Martin, S.; Leary, E.; van Zalinge, H.; Higgins, S. J.; Bouffier, L and Nichols, R. J. *J. Phys. Chem. C.* **113**, 5823-5833. (2009).
11. Haiss, W.; Nichols, R.; Zalinge, H. V.; Higgins, S. J.; Bethell, D.; Schiffrin, D.J. *Phys. Chem. Chem. Phys*, **6**, 4330-4337. (2004).
12. Suzuki, M.; Fujii, S.; Fujihira, M. *Japanese Journal of Applied Physics*, **45** (3B), 2041-2044. (2006).
13. Lindsay, S. M and Ratner, M. A. *Advanced Materials*, **19**, 23-31. (2007).
14. Wang, W.; Lee, T and Reed, M. A. *Rep. Prog. Phys*, **68**, 523-544. (2005).

15. Kang, Y.; Won, D-G.; Kim, S. R.; Seo, K.; Choi, H-S.; Lee, G.; Zaesung, N.; Lee, T. S and Lee, C. *Materials Science and Engineering C*, **24**, 43-46. (2004).
16. Sing, A.; Dahanayaka, D. H.; Biswas, A.; Bumm, L. A and Halterman, R. L. *Langmuir*, **26**(16), 13221-13226. (2010).
17. Haiss, W.; van Zalinge, H.; Bethell, D.: Ulstrup, J.: Schiffrin, DJ and Nichols, R. J. *Faraday Discuss*, **131**, 253-264. (2006).
18. Haiss, W.; van Zalinge, H.; Higgins, S. J.; Bethell, D.; Hobenreich, H.; Schiffrin, D. J and Nichols, R. J. *J. Am. Chem. Soc*, 15294-15295. (2003).
19. Haiss, W.; Martin, S.; Scullion, L. E.; Bouffier, L.; Higgins, S. J and Nichols, R. J. *Phys. Chem. Chem. Phys*, **11**(46), 10831-10838. (2009).
20. Jang, S. Y.; Reddy, P.; Majumdar, A and Segalman, R. A. *Nano Lett.* **6** (10), 2362-2367. (2006).
21. Simmons, J. G. *J. Appl. Phys*, **34** (6), 1793-1803. (1963).
22. Majumdar, N.; Gergel, N.; Routenberg, D.; Bean, J.; Harriott, L.; Li, B.; Pu, L.; Yao, Y and Tour, J. M. *J. Vac. Sci. Technol*, **23** (4), 1417-1421. (2005).
23. Tivanski, A.; He, Y.; Borguet, E.; Liu, H.; Walker, G and Waldeck, D. *J. Phys. Chem. B*, **109**, 5398-5402. (2005).
24. Akkerman, H.; Naber, R.; Jongbloed, B.; van Hal, P.; Blom, P.; Leeuw, D and de Boer, B. *Proc, Nat, Acad, Sci*, **104** (27), 11161-11166. (2007).
25. Innes, R. A and Sambles J. R. *J. Phys. F. Met. Phys*, **17** (1), 277-287. (1987).
26. Tomfohr, J. K and Sankey, O. F. *Phys. Rev. B*, **65**, 245105. (2002).
27. McDermott, S.; George, C.; Fagas, G.; Greer, J and Ratner, M. A. *J. Phys .Chem .C*, **113**, 744-750. (2009).
28. Engelkes, V.; Beebe, J and Frisbie, C. D. *J. Am. Chem. Soc*, **126**, 14287-14296. (2004). (in papers 10)

Chapter 4. Single Molecule Conductance of Ethers

4.1 Introduction

As described in Chapter 3, the conductance of *n*-alkanedithiols is fairly well understood with their electron transport proceeding via through bond tunnelling. Their measured conductance should be rather sensitive to chemical alteration in these molecular bridges. In the simplest barrier tunnelling model changes to the chemical nature of the bridge would alter the tunnelling barrier height and width and consequently impact on the barrier transmission. The three molecules introduced in Chapter 1 were synthesised with the same linking groups but substituted atoms in the backbone, in order to determine experimentally if simple atom substitution affects conductance. Again, no deprotection of the acetate groups was performed as the molecules were shown to form sulfur gold bonds upon adsorption. These structures are shown in Figure 4.1.

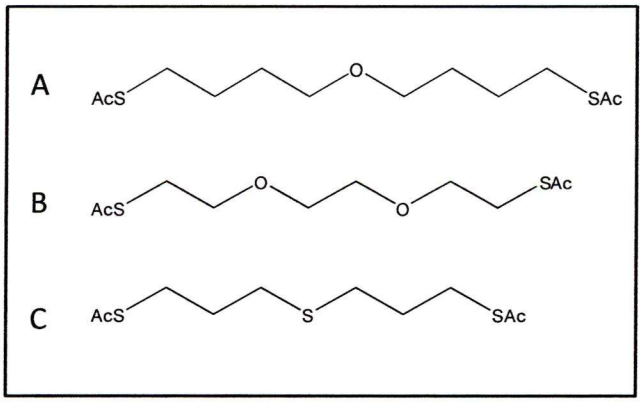

Figure 4.1. Structure of three molecules under investigation a) DBE, b) TEG and c) DPTE.

The oxygen atoms are broadly similar in size to the carbon atom they replace enabling direct comparison with similar length alkanedithiols. Using the $I(s)$ and $I(t)$ techniques described previously, the conductance for hexanedithiol, octanedithiol and nonanedithiol were determined as

2.5 nS, 0.99 nS and 0.49 nS respectively for the low A_1 conductance group.[1,2] The conductance of heptanedithiol has now also been determined as 1.42 nS and by using this comparison it will be possible to understand how even simple changes to a molecule affect its electrical behaviour within metallic contact junctions

4.2 Previous Work

Few studies so far have focused on how simple internal atom substitution affects electron transport through single molecules, with the exception of experiments regarding alternative anchoring groups. Most work to date involving atom substitution is based on the electron transfer rates in self-assembled monolayers. Cheng *et al*[3] reported an approach to investigate the effects of bridging units in 1995, however, this study focused on the effects of atom substitution on long-range electron transfer rates. They synthesised several ω-hydroxyalkanethiol molecules with centrally modified groups including several single ethers which were immobilized on gold electrodes through self-assembly. The electron transfer from the gold electrodes to redox species tethered to the top of the monolayers was recorded. They deduced that the ether modified SAMs resulted in decreased electron transfer rates and attributed this to a lower electronic coupling for the ether molecules compared to corresponding alkanethiols. Similarly, work was carried out by Napper *et al*[4] a few years later on electron transfer rates from gold electrodes to ferrocene groups on mixed SAMs of alkanethiol and alkanes containing single ether linkages. Again electron transfer rates were found to decrease upon introduction of oxygen atoms into the SAM and the observations were attributed to the same decrease in electronic coupling as Chen *et al.*

Sek *et al*[5] on the other hand reported enhanced electron tunnelling efficiency through SAMs where single methylene groups of alkanethiols were replaced by a single amide moiety. They attribute the effect to lateral hydrogen bonding throughout the monolayers; however, the effect of this substitution on electron transfer through just a single molecule

has not been investigated. Intermolecular hydrogen bonds involving amide groups through monolayers may have implications in the study of peptide monolayers which will be discussed in Chapter 5.

4.3 The Molecules

4.3.1 DBE

S,S'-(oxybis(butane-4,1-diyl))diethanethioate was synthesized according to the scheme shown below in Figure 4.2. Ring-opening polymerization of THF using phosporylchloride was followed by substitution of the chlorine atoms with thioacetate groups. The full synthesis with characterisation data can be found at the end of this chapter.

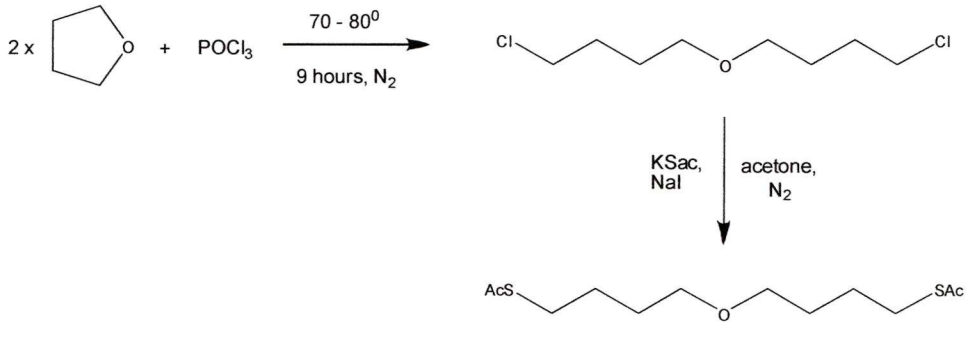

Figure 4.2. Reaction scheme for the synthesis of DBE.

DBE is a simple symmetrical ether, in its base form $C_8H_{18}O$ is it generally used as a solvent for hydrocarbons and alcohols. It has two methyl chains four carbons in length bridged by a single oxygen atom, the presence of which result in the molecule being weakly polar. The introduction of the terminal thioacetate groups should allow the molecule to chemically bind to the electrodes and so enable measurement using the $I(s)$ and $I(t)$ techniques described. The monolayer method by Sek[6] will also be introduced here. Infrared reflection-absorption measurements on monolayers of similar molecules[7] indicate that this type of molecule can form stable monolayers and that the presence of the oxygen bridge does not significantly alter the monolayer tilt angle with comparison to alkane chains, both appearing around 30^0.

4.3.2 TEG

The second molecule under investigation, *S*'-((methylenebis(oxy))bis(ethane-2,1-diyl)) diethanethioate was synthesised according to the scheme in Figure 4.3 and involved the simple reaction of the tosylated triethylene glycol with potassium thioacetate. The full synthesis can be found at the end of this chapter.

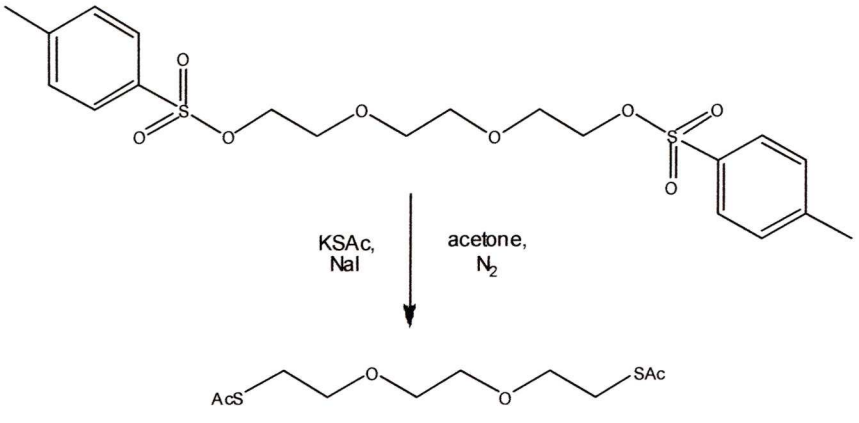

Figure 4.3. Synthesis of *S*,*S*'-((methylenebis(oxy))bis(ethane-2,1-diyl)) diethanethioate from Tri(ethylene glycol) di-*p*-toluenesulfonate.

Tri(ethylene glycol) ($C_6H_{14}O_4$) is a member of a homologous series of dihydroxy alcohols. It is used commercially in disinfectant products[8-10] and as dehumidifying agent for air and natural gas[11]. Its polymerized form, poly(ethylene glycol) (PEG) is used extensively in applications due to the fact that it is non-toxic, soluble in a variety of solvents and is biocompatible. Thiolated TEG and PEG can both be used as ligands for the stabilisation of gold nanoparticles[12] Thiolated PEG is often used to modify substrates for applications such as the non specific adsorption of proteins or cells[13-15] and to increase the hydrophilicity of surfaces, however, studies on PEG thiol SAMs have shown that the monolayers are subject to degradation upon exposure to air for two weeks and cannot withstand high temperatures[13]. Ethylene glycol units are often found attached to alkane chain linkers as pure ethlylene glycol chains over a certain length have a tendency to fold in on themselves due to the

constraints of the C-O-C bond angles This can lead to less densely packed monolayers so the alkyl chains are included to help to 'straighten out' the glycols. The dithioacetate substituted version of TEG used here should again enable contact between the STM tip and substrate and should also be able to form reasonably ordered monolayers as it only has two ether oxygens.

4.3.3. Thioether

The third and final molecule to be studied is *S,S'*-(thiobis(propane-3, 1-diyl))diethanethioate which was synthesised according to the scheme in Figure 4.4. The full synthesis can be found in Appendix 5.

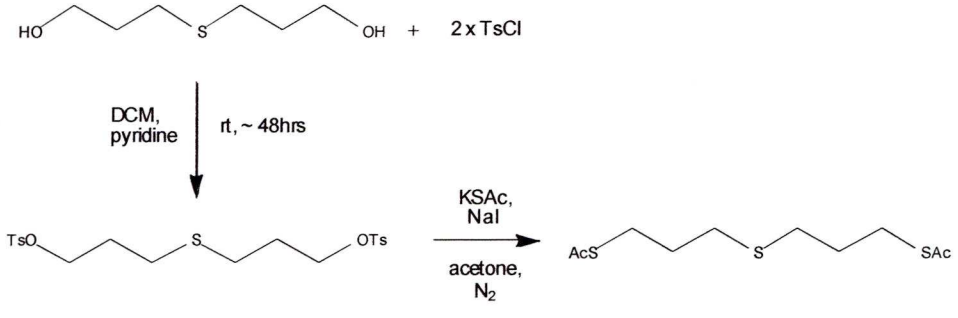

Figure 4.4. Synthesis of DPTE from 3,3'-thiodipropan-1-ol.

The aim of using this thioether in single molecule studies is to examine the effect of the bridging sulfur atoms. Studies have been performed on molecules with sulfur containing bridging units such as thiophenes[16,17] that display switching behaviour however, substitution by single sulfur atoms has not been addressed.

4.3.4 Barrier Indentations

The studies performed on viologen molecules[18-20] showed that inclusion of the 4, 4'-bipyridinium moiety resulted in a double tunnelling barrier system. The frontier orbital energies for alkyl groups are far from the Fermi energy of gold as shown in Chapter 3. The conjugated π-system of the viologen has frontier orbitals that are much closer to the Fermi energy of gold and results in the viologen forming a barrier indentation. More recently studies on simple substituted aromatic units[20] showed that non-

redox-active central benzene groups can act as barrier indentations resulting in measured conductance values that are significantly higher than alkanedithiols of similar lengths. The effect of the indentation can be modified by the introduction of electron donating moieties such as methoxy groups to the central aromatic units. With the three molecules presented here we would like to probe the limits for barrier indentations and see if single molecule bridges can produce these effects.

4.4 Environmental Effects

The two oxygen containing molecules will be studied using the $I(s)$ method in a water environment. The reason for these measurements is to see how the presence of water affects conduction through the molecule. Although several groups study single molecule conductance under UHV conditions, many experiments on single molecules are often carried out under ambient conditions where the presence of water and impurities from the air may have an effect on the measured conductance.

This is an important factor to consider if organic molecules are to be used in electronic devices as it is not always possible to control precisely the environment in which they function. The two studies mentioned briefly in Chapter 1 represent efforts to address this issue and will be revisited now.

Long *et al*[21] used magnetically assembled silica microsphere junctions to probe the effect of hydration on a variety of SAMs. The molecules used to prepare the SAMs were mono-and dithiolated nonane, dodecanethiol and mono- and dithiolated oligo(phenylene ethylene). SAMs were prepared in the junction and the I-V characteristics recorded for each molecular SAM under different environmental conditions. The I-V curves for OPE and dodecanethiol SAMs were initial recoded under vacuum conditions, after which a variety of gas or gas mixtures were introduced into the junction. For both systems in was found that the molecular conductance remained constant for measurements performed in vacuum, under Ar/N_2 and Ar/O_2 in a 1:1 ratio. When water vapour was introduced into the junction, however, a marked decrease in

conductance was observed. Similar results were obtained for the nonanethiol and nonanedithiol molecules upon changing from a vacuum environment to one where water vapour was present, the nonanedithiol producing the largest decrease in current. The group attributes these observations to hydration at the gold-thiol contact where the polar water molecules interact with negatively charged thiolate sulfur atoms. This was used to explain why the dithiols produce a larger current decrease than monothiols. They supplemented these experiments with inelastic tunnelling spectroscopy (IETS) to measure the changes in the vibrational spectra of the junction under each environment. Again these results indicated that water associated with the electronegative thiolate.

These results are in direct contrast with the results of the studies by Li *et al*[22] who measured single molecule conductance using STM and AFM break junction techniques. Single molecule conductance measurements of octanedithiol were performed in different solutions, toluene, dodecane, 0.1 M $NaClO_4$ and pure water. The conductance values recorded were identical in each case indicating that the environment had no effect on the conductance through alkanedithiols. This result is in agreement with the experiments performed at Liverpool where no change in conductance was observed for alkanedithiols under inert and ambient conditions. [23,24] This is to be expected as the alkanes are simple saturated chains with no readily polarisable moieties on the molecular backbone.

It has been shown previously that some molecules exhibit enhanced electrical conductance in the presence of water. The study by Leary *et al*[16] on a series of oligothiophenes showed that when measured in the presence of water vapour, the conductance of thiophenes was higher than when measured under a dry argon environment and this observation was attributed to the formation of a solvent shell. Water molecules of this hydration shell interact with the thiophene rings which 'gated' the conductance and this gating of conductance by the addition or removal of water was found to be reversible. Water environment was produced by exposure of the sample to an ambient environment. Under conditions of normal humidity a film of water is expected to be present on the gold surface. The observation of conductance gated by water for this

thiophene bridge system differs from the results obtained for the ether molecules which will be discussed later in the chapter.

The molecules under investigation contain one and two oxygen atoms respectively with a small dipole present due to the electronegative oxygen. Also, the oxygen lone pairs in both molecules are able to participate in hydrogen bonding in the presence of water; this may produce interesting effects when performing measurements in aqueous conditions. It has been reported that ether oxygens when present in self-assembled monolayers can introduce internal dipoles into the film structure and studies of PEG SAMs on gold have shown that when hydrated, PEG is surrounded by a water cage with at least two to three water molecules per ethylene glycol unit[13] Here, the oxygen atoms act as hydrogen bond acceptors and this effect has been observed for TEG-OMe SAMs where the association of water with these monolayers was high. So the aim of these measurements is to ascertain whether the molecules from the surrounding environment interact with the molecular electrical junctions thus changing their conductance.

4.5. Results

For experiments carried out in aqueous environments, the gold STM tip was coated with Apiezon wax and only tips which resulted in a very small leakage current < 5-10 pA were used. For measurements performed under argon an open STM cell was placed into a PicoAPEX Environmental Control chamber and the argon introduced using double lined rubber tubing. The system was purged for a minimum of two to three hours before experiments commenced and the flow of argon was monitored using a Dreschel bottle.

4.5.1DBE

4.5.2 *I*(*s*) Measurements

I(*s*) measurements were performed in air according to the description in Chapter 2. The histogram in Figure 4.5 a) is constructed from 100 *I*(*s*) scans, examples of which are found in Figure 4.5 b).

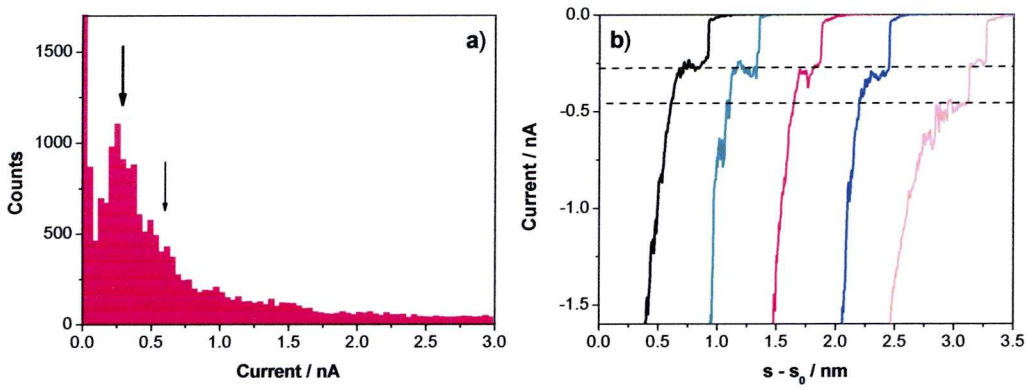

Figure 4.5. a) All current histogram for DBE at a bias voltage of 0.2 V, I_0 = 20 nA, b) *I*(*s*) scans used to construct the histogram.

The main peak seen in the histogram is the A_1 peak which gives a conductance of (1.39 ± 0.43) nS or (1.80 x 10^{-5}) G_0 at 0.2 V, the smaller A_2 peak attributed to two molecules in the junction can also be seen with a conductance of (2.79 ± 0.33) nS. The *I*(*s*) plateaus in b) are well defined with sharp break off points and only appear in the presence of adsorbed molecules. It can be immediately noted that this molecule, which has a backbone composed of nine atoms, has a higher conductance than nonanedithiol (0.49 nS).

The break off distance, $S_{1/2}$, was measured for all the plateaus displayed in the *I*(*s*) scans and used to construct the histogram shown in Figure 4.6. The average break off value was determined to be 0.705 nm and the initial tip-sample separation was calculated using the equation discussed in Chapter 2 and was found to be 0.712 nm. This gives a total distance of (1.42 ± 0.12) nm. The S-S distance calculated from SPARTAN® for the fully extended *all trans* molecule was 1.29 nm, so the two values are in reasonable agreement.

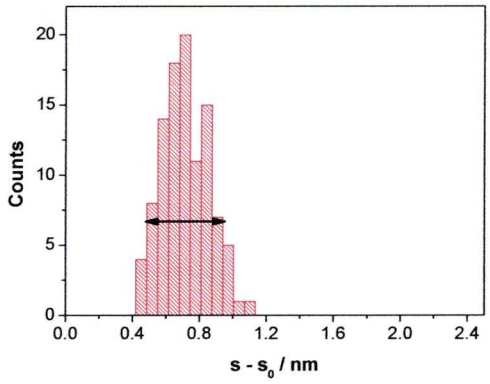

Figure 4.6. Average break off distances for DBE at 0.2 V, I_0 = 20 nA

Different set point currents

The set point current used in these experiments, 20 nA, is relatively high compared to the set point used in previous measurements of alkanedithiols. It has been shown that high set points used in *I*(*t*) measurements can lead to tilting of the molecule in the junction which can lead to increased current values[25]. As the *I*(*s*) method involves retraction of the tip from the surface the effect of the initial tip sample separation should be minimal. However, to ensure a consistent comparison conductance values, the *I*(*s*) measurements for this molecule were repeated using a smaller I_0 value of 5 nA and a large I_0 value of 60 nA. The results of these experiments are shown below in Figure 4.7.

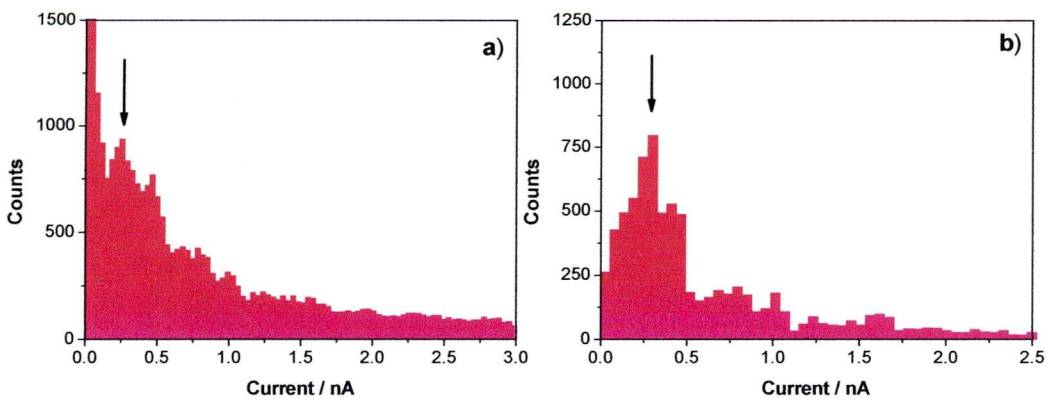

Figure 4.7. a) All current histogram for DBE at 0.2 V, I_0 = 5 nA, b) All plateau current histogram.

At a set point of 5 nA, the peak from the all current histogram in Figure 4.7 a) gives a conductance of around (1.27 ± 0.24) nS. The peak is slightly obscured however, so to resolve the peak, a histogram (Figure 4.7 b)) was constructed from just the plateau data to determine the value of the current through the molecule. This plateau only data allowed resolution of the peak and gave a conductance of (1.39 ± 0.59) nS, which is consistent with the data obtained at 20 nA.

The measurements carried out at high set point currents (Figure 4.8) are less straightforward. The main peak is split and complications arise when using such high set points, such as higher probabilities of contacting multiple molecules. Using the available data however, the conductance at 60 nA was calculated at (1.79 ± 0.44) nS which is slightly higher than the first two values but is within error limits.

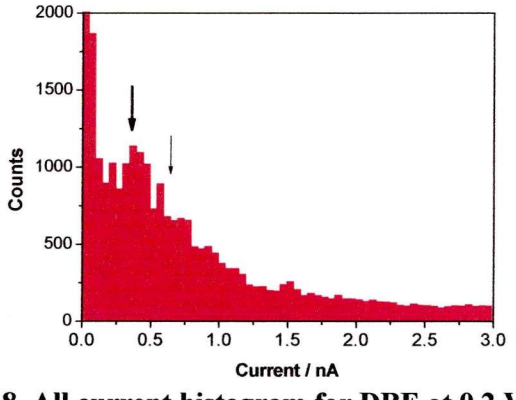

Figure 4.8. All current histogram for DBE at 0.2 V, I_0 = 60 nA.

4.5.3 Current – Voltage Data

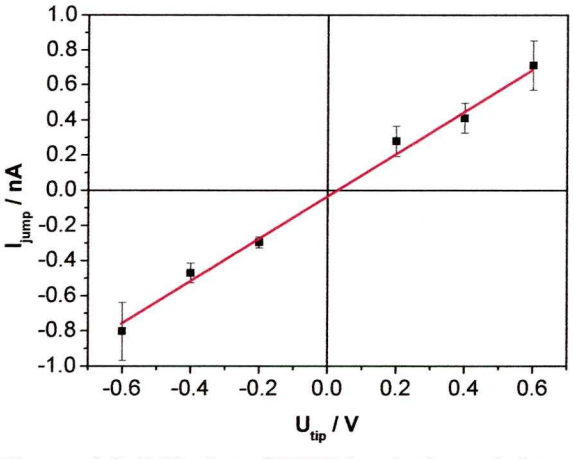

Figure 4.9. I-V plot of DBE in air from 0.6 to -0.6 V

All the current values obtained were plotted against the respective bias voltage to give the current-voltage relationship in Figure 4.9. The I-V plot is linear displaying no asymmetry as expected for the symmetrical molecule, indicating that the molecule has the same coupling strength at both tip and substrate. It gives an overall conductance of (1.20 ± 0.07) nS or (1.55 x 10^{-5}) G_0. The reported conductance of the nonanedithiol molecule using $I(s)$ and $I(t)$ techniques is (0.49 ± 0.08) nS[1] so the DBE molecule has a higher conductance by more than a factor of two.

4.5.4 Break Junction

Measurements were performed using the break junction technique as described in Chapter 2. The current data obtained at 0.2 V is shown below in Figure 4.10.

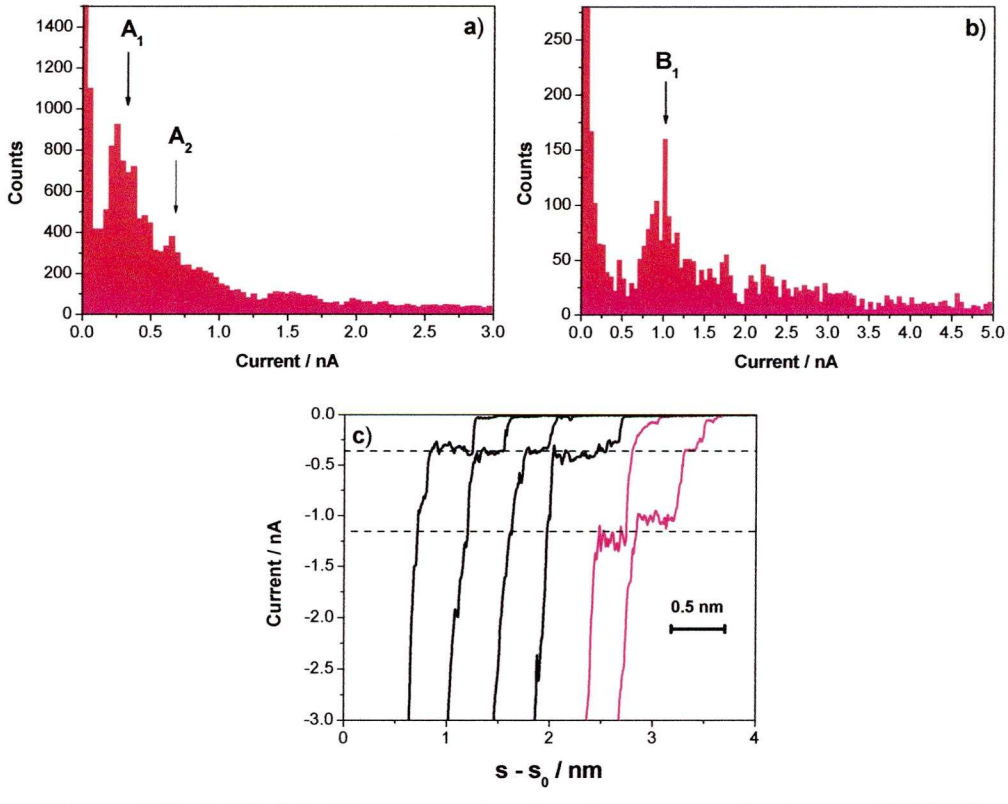

Figure 4.10 a) All data histogram showing A group conductance at 0.2V 20 nA in air b) B group conductance and c) Example $I(s)$ scans, A group (black), B group (red).

The conductance measured using the break junction technique is slightly higher that that obtained with the *I*(*s*) method at the same potential giving the A_1 group as (1.55 ± 0.40) nS or (2.0×10^{-5}) G_0 and an A_2 conductance of (3.27 ± 0.17) nS. The values are within error limits however. Using the BJ method is was also possible to observe B group events with a conductance of (5.14 ± 0.88) nS or (6.64×10^{-5}) G_0 as shown in Figure 4.10 b) both sets of current plateaus can be seen in Figure 4.10 c).

4.5.5 Monolayer measurements

Monolayer measurements were carried out according to the procedure described in Chapter 2. The initial set point current was increased systematically from 1 nA in increments of 0.5 nA until molecular-junction-forming events were observed. The results from these experiments are shown in Figure 4.11.

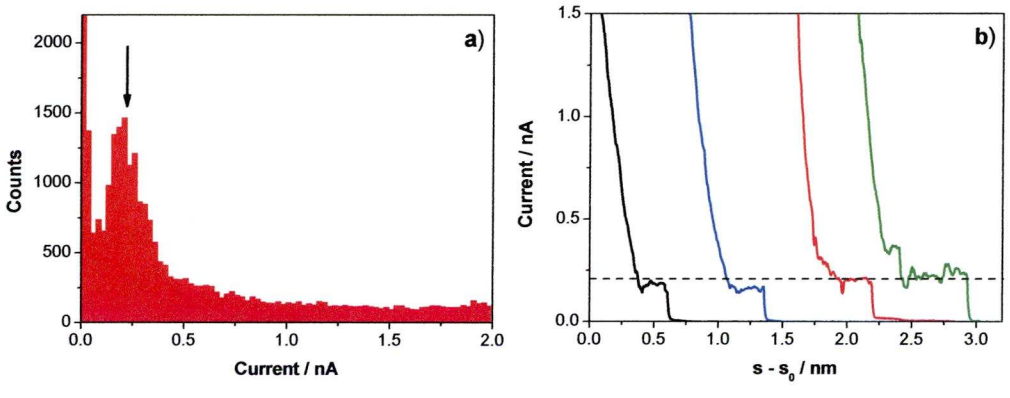

Figure 4.11. a) All data histogram from monolayer measurements at -0.2 V, I_0 = 2 nA, b) I(s) scans recorded for DBE

The monolayer measurements result in a conductance of (1.11 ± 0.28) nS at 0.2 V. This is lower than that calculated from the *I*(*s*) and break junction methods, however, the values are within error limits.

4.6 Environmental Results

4.6.1 Under Argon

Figure 4.12 a) shows the all data histogram of DBE under argon at 0.2 V with a set point of 20nA. The corresponding *I*(*s*) scans are shown in Figure 4.12 b). The scans obtained were often noisy as a result of mechanical tip vibrations due to the argon flow.

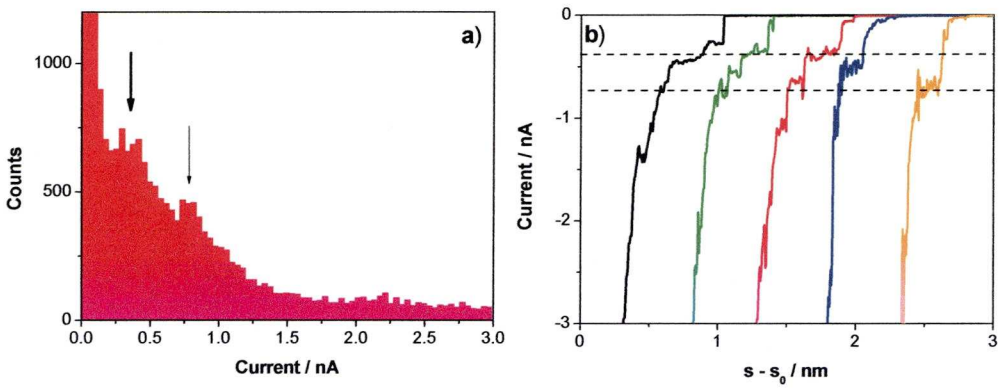

Figure 4.12.a) All data histogram of DBE under argon at 0.2 V, I_0 = 20 nA, b) example *I*(*s*) data.

The main conductance peak gives a value of (1.71 ± 0.39) nS, the second peak corresponds to the A_2 peak and gives a value of (3.88 ± 0.31) nS. Measurements were carried out over a range of potentials to give the current voltage plot shown in Figure 4.13.

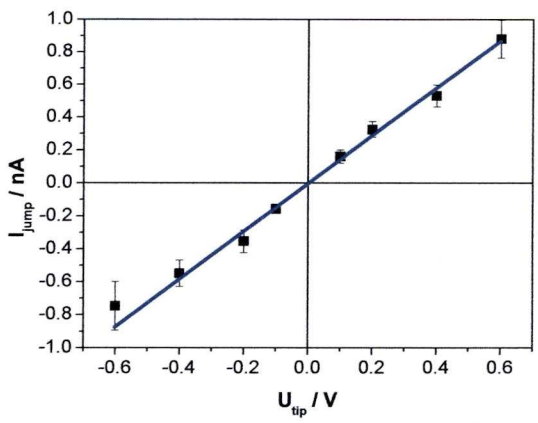

Figure 4.13. I-V relationship for DBE measurements performed under argon.

Again the relationship between the current and applied bias is linear for this range of voltages. The linear fit of the I-V plot gives an overall conductance under argon of (1.45 ± 0.06) nS or (1.87 x 10^{-5}) G_0, which is slightly higher for that recorded for the same molecule measured in air (1.20 ± 0.07) nS and the two value lie slightly also just outside of each others respective error bar limits.

4.6.2 Water Measurements

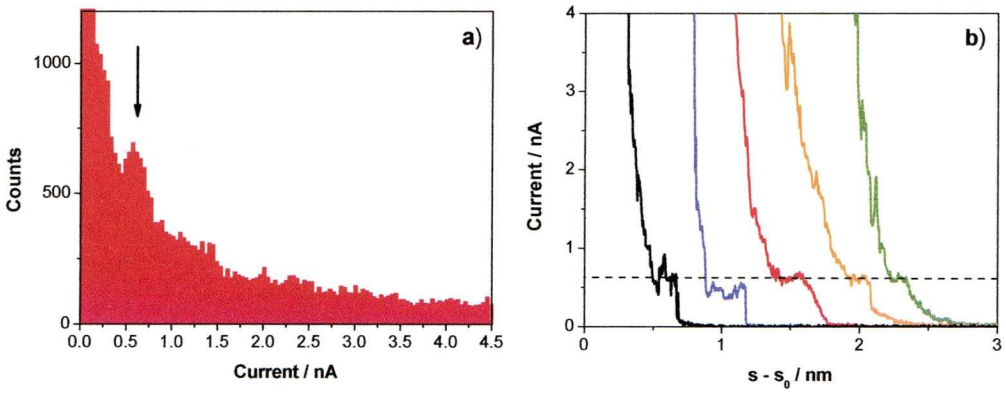

Figure 4.14. All current histogram for DBE in water environment at -0.2 V, I_0 = 10 nA, b) sample *I*(*s*) traces for the same conditions.

I(*s*) measurements performed in aqueous environments are less straightforward than in air or under inert gas. Fluctuations in the tunnelling current are produced by the water environment and leakage currents are often present if the tip is not adequately coated. Full data sets were obtained for the 0.6 to -0.6 bias voltage range, the results of which are shown in Figure 4.14. It can be observed in the *I*(*s*) scans shown in 4.14 b) that the current decays less abruptly upon detachment of the molecule from the tip. The calculated conductance for the DBE in water at -0.2 volts is (2.98 ± 0.51) nS.

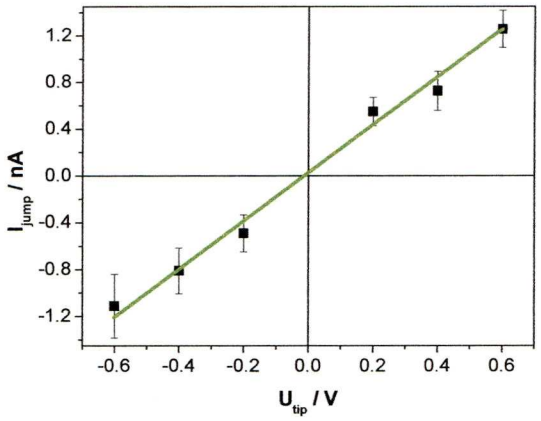

Figure 4.15. I-V plot with linear fitting for DBE measured in a water environment from 0.6 to -0.6 V.

The linear fit of the current voltage data (Figure 4.15) gives a conductance value of (2.05 ± 0.13) nS or (2.65 x 10^{-5}) G_0. This is significantly higher than the values obtained in both ambient and argon environments. The conductance in water is higher than in air by around 40%. A comparison of the measurements in all three environments is shown in Figure 4.16.

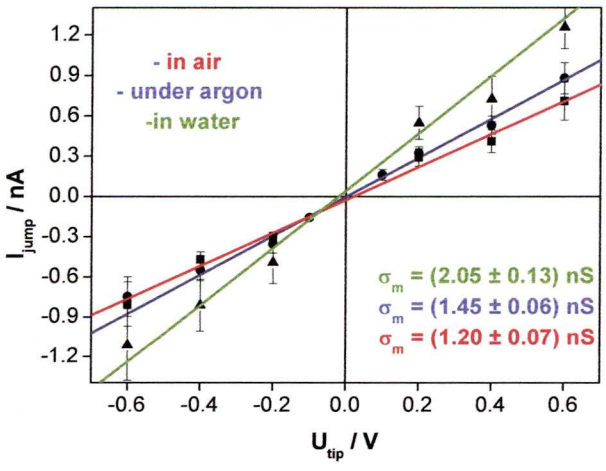

Figure 4.16. Comparison of *I*(*s*) measurements in different environments for DBE.

It is clear from the graph that in the water environment the molecular conductance significantly increases. It seems likely that this is due to hydrogen bonding effects between water and the lone pair of the ether oxygen. However, this conclusion has to be treated with caution since measurements in an inert environment led to an unexpected increase in conductance of around 17.3 % when compared to the conductance in air.

If indeed the presence of the water produces an increase in conductance, this is an unexpected result. Water is naturally present in the ambient environment and produces water films on the sample, so the conductance measured under argon would be expected to be lower than that in air. Clearly this is not the case here.

4.7 TEG Results

4.7.1 XPS

XPS was performed as described in Chapter 2 on both low and high coverage samples at take off angles of 10 and 90^0. A selection of the resulting spectra are shown below in Figure 4.17.

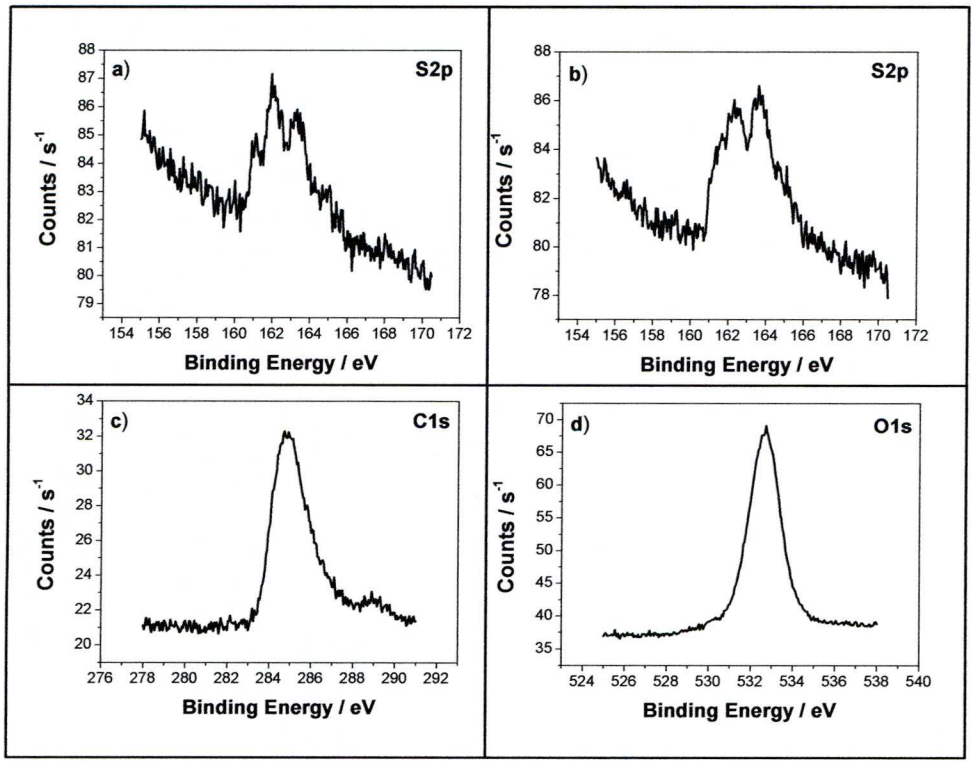

Figure 4.17. XPS spectra a) S2p low coverage 90^0 b) S2p high coverage 90^0, c) C1s low coverage 10^0 and d) O1s low coverage 10^0.

The spectrum in Figure 4.17 a) shows the S2p region for low coverage TEG. The peak for the S-Au bond at 162 eV is larger than that of unbound sulfur at 163.5 eV. Figure 17 b) shows the same region for the high coverage sample. Here, the ratio of the two peaks is almost 1:1 indicating that the molecules are standing upright with one terminal sulfur bound to the substrate and one at the top of the monolayer. The presence of the peaks at 162 eV in both spectra also confirm that deprotection of the thioacetate group is not necessary for covalent binding of the sulfur atom to the gold substrate. The final two spectra shown in Figure 4.17 c) and d) are the C1s and O1s regions of the low coverage sample taken at 10^0. The C1s spectrum shows a single peak at 284.85 eV which is in excellent agreement with reported C1s values of ethylene glycols on gold. Likewise the single peak in the O1s region at 532 eV corresponds to the glycol oxygens[26]. All the spectra, therefore, confirm the presence of the molecule on the substrate with the adsorption conditions used.

4.7.2 *I*(*s*) Results

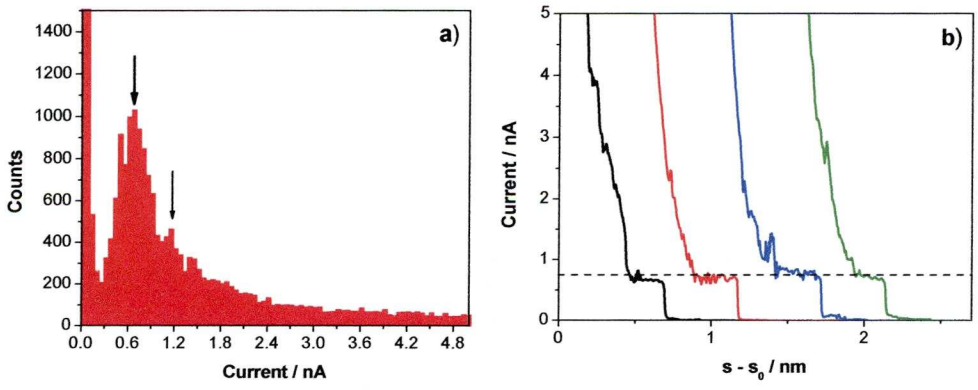

Figure 4.18. a) all data histogram for TEG at -0.2 V with I_0 = 20 nA

The *I*(*s*) results for TEG measured in air at -0.2 V are shown in Figure 4.18. The histogram peak compiled from over 100 scans in a) is well defined reflecting the high quality of *I*(*s*) traces as shown in Figure 18 b). The calculated conductance at this potential is (3.40 ± 0.61) nS or (4.39 x 10^{-5}) G_0 with a visible A_2 peak giving just under double the conductance

value at (5.84 ± 0.42) nS. The break off distance measurements were obtained in the same manner as DBE giving an overall break off value of 1.52 nm, which is slightly higher than the S-S distance calculated by SPARTAN® of 1.15 nm. This molecule however is significantly folded in molecular modelling simulations due to the C-O-C bond angles in the molecule. The longer, experimental break off distance therefore, can be rationalised by the extension of the molecule in the junction. Again it is immediately obvious that the conductance for this molecule is higher than its alkanedithiol analogue, octanedithiol, which has a conductance value of 0.99 nS when measured with either the *I*(*s*) or *I*(*t*) technique.

4.7.3 Current-Voltage Data

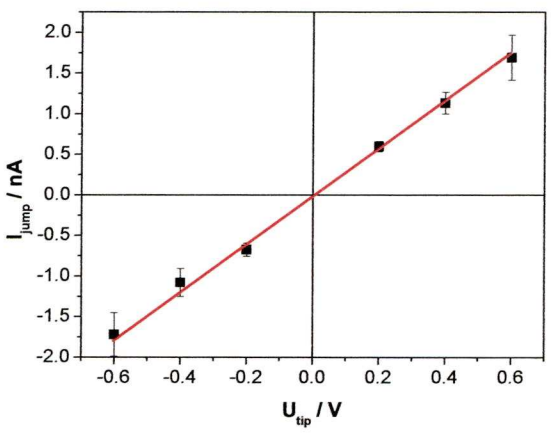

Figure 4.19. I-V plot with linear fitting for TEG in air.

The current-voltage plot for the TEG molecule is also linear in the 0.6 to -0.6 V region. The linear analysis gives a conductance value of (2.95 ± 0.10) nS or (3.81 x 10^{-5}) G_0.

4.7.4 Break Junction Experiments

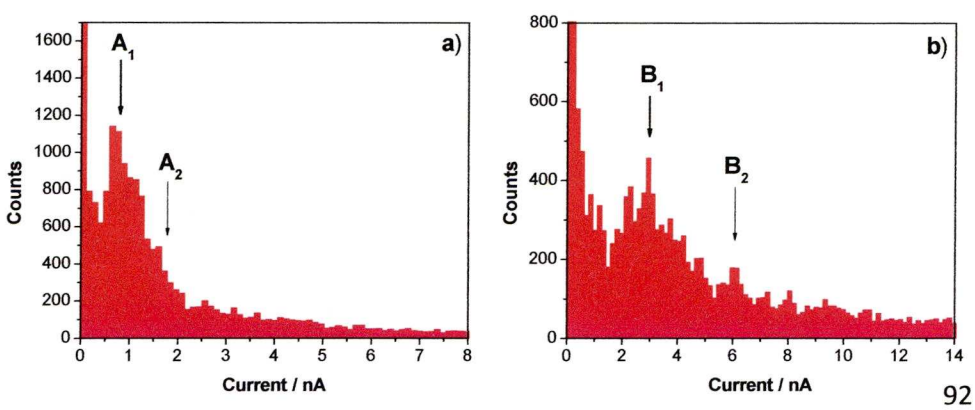

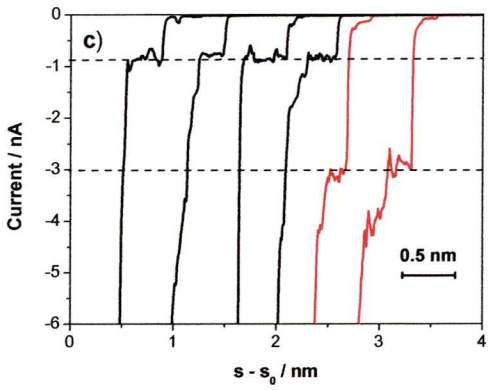

Figure 4.20 a) All data histogram to show break junction measurements in air, a group, at 0.2V, I_0 = 20nA b) b group histogram.

As shown in Figure 4.20 a) and b) the break junction experiments for this molecule were successful with both A and B groups events observed. The conductance value for the A_1 groups is calculated at (4.42 ± 1.16) nS or (5.71 x 10^{-5}) G_0 with an A_2 group conductance of (8.12 ± 0.54) nS. The higher B group conductance was calculated as (14.69 ± 3.67) nS or (1.90 x 10^{-4}) G_0 with B_2 equal to (30.11 ± 1.57) nS. These values are again higher than those obtained with the *I*(*s*) technique at this potential but are within error bar determinations.

4.7.5 Monolayer Measurements

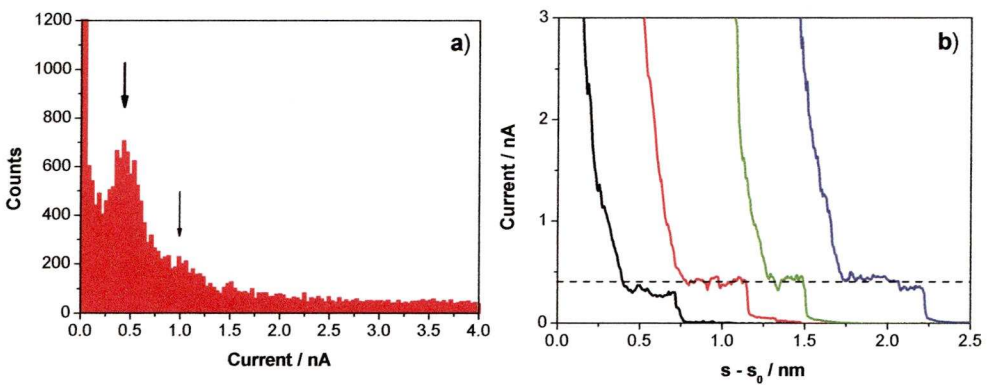

Figure 4.21. a) All current histogram for monolayer measurements of TEG, at -0.2 V, I_0 = 5 nA, b) Example *I*(*s*) scans.

Monolayer measurements were performed in the same way as for the DBE molecules. Molecular events were observed only when the initial set point

currents were increased to 5 nA, at which point the tip was around 0.8 nm from the surface. This value (0.8 nm) was obtained through use of the distance calibration equation. The average 'raw' break off distance recorded during these measurements was 0.65 nm. This gives a total distance of 1.45 nm which correlates well with the distances measured using the *I*(*s*) method and gives further confirmation that the molecule is extending during the measurements. As with the first molecule, this technique again results in a lower conductance value than the *I*(*s*) or break junction methods with a value of (2.22 ± 0.53) nS or (2.87 x 10^{-5}) G_0.

4.7.6 Under Argon

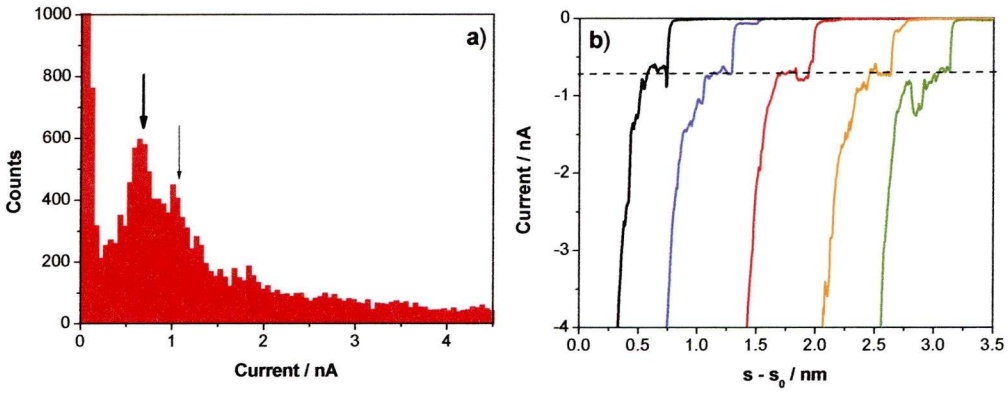

Figure 4.22. a) All data histogram for TEG under argon at 0.2 V, I_0 = 20 nA, b) Example *I*(*s*) scans.

Measurements under argon were performed on TEG at 0.2 V with a set point current of 20 nA. The main histogram peak gives a conductance value of (3.30 ± 0.63) nS or (4.26 x 10^{-5}) G_0. There is also a pronounced A_2 peak at just under double the current value giving a conductance of (5.26 ± 0.31) nS. The main conductance value is almost identical to the value measured by the *I*(*s*) method at the same potential, suggesting that there is no change in conductance for this molecule when measured in an inert environment. This is a surprising result considering that the single ether experiences a slight rise in conductance upon moving from ambient to inert gas environment. Unfortunately a full range of measurements

over the potential range was not obtained for this molecule. This means that we are unable to compare the I-V plots for the two systems.

4.7.7 Experiments in Water.

A full range of measurements was obtained for TEG in water environments. These are summarised in 4.23 a). Again the *I*(*s*) traces shown in Figure 4.23 b) show a gradual drop in current as the contact is broken between tip and molecule in water.

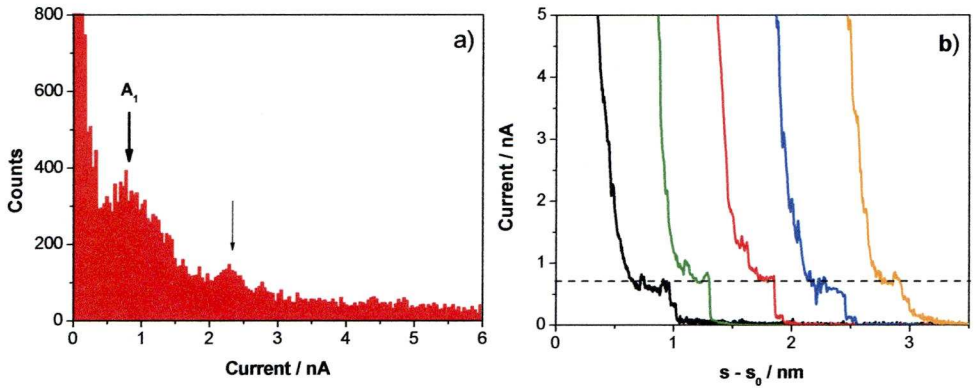

Figure 4.23 a). All current histogram for TEG in H_2O at -0.2 V, I_0 = 20 nA. b) Resulting I(s) scans.

The resultant peak is broad due to the high noise that can be associated with measurements performed in aqueous environments. This is reflected in the *I*(*s*) scans shown in b). The main peak is clear, however, giving a conductance value of (4.17 ± 1.21) nS or (5.39 x 10^{-5}) G_0. There is also a peak at (11.4 ± 0.78) nS which is too high to be the A_2 group and is more representative of A_3 events. Similar to the DBE measurements, the conductance found in a water environment is significantly higher than in ambient or inert gas environments. This can be graphically demonstrated by comparing the available I-V curves as shown in Figure 4.24. Here the conductance in water over the bias potential range 0.6 to -0.6 V is (3.72 ± 0.08) nS which is larger than the conductance in air by around 21%.

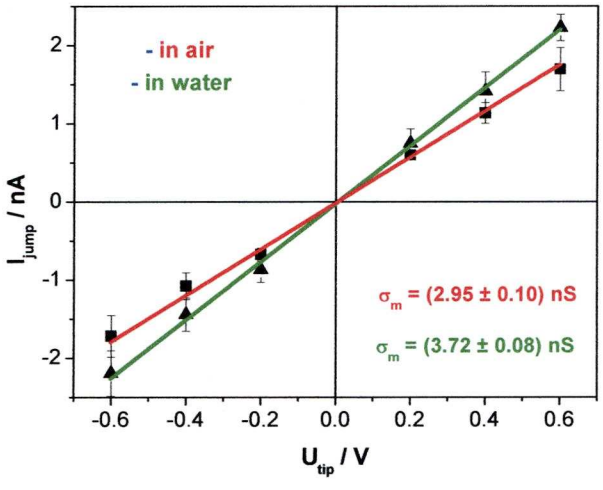

Figure 4.24. IV plots for TEG in air and in water from 0.6 to -0.6 V.

4.8 Thioether Results

STM measurements using the *I*(*s*) method were performed in air for DPTE over a range of bias potentials from -0.6 to 0.6 V. It was immediately obvious when carrying out these experiments that this molecule was difficult to measure. Although plateaus were observed, their frequency was low and both the current value of the plateau and the length of the plateau varied greatly so it was necessary to use very high set points in the order of 40 – 60 nA. However, a full set of data was obtained and Figure 4.25 a) shows the histogram obtained at -0.2V using a set point of 40nA. Figure 4.25 b) shows the corresponding break off lengths. For this particular data set, the break off length does not vary considerably, however the distance measurements for alternate potentials (not shown) showed a wide distribution. The S-S distance calculated by SPARTAN® is 0.957 nm and the C-S-C bond angle causes significant distortion of the molecule.

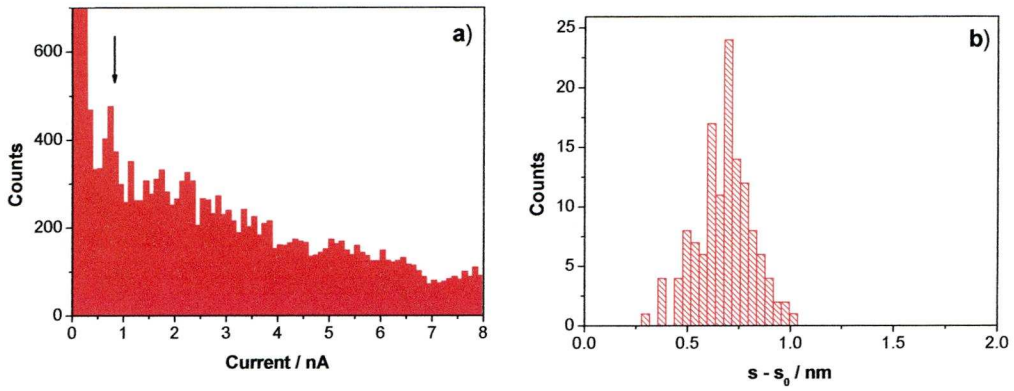

Figure 4.25. a) All current histogram for DPTE at -0.2 V, I_0 = 40 nA, b) break off distance distribution.

Over the six potentials measured, the histograms show no clear peak. Instead the peaks are broad with no clear apex or comprised of numerous smaller peaks as in Figure 4.25 a). At least one hundred scans were used to construct each histogram as explained in the description of the "data selection process" earlier. As Figure 4.26 a) shows, the *I*(*s*) scans obtained exhibit clear plateaus, indicating that the STM tip is indeed picking up the molecule. The measurements were performed again with no data selection to see if the selection process had affected the outcome. The resulting graphs (not shown here) constructed from one thousand *I*(*s*) scans showed no discernable current peak and examination of the "plateau-only" data showed only a handful of current jumps, highlighting the difficulty encountered when an additional sulfur atom is incorporated into the polymethylene chain.

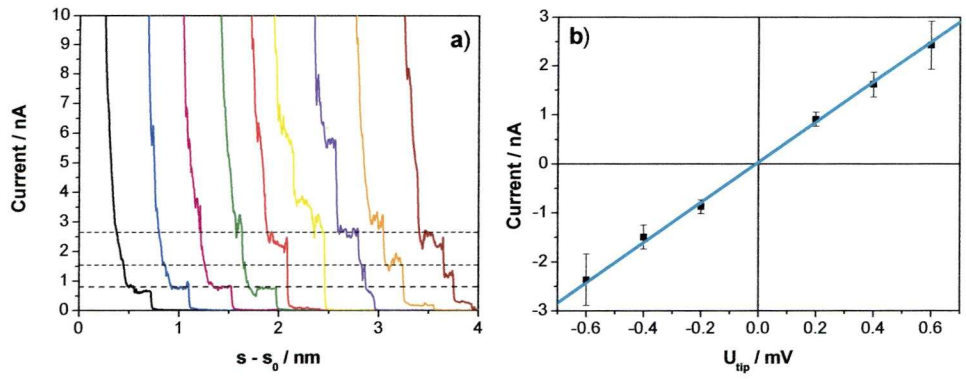

Figure 4.26. a) Example I(s) curves taken at -0.2V, I_0 = 40nA, b) IV plot for DPTE form 0.6 to -0.6 V.

A tentative I-V plot was constructed from the available data using the lowest identifiable current peak and is shown in Figure 4.26 b). It suggests that the conductance of the molecule is around (4.10 ± 0.29) nS or (5.3 x 10^{-5}) G_0. As demonstrated in Chapter 3, the measured conductance of the alkane analogue of this molecule is 1.42 nS. Based on the poor quality of data, no definite conclusions can be drawn, however, it is reasonable to conclude that the sulfur bridge results in a higher molecular conductance.

4.9 Measurements at High Potentials.

In order to fit the I-V data for these molecules using the Simmons model described in Chapter 3, the voltage range for measurements was increased to 1.2 to -1.2 V. This is because in the range 0.6 to -0.6 the I-V plots are linear and Simmons fitting to this data results in unrealistic fitting parameters. Measurements at such high potentials encounter difficulties, as when the bias is increased the plateaus in the *I*(*s*) scans become increasingly noisy because of current induced instability. Full sets of measurements for ± 0.8, 1.0 and 1.2 V were obtained for each of the ether molecules. The thioether was not included in the rest of the study due to the difficulties outlined earlier in forming convincing molecular junctions. Figure 4.27 below shows two examples of the high potential histograms obtained for DBE, each constructed from around 120 *I*(*s*) scans.

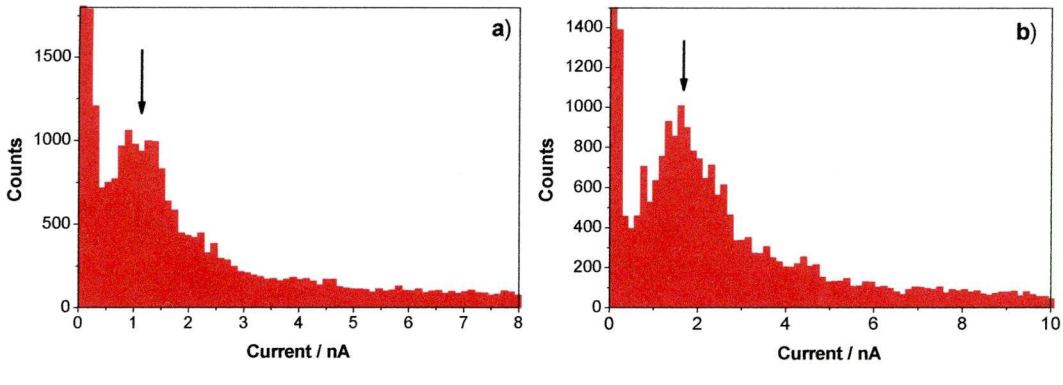

Figure 4.27. All current histograms for DBE, a) -0.8 V, I_0 = 20 nA, b) -1.0 V, I_0 = 20 nA.

4.9.1 Simmons Model.

The main current peak in the histograms in Figure 4.27 a) and b) give conductance values of (1.37 ± 0.33) nS and (1.67 ± 0.53) nS respectively. All the current values were then compiled to form an I-V curve from 1.2 to -1.2 V. Using the modified Simmons equation with d = 1.5 nm for the through bond length as calculated by SPARTAN® and A = 0.217 nm^2 as the molecule is assumed to occupy an area similar to that of equivalent alkanedithiols, the Simmons equation was applied to determine the barrier height and α values which best describe the voltage dependence of the measured currents. The resulting fit is shown in Figure 4.28.

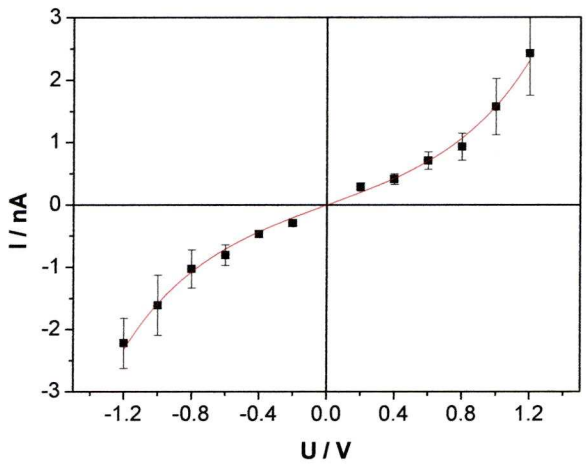

Figure 28. I-V curve for DBE from 1.2 to -1.2 V fitted using the Simmons model.

The Simmons model fitting of the I-V data results in a barrier height ϕ of 0.94 eV with an α value of 0.50. This α value is similar to that determined for ODT previously (0.53), again indicating that the charge transport through the molecule predominately involves the HOMOs. Although the DBE molecule has an extra atom in length, it still has just eight carbons and has a lower overall barrier height than for octanedithiol which is reflected in its higher conductance of around 20 %.

4.9.2 TEG Results

High potential measurements for the TEG molecule proved less straightforward. Figure 4.29 shows several of the histograms produced for TEG at 0.8 V and 1.2 V. The current peaks in these histograms are extremely broad. In particular the peak at 1.2 V ranges in current values from 1.5 to 5.6 nA.

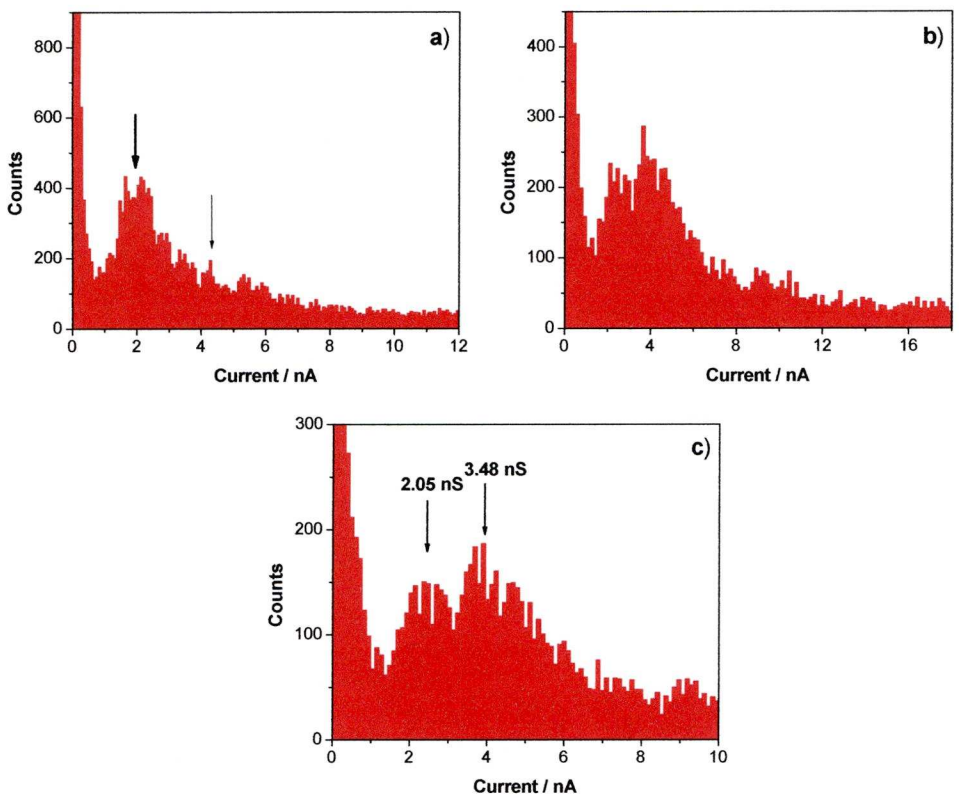

Figure 4.29 a) -0.8, I_0 = 20 nA, b) 1.2 V, I_0 = 40 nA c) enlargement of main peak at 1.2 V, I_0 = 40 nA.

In Figure 4.29 b) two peaks are visible, one at (2.05) nS and the second at (3.48) nS. The *I*(*s*) measurements at -0.2 V for this molecule gave a conductance value of (3.40 ± 0.61) nS which closer in value to the second peak. However, both 1.2 and -1.2 V histograms have a very broad peak which upon closer inspection can possibly be resolved into two peaks. To investigate further, *I*(*t*) measurements were performed at these high potentials. As already stated, it has been observed that the *I*(*t*) technique has a propensity to record only the lowest conductance, i.e. the A_1 conductance group. The results for these *I*(*t*) measurements are shown below in Figure 4.30.

4.9.3 *I*(*t*) results

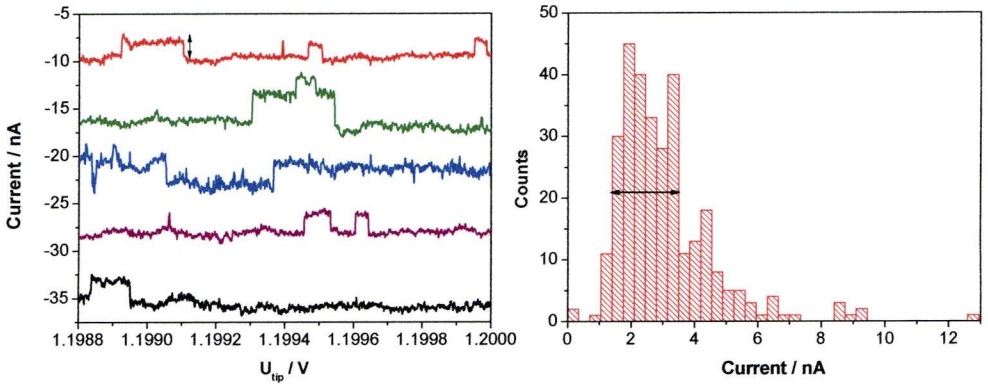

Figure 4.30. Example of *I*(*t*) scans taken at 1.2 V for TEG, I_0 = 40nA in air b) resulting hand analysed histogram at 1.2 V.

There is a clear peak in the *I*(*t*) histogram which corresponds to a conductance of (2.04 ± 0.51) nS. This indicates that the previous *I*(*s*) histogram does indeed contain two unresolved peaks. This can arise from using high set point currents, as the closer the tip is to the surface, the higher the probability for picking up multiple molecules.

In the same way as for the DBE, an I-V plot was constructed from all the current values in the bias voltage range 1.2 to -1.2 V (Figure 4.31). It is immediately clear from the I-V curve that this molecule has a different current voltage relationship to that of DBE.

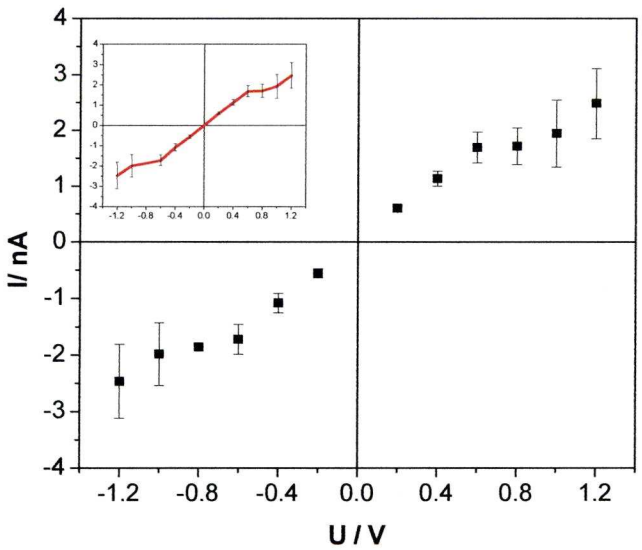

Figure 4.31. Current – voltage curve for TEG between 1.2 and -1.2 V.

Fit to point line to highlight plateau regions in the current- voltage curve (inset).

The curve is not sigmoidal in nature; instead the current appears to plateau at around 0.6 – 0.9 V before increasing again at 1 V (inset). This voltage dependence cannot be fitted with the Simmons model with any parameters and suggests a more complicated charge transfer mechanism than the DBE molecule.

4.10 Density Functional Calculations

Calculation of the MOs for both molecules with one gold atom attached to both terminal sulfurs was carried out using the SPARTAN® DFT calculations in a similar manner to that employed for ODT described in the previous chapter.

4.10.1 DBE

The first six LUMO orbitals for DBE are shown below in Figure 4.32.

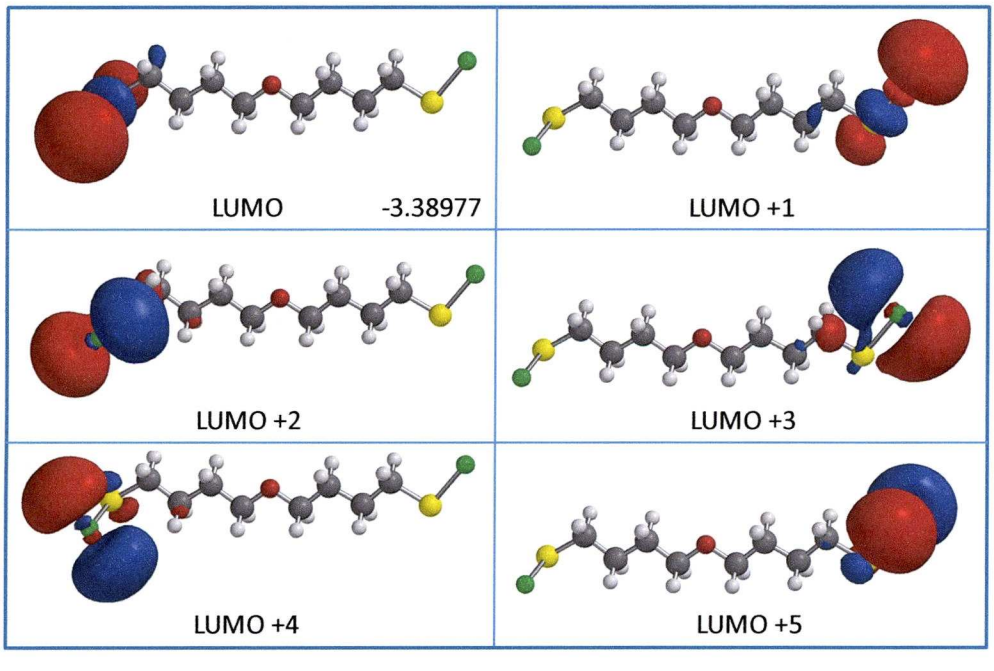

Figure 4.32 Density of the first six LUMO orbitals of DBE in eV

Examination of the energetic position of the molecular orbitals show that similar to the alkanedithiols, the LUMOs are located at the contacts and are not involved in charge transport. This was also found to be the case

for the LUMO energies of TEG indicating hole transport as the main electron transfer mechanism.

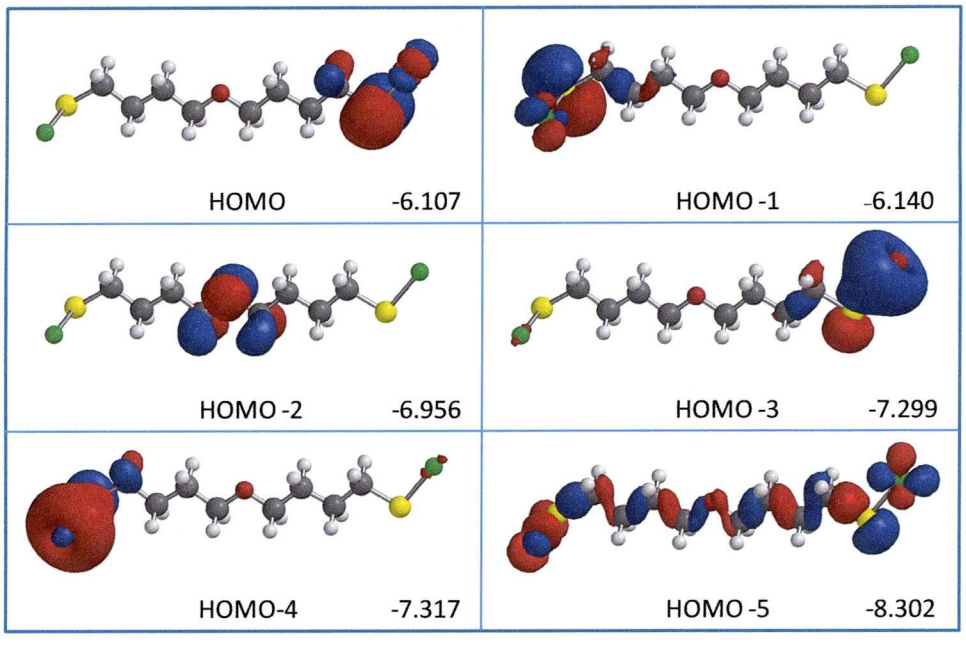

Figure 4.33 Density of the first six HOMO orbitals of DBE in eV

Figure 4.33 shows the positions of the first six HOMO orbitals for DBE. The HOMO and the HOMO -1 are almost degenerate, appearing at -6.107 and -6.139 eV respectively. The same can be seen for the HOMO -3 and HOMO -4 orbitals which do not contribute to conduction through the molecule. The lowest energy HOMO orbital that spans the whole of the molecule is the HOMO – 5, which appears at an energy of 8.30 eV giving an estimated barrier height of 3.1 eV which can be corrected with the image charge correction equation.

$$\phi_i = \phi_0 - \frac{2\phi_0 c}{\Delta s} ln\left(\frac{s_0+\Delta s}{s_0-\Delta s}\right) \qquad (1)$$

After the image charge correction, the barrier height is 2.43 eV. This value is comparable to the values of the frontier orbital calculated using the same SPARTAN® DFT in nonanedithiol which is located at 2.86 eV from the gold Fermi level as shown in Figure 4.34.

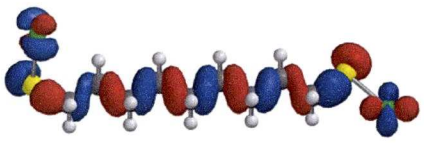

8.06 eV

Figure 4.34. Frontier orbital of nonanedithiol calculated using SPARTAN®.

With the image charge correction this value then corresponds to 2.22 eV. If this HOMO -5 orbital in DBE was solely responsible for the conductance through the DBE molecule then a conductance value similar to NDT would be expected. However, the lower lying HOMO -2 orbital which appears at -6.95 eV in Figure 4.33 shows the orbital density located in the middle of the molecule directly over the oxygen atom. This suggests that this HOMO -2 orbital is acting as a barrier indentation or well as shown in Figure 4.35. As no well is present in alkanedithiol molecules this may account for the higher conductance measured for DBE as the well provides a hopping site. If this is the case then this would also account for the discrepancy in the barrier height calculated from the Simmons model (0.94 eV) and the molecular orbital calculations (2.43 eV) as the Simmons model assumes tunnelling through a square potential barrier as opposed to a double barrier system.

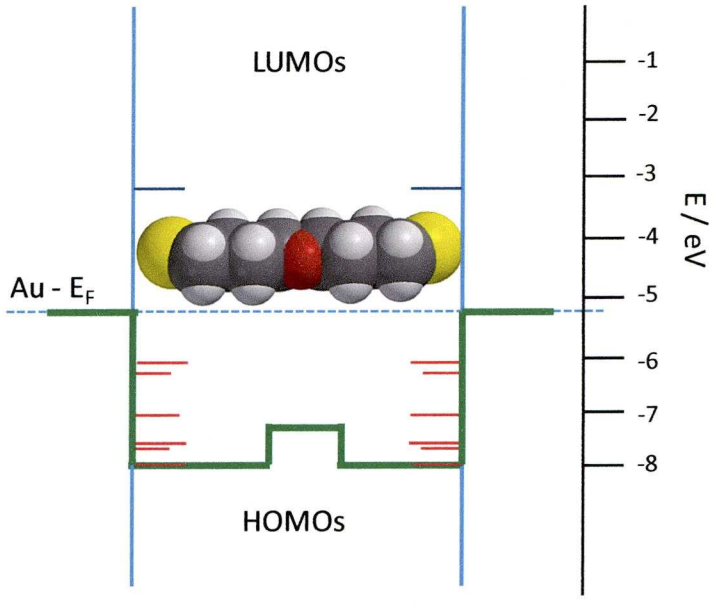

Figure 4.35. Energy level model for charge transport through a double tunnelling barrier with E_F = 5.2 eV.

4.10.2 TEG

The DFT SPARTAN® calculations were also performed on TEG to determine the energetic position of the MOs to investigate the orbitals involved in the unusual voltage dependent charge transport through this molecule. The DFT results are shown below in Figure 4.36.

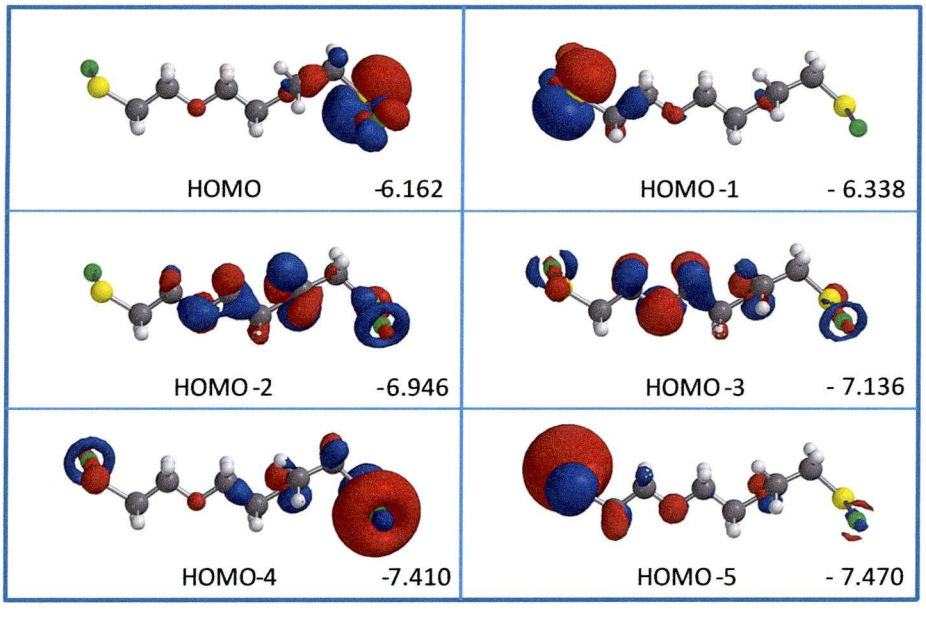

Figure 4.36. Density of the first six HOMO orbitals of TEG in eV

The orbital responsible for charge transport appears to be the HOMO-2 and HOMO -3 levels where the orbital density is located on both oxygen atoms and at the gold sulfur contact. The HOMO -2 appears at a very similar energy to the DBE HOMO -2 level. Unlike the DBE molecule, the density of this orbital is not exclusively located at the oxygen atoms suggesting a double tunnelling barrier model is not applicable here. This HOMO -2 level is 1.75 eV from the gold Fermi energy and using the image charge correction equation gives a corrected barrier height of 1.31 eV which is slightly less than the equivalent alkanedithiol ODT corrected barrier height of 1.36 eV obtained using the same DFT calculations[24]. This DFT model therefore, does not account for the large increase in conductance upon the introduction of the two oxygen atoms even though TEG and ODT are comparable in length and their through bond distances are very similar. Although in its normal conformation the TEG molecule is twisted due to the restricted bond angles of the C-O-C bond, the previously described distance results indicate that it is fully extended during the measurements. A possible explanation could be that in the case of the TEG the charge transfer does not proceed via through bond tunnelling although there is no alternative explanation at present.

4.11 Discussion

The introduction of oxygen atoms into a simple methylene chain clearly increases the conductance of the molecule as shown by a variety of different techniques to measure single molecule conductance. In the case of DBE, as suggested by Sinniah *et al*[7], the introduction of oxygen disrupts the near degeneracy of the CH_2 orbitals resulting in an indentation of the tunnelling barrier height at the HOMO-2 level. In the case of the alkanedithiols, the conductance is dominated by occupied orbitals, however, in the case of DBE the HOMO -2 orbital is closer to the gold Fermi level due to the lone pair character of the oxygen heteroatom. The

observed higher conductance of this molecule may therefore be attributed to this tunneling barrier indentation.

For the TEG molecule, examination of the molecular orbital energies does not present an immediate reason for the observed conductance increase as the frontier orbitals appear at similar levels to those of its alkane analogue. Additionally the projected orbital densities give no indication of any tunnelling barrier indentations. The I-V data collected for this molecule showed unusual voltage dependence where the current leveled-off at high potentials 0.6-0.9 V before increasing again at 1 V. This does not match the sigmoidal, rectification or NDR behaviour discussed previously, however the molecule clearly does not fit a single barrier model. The symmetry of the I-V plot indicates that this behaviour is not due to erroneous results as the current measured at ± 0.6-1.2 V is the same despite the difficulties associated with measurements performed at high bias voltage.

Both ether molecules exhibit an increase in conductance in an aqueous environment, a behaviour which is not observed for the alkanedithiols that may be attributed to the hydrogen bonding capabilities of the ether oxygens. The conductance data resulting from measurements performed under argon suggest that the conductance increase is sensitive to the amount of water present. Normally ambient environments contain a certain amount of water and possible contaminates, however, no large change in conductance was observed until measurements were made under liquid water as opposed to ambient environments.

Electrical data recorded with monolayer films (high surface coverage samples) produced consistently lower conductance values than any of the other techniques. It has been proposed that the nature of the binding of sulfur on gold changes with increasing coverage, with more S-S dimers being present as monolayer coverage is reached.[27] This suggests that the relative strength of the Au-S bonds on the high coverage surfaces is different to that of the molecules adsorbed in a low coverage phase which may be a contributing factor to the observed lower conductance as weakened Au-S bonds may result in a reduction in transmission at the Au-S bond. In addition, intermolecular hydrogen bonding throughout the

monolayer may also influence the measured conductance. However, in the absence of high level ab-initio computations it is not possible to reliability predict such effects.

Clearly electron transport mechanisms are difficult to determine experimentally for these molecules. For the DBE, synthesis and electrical measurements of additional molecules with varying numbers of polymethylene groups either side of the central oxygen would provide a clearer picture of the orbitals involved in the electron transfer process for these molecules. Studying a homologous series of these molecules would enable a length dependence of the electrical conductance to be determined, which by analogy to alkanedithiols may also give an insight into the electron transfer process. The thioether molecule may be a good candidate for matrix isolation measurements; the single molecule techniques used here do not produce a reliable conductance value as the central sulfur can bind strongly to the gold substrate inhibiting the formation of defined molecular bridges. As discussed in Chapter 1, in matrix isolation methods it appears that molecules adsorbs into defect sites or on step edges in insulating matrices. They generally adsorb in upright positions, thus helping to eliminate the problem of multiple adsorption sites encountered during measurement of the DPTE on the gold substrate. The thioacetate groups on each end of the molecule would provide an excellent terminal point with which to bind to gold nanoparticles.

4.12 Conclusions

$I(s)$ and $I(t)$ techniques have been used to determine the single molecule conductance of three molecules composed of polymethylene groups with central atom substitutions. The first two molecules, DBE and TEG contain one and two oxygen atoms respectively. The conductance of DBE in ambient conditions was determined to be (1.20 ± 0.07) nS which is higher than that of its alkane analogue. The conductance of TEG under the same conditions was determined to be (2.95 ± 0.10) nS which again is higher than that of its respective alkanedithiol. Alternative break junction and monolayers techniques were then employed to verify the conductance

measurements presented. The conductance found in a water environment for both DBE and TEG was significantly higher than that found in ambient or inert environments. Simmons model fitting was applied to the I-V plots of both molecules, the DBE I-V data resulted in a barrier height of 0.94 eV. The I-V data for TEG exhibited unusual behavior and could not be fitted with this model. SPARTAN® DFT calculations were performed on DBE and TEG, the results of which indicated a double tunneling barrier system for DBE, however, these calculation could not provide an explanation for the enhanced conductance values of TEG. The single molecule conductance of DPTE proved difficult to measure although results obtained using the *I*(*s*) technique indicate a conductance value of (4.10 ± 0.29) nS.

4. 13 Syntheses

All chemicals were purchased from Sigma Aldrich and used as received.

4.13.1 1-chloro-4-(4-chlorobutoxy)butane

This was prepared by a modification of the method of Alexander *et al* [28] THF (72.1 g, 1mol) and $POCl_3$ (76.7 g, 0.5 mol) were combined and refluxed under N_2 for 9 hours. The mixture was cooled to 0 °C and water (30 cm3) was added. The resulting mixture was extracted with diethyl ether (30 cm3), the organic layer was dried, ether was evaporated and the residue was fractionally distilled (B. Pt. 153 °C/0.2 mmHg). Yield 141.4 g, 71 %. Mass spec (CI: NH_3) 216, 218 $[M+NH_4]^+$. ^1H NMR ($CDCl_3$) δ 3.56 (t, 4H, 6.2 Hz) 3.44 (t, 4H, 6.2 Hz), 1.87 (m, 4H), 1.70 (m, 4H). $^{13}C\{^1H\}$ NMR ($CDCl_3$) δ 70.27, 45.27, 29.85, 27.40.

4.13.2 *S,S'*-(oxybis(butane-4,1-diyl))diethanethioate

To 1-chloro-4-(4-chlorobutoxy)butane (1.4 g, 7 mmol) was added KSAc (2 g, 17.6 mmol) and a catalytic amount of NaI (0.11g) in acetone (25 cm^3) under nitrogen. The mixture was refluxed for 48 hours, extracted with water and ethyl acetate and dried. Purification by column

chromatography (hexane/CH_2Cl_2 9/1) gave the final product. Mass spec (CI: NH_3) 279 $[M+H]^+$ (48); 296 $[M+NH_4]^+$ (100). ^1H NMR ($CDCl_3$) δ 3.40 (m, 4H) 2.90 (m, 4H), 2.32 (s, 6H), 1. 65 (m, 8H). ^{13}C NMR ($CDCl_3$) δ 196.16, 70.55, 30.96, 29.30, 29.20, 26.76. The NMR and Mass Spectrometry data can be found in Appendix 3.

4.13.3. *S,S'*-((methylenebis(oxy))bis(ethane-2,1-diyl)) diethanethioate

Tri(ethylene glycol) di-*p*-toluenesulfonate (0.5 g, 1.2 mmol) was treated with KSAc (0.688 g, 6 mmol) and a catalytic amount of NaI (0.016 g) in acetone (30 cm^3) under nitrogen and the mixture was refluxed for 24 hours. The addition of water was followed by extraction with ethyl acetate. The product was then dried and placed under high vacuum to give the tri(ethylene glycol)dithioacetate without further purification. Mass spec (CI: NH_3) 267 $[M+H]^+$ (23); 284 $[M+NH_4]^+$ (100). ^1H NMR ($CDCl_3$) δ 3.61 (s, 4H), 3.60 (t, 4H, 6.4 Hz), 3.10 (t, 4H, 6.4 Hz) 2.34 (s, 6H). ^{13}C NMR ($CDCl_3$) δ 196.0, 70.6, 70.2, 31.0, 29.2. The NMR and Mass Spectrometry data can be found in Appendix 4.

References

1. Haiss, W.; Nichols, R.; Zalinge, H. V.; Higgins, S. J.; Bethell, D.; Schiffrin, D.J. *Phys. Chem. Chem. Phys*, **6**, 4330-4337. (2004).
2. Haiss, W.: Albrecht, T.: van Zalinge, H.: Higgins, S. J.: Bethell, D.: Höbenreich, H.: Schiffrin, D. J.: Nichols, R. J.: Kuznetsov, A. M.: Zhang, J.: Chi, Q.: Ulstrup, J. *J. Phys. Chem. B*, **111**, 6703-6712. (2007)
3. Cheng, J.; Saghi-Szabo, G.; Tossell, J and Miller, C. *J. Am. Chem. Soc*, **118**, 680-684. (1996).
4. Napper, A. M.; Liu, H and Waldeck, D. H. *J. Phys. Chem. B*, **105**, 7699-7707. (2001).
5. Sek, S.; Palys, B and Bilewicz, R. *J. Phys. Chem, B*, **106**, 5907-5914. (2002).
6. Sek, S.; Swiatek, K.; Misicka, A. *J. Phys. Chem. B,* **109** (49), 23121-23124. (2005).
7. Sinniah, K.; Cheng, J.; Terrettaz, S.; Reutt-Robey, J and Miller, C. *J. Phys. Chem*, **99**, 14500-14505. (1995).
8. Kethley, T.; Fincher, E and Cown, W. B. *Applied Microbiology*, **4**, 237-243. (1956).
9. Puck, T. *Journal of Experimental Medicine* 729-739. (1947).
10. Rudnick, S.; McDevitt, J.; First, M and Spengler, J. *Am. J. Infec. Control.* **37** (10), 813-819. (2009).
11. Zurigat, Y.; Abu-Arabi, M and Abdul-Wahab, S. *Energy Conversion and Management*. **45** (1), 141-155. (2004).
12. Pengo, P.; Pasquato, L and Scrimin, P. *Journal of Supramolecular Chemistry*, **2**, 305-310. (2002).
13. Cerruti, M.; Fissolo, S.; Carraro, C.; Ricciard, C, Majumdar, A and Maboudian R. *Langmuir*, **24**, 10646-10653. (2008).
14. Dicke, C and Hahner, G. *J. Am. Chem. Soc*, **124**, 12619-12625. (2002).
15. Hodneland, C and Mrksich, M. *J. Am. Chem. Soc*, **122**, 4235-4236. (2000).

16. Leary, E.; Hobenreich, H.; van Zalinge, H.; Haiss, W.; Nichols, R. J.; Finch, C. M.; Grace, I.; Lambert, C. J.; McGrath, R and Smerdon, J. *Phys. Rev. Lett*, **102**, 086801. (2009).
17. Xu, B.; Li, X.; Xiao, X.; Sakaguchi and Tao, N. *Nano Lett*, **5** (7), 1491-1495. (2005).
18. Haiss, W.; van Zalinge, H.; Higgins, S. J.; Bethell, D.; Hobenreich, H.; Schiffrin, D. J and Nichols, R. J. *J. Am. Chem. Soc*, 15294-15295. (2003).
19. Haiss, W.; Nichols, R. J.; Higgins, S. J.; Bethell, D.; Hobenreich, H and Schiffrin, D. J. *Faraday. Discuss*, **125**, 179-194. (2004).
20. Leary, E.; Higgins, S. J.; Van Zalinge, H.; Haiss, W and Nichols, R. J. *Chem. Commun*, 3939-3941 (2007).
21. Long, D. P.; Lazorcik, J. L.; Mantooth, B. A.; Moore, M. H.; Ratner, M. A.; Troisi, A.; Yao, Y.; Ciszek, J. W.; Tour, J. M and Shashidhar, R. *Nature Materials*, **5**, 901-908. (2006).
22. Xiulan, Li.; He, J.; Hihath, J.; Xu, B.; Lindsay, S. M and Tao, N. *J. Am. Chem. Soc*, **128**, 2135-2141. (2006).
23. Nichols, R. J.; Haiss, W.; Higgins, S. J.; Leary, E.; Martin, S and Bethell, D. *Phys. Chem. Chem. Phys*. **12**, 2801-2815. (2010).
24. Haiss, W.; Martin, S.; Scullion, L. E.; Bouffier, L.; Higgins, S. J and Nichols, R. J. *Phys. Chem. Chem. Phys*, **11**(46), 10831-10838. (2009).
25. Haiss, W.; Wang, C.; Grace, I.; Batsanov, A.; Schiffrin, D. J.; Higgins, S. J.; Bryce, M. R.; Lambert, C. J and Nichols, R. J. *Nature Materials*, **5**, 995-1002. (2006).
26. Zharnikov, M. *J. Electr. Spec. Rel. Phenom*, **178-179**, 380-393. (2010).
27. Rodriguez, J.; Dvorak, J.; Jirsak, T.; Liu, G.; Hrbek, J.; Aray, Y and Gonzalez, C. *J. Am. Chem. Soc*, **125**, 276-285. (2003).
28. Alexander, K and Schniepp, L. E. *J. Am. Chem. Soc*, **70** (5), 1839-1842. (1948).

Chapter 5. Peptides

5.1 Introduction

Peptides are the building blocks of proteins and peptide sequences are polymers of α-amino acids. Peptide sequences containing over fifty amino acid residues are classed as polypeptides while those containing more than one hundred residues are proteins. Amino acids contain amine (NH_2) and carboxyl (COOH) functional groups and there are 20 primary amino acids that are coded for by DNA in addition to several essential amino acids which cannot be made by the body and must, therefore, be supplied by other means. Amino acids are characterised by the nature of the side group, R (Figure 5.1), which ranges from a simple hydrogen in glycine to more complex groups such as the imidazole ring of histidine and the aromatic rings of tyrosine and tryptophan. Amino acids can be broadly categorised into hydrophilic and hydrophobic residues depending on the structure of their side chain and the molecules with the exception of glycine are all chiral.[1,2] Careful selection of amino acid sequences results in numerous secondary structures, the most common of which are the α-helix and the β-sheet, [3,4] also formed in less abundance are 3_{10} helices [1,5]

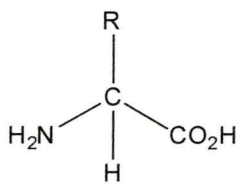

Figure 5.1. Illustration of generic amino acid structure.

Individual residues are joined by planar, covalent peptide bonds. The bonds are formed through a condensation reaction that joins the carboxyl group of one residue to the amino group of another and different sequence combinations possible are vast. Synthetic peptide sequences are generally synthesised from the C-terminus and sequences are conventionally written

with the N-terminus on the left and the C-terminus on the right, an illustration of which is shown in Figure 5.2.

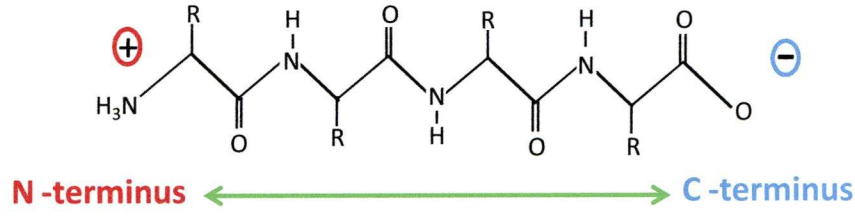

Figure 5.2. Illustration of a short peptide sequence with C- and N-terminals.

It is important to study the conductance of single peptide molecules, particularly those of α-helices and β-sheets as they are responsible for the mediation and control of electron transfer in proteins.[6-8] Calculated decay constants for helical peptides have been reported as 0.5 to 0.7 $Å^{-1}$ [7,9,10] which are smaller than those of alkane chains indicating enhanced electron transport through peptide systems. This is one of the reasons why they are attractive candidates for single molecule conductance measurements. An examination of the secondary structure and bonding properties for different peptide sequences is required to understand how electron transfer proceeds through such molecules.

The carbon-nitrogen peptide bond has around 40% double bond character which is sufficient to prevent rotation. As a consequence of this, the peptide bond exists only in its *trans* or *cis* rotational isomer with the *trans* form being the most prevalent.[1,11] The resonance forms of this amide bond means that is also slightly polar with a negative charge on the oxygen and a positive charge on the nitrogen, this characteristic provides the means to stabilise secondary structures through intramolecular hydrogen bonding. Secondary structures often possess a net dipole due to an addition of these smaller dipoles which results in a partial positive charge at one terminal and a negative charge at the other as shown in Figure 5.2.

5.1.2 Peptide Secondary Structure

As stated, the two most common local conformations of peptides are the α-helix and the β-sheet with the α-helix being the most abundant. In an α-helical structure intramolecular hydrogen bonds between the N-H group and the O=C group help to stabilise the structure and account for its rigidity. The α-helix has 3.6 residues per turn with the carbonyl of residue *i* hydrogen bonded to the amide NH of the *i* + 4 residue.[1,4,5] It is characterised by its dihedral angles ω, φ and ψ that constrain the amino acids within the structure.[1,12] The β-sheet conformation is an extended structure requiring two peptide strands that are stabilized by intermolecular bonds between the carbonyl and amide groups of every second backbone residue.[1,13,14] The secondary structure has many purposes such as mechanical rigidity, for example, it may be necessary for protein structures to secure substrates in certain positions, transport other molecules or function in gene expression.[1,2] Many techniques exist with which to identify the secondary structure of peptides. For example, solid state NMR can be used to directly identify secondary structures, this is due to the chemical shifts of the C=O and the C_α in ^{13}C NMR which are distinctive for both helical and β-sheet structures.[14] Circular Dichroism and IR spectroscopy are also used routinely to help elucidate secondary structure.[15]

Several polypeptides favour the α-helix motif, notably those incorporating alanine, glutamic acid and lysine residues[13] and secondary structure can often be predicted using the knowledge and preference of individual and sequences of amino acids. Much work has been carried out to explore the factors that promote helical secondary structures, the introduction of metal ions,[4] pH[16,17] and sequence design[18] are all known to influence helix formation. For example it is known that incorporating a proline residue at the N-terminal of a sequence helps to instigate the first turn within the helix, possibly due to the *cis-trans* isomerism of its subsequent amide bonds. [1,7] Higashi *et al.* showed that immobilisation and assembly of a benzyl fuctionalized, glutamic acid peptide on gold nanoparticles led to an

increase in helicity compared to the peptide in solution.[19] The solvent can also play a crucial role in promoting helix formation[20-22]

5.1.3 Self-Assembly of Peptides

Peptides can form self-assembled monolayers that may be stabilised due to several different interactions including hydrogen bonding, interchain H-N---C=O bonds and interchain dipole interactions. In the case of cysteine containing peptides, disulphide bridges can also stabilize the monolayers.[2,23] The cysteine residue, Figure 5.3, contains a weakly-polar thiol side chain.

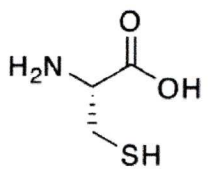

Figure 5.3. The amino acid Cysteine

The adsorption of cysteine on gold is influenced by intermolecular interactions involving the carboxylic acid group and infrared studies have shown that it is possible for this group to form an additional anchor to the gold surface.[24] When a peptide adopts a regular secondary structure on a surface, its IR spectrum exhibits two highly characteristic vibrational modes, known as Amide I and Amide II. The Amide I mode is a result of the stretching of the C=O peptide bond and the Amide II mode is a mixture comprising mainly of the in plane bending of the N-H peptide bond and also stretching of the C-N bond.[25] Information about the structure of peptide monolayers can be determined from the position and intensity of these amide bands enabling the tilt angle of the peptide with respect to the surface to be calculated; it is also possible to calculate the surface coverage. It has also been reported that peptide monolayers generally incorporate water within the layer[26] that contributes to the observed fast electron transport.

Several groups employ protection groups such as Acm[10] and Boc[27] groups, deprotection being used to control the orientation of the peptide within the monolayer. This strategy is often necessary as the macrodipole of peptides can affect its electrical properties when present in films as will be described shortly. This dipole can also affect packing densities in monolayers, for example, packing densities are increased when peptides are bound to gold via the N-terminal compared with the C-terminal due to the alignment of the peptide dipole,[9,28,29] which is a consideration when designing and assembling monolayers for use in molecular electronics.

5.1.4 Electron Transfer in Peptides

There are many factors that influence the efficiency and the kinetics related to electron transfer within peptides, these include the amino acid sequence,[16,30] the nature of the scaffold and the secondary structure,[12,35] the length of the peptide sequence and the distance between electrodes.[16,23,30-32] It has been reported that generally the amino acid LUMO is localised around the carbonyl group, C- terminus and the HOMO at the N-terminus[12,33] and it is generally assumed than electron transfer proceeds via the HOMO.[9] A hopping mechanism has been assigned by many groups to describe the electron transfer through peptide junctions and is reliant on the presence of suitable intermediates between terminal groups in photo-physics experiments, or between the terminal groups in metal | peptide | metal electrical junctions.[8,27] Other groups, however, such as Mandel *et al.*[29] have proposed molecular motion assisted electron transfer involving thermal fluctuations of the peptide bridge. This theory was based on decreased electron transfer rates through tightly packed monolayers.

5.2 Peptides in Molecular Electronics

Much of the work done in the last few years to investigate the electron transport characteristics of short peptide chains has been undertaken by Sek et al[10,26,30,31,34] and Kimura et al[6,7,9,27,35,36] who have studied a wide range of peptide sequences, mainly present in self assembled monolayers or isolated in a matrix of alkanethiols. Many studies have been carried out on alanine based peptides due to their propensity to form helices and the fact that they possess a simple methyl group side chain which avoids multiple non covalent interactions encountered with other, polar side groups. A small selection of these studies are summarised below in Table 1 and are discussed in detail in the following text.

Research Group	Peptide sequences studied	Linkers and metal surface	Phenomena studied	Year
Kimura	$SPh(L\text{-}Aib)_8Ph$ $SPh(L\text{-}Aib)_8Ph$	Au -S	Current-voltage rectification of helical peptides	2005[36]
Kimura	SS18Fc Fc18SS (see text for details)	Au-SS	Linker and dipole effects.	2005[7]
Kimura	$SS(Aib\text{-}A)_nFc$	Au-SS	Distance dependence of electron transfer rates in helical peptides.	2007[35]
Sek	$S(CH_2)_2\text{-}NH\text{-}A\text{-}(K\text{-}A_3E)_2\text{-}K\text{-}A\text{-}Cys$	Au-S	Single molecule conductance of helical peptides.	2005[31]
Sek	$Cys\text{-}(A\text{-}K)\text{-}(EAAAK)_2\text{-}A\text{-}S$	Au-S	Conductance of helical peptides and distance dependence.	2006[10]
Sek	CSA-A-Cys	Au-S Au-N	Different contact effects on conductance through short peptide sequences.	2008[34]

Table 1. A selection of research into the electron transport characteristics of peptides.

The first study shown in Table 1 by the Kimura group, demonstrated rectification behaviour for a helical peptide upon the introduction of a redox group at one terminal. The peptide backbone consisted of alternating leucine and aminoisobutyric acid, both employed for their helix favouring properties and a thiobenzoic acid linker was used to immobilize the peptides in monolayers on a gold surface. The I-V behaviour obtained using an STM showed slight rectification behaviour. When a ferrocene group was introduced to the peptide, this rectification behaviour became more pronounced and was attributed to the regulation of the electron transfer by the ferrocene.

The Kimura group have also studied the long range transfer through ferrocene terminated octadecapeptides.[7] The SS18Fc peptide (Table 1) contained a disulfide group at the N-terminus with a ferrocene moiety at the C-terminus. The peptide backbone was comprised of alternating alanine and aminoisobutyric acid residues with two glutamic acid derivatives inserted into the sequence. The same sequence with the disulfide at the C-terminus and the ferrocene at the N-terminus was also investigated, as upon adsorption to gold this molecule was expected to have a dipole direction opposite to the SS18Fc. The long range transfer was studied on SAMs of both molecules using electrochemical methods and it was determined that the change in dipole direction did not significantly alter the measured rate constants through the monolayer. During this study, the group also investigated the replacement of linkers formed from methylene chains with those composed of phenylene groups. This dramatically increased the observed electron transfer rate and led the authors to conclude that the rate determining step in electron transfer through helical peptides is the local electron transfer between the gold and the molecular terminal of the peptide. The long range electron transfer was predicted to occur through the HOMOs of the peptides via a hopping mechanism, where the amide groups within the molecular backbone act as hopping sites. This theory was reinforced by the studies of the distance dependence on long range electron transfer in 2007.[35] Here, helical peptides of various lengths were studied and electron transfer rates between 16 residue peptides and 24 residue peptides were found to be

similar, a phenomenon that cannot be explained by the use of a simple tunnelling model. They have also reported that the mechanism of electron transfer in peptides can switch from superexchange to hopping at a certain threshold distance.[9]

The experimental work of Sek *et al*,[31] demonstrated that the conductance of an α-helical peptide fourteen residues in length is comparable to that of dodecanedithiol. The amino acid sequence was chosen to be helix favouring as it contained mainly alanine and lysine residues with a cysteamine linker at one terminal and a cysteine residue at the other. The electrical measurements were carried out with STM using the groups' monolayer/*I*(*s*) method at a bias voltage of 0.2 V and current was measured from –0.4 to +0.4V. The resulting current voltage curves for the α-helical peptide and a dodecanedithiol molecule showed very similar values despite a length difference of around 8.1 Å. and the authors attributed this relatively high conductance of the peptide bridge to electron transport mediated by a hopping mechanism, in agreement with the predictions by Kimura. In a hopping process, the distance dependence of electron transfer is much weaker than that of superexchange. Sek also found that the I-V curve for the peptide was asymmetric, recording lower currents at a positive bias, with the current at negative bias being up to four times larger, indicating that in their experiments the electron transfer from the substrate to the tip is more efficient than from the tip to the substrate. This is explained by the fact that the electron transfer rates in α-helical peptides are dependent on the direction in which it proceeds. α-helical peptides have a dipole moment of 3.5 D per residue,[9,23,29,31] along the complete length of a peptide strand this leads a macrodipole. This produces an effective positive charge at the N terminus and an effective negative charge at the C-terminus as described earlier;[37] electron transport, therefore, is more efficient along the molecular dipole of the helix. The same group[30] also observed this rectification behaviour for α-helical polyalanine derivatives on gold and many other groups have observed this directional dependence.[38,39] *β*-sheet peptide conformations on the other hand, have a much smaller dipole moment producing little or no directional dependence[40]

Rectification behaviour has also been studied theoretically, for example, current – voltages curves with large asymmetry have been simulated using *ab initio* density functional theory and Green's function formalisms by Cristancho *et al.*[41] They applied an electric field antiparallel to the intrinsic molecular dipole of polyglycine and polyL-alanine with terminal S-Au groups. They predicted that conduction was only possible after a threshold of 2.2V and attributed this to a decrease of the HOMO-LUMO gap as the bias was increased. Practically zero conduction was calculated at parallel fields. They also found larger currents in polyalanine than in polyglycine due to its enhanced conformational stability.

The final study in Table 1 is an STM study carried out by Sek[34] on different peptide binding modes for short peptides showed that junctions incorporating an Au-N contact had a lower conductance than those with Au-S contacts at both terminals. This is similar to the observations of amide binding characteristics for alkanes on gold discussed previously and was explained by the difference in binding strength of the two groups with the gold STM tip. The different binding modes were obtained by alternatively removing either the Boc or Acm protecting groups from the peptide sequence. These results were complemented by control experiments on alkanethiol systems with similar terminal linkers to those of the peptides, where this conductance difference was also observed. The Sek monolayer technique has been used in the work presented here for both peptides and ether molecules. The group has performed many experiments on single peptides and peptide SAM's and a full review is outside the scope of this thesis.

Work carried out by other groups includes AFM experiments by Afrin *et al.* in which the tensile strength and helix extension of an alanine based polypeptide with terminal cysteine residues was investigated.[13] It was concluded that the tensile strength of an α-helical peptide was very similar to that of a non helically coiled chain. Experiments performed on structural transitions include those by Moretto *et al.*[5] who reported a solvent driven, reversible transition between the α-helix and 3_{10} helix conformations of a substituted Ac-$[_L$-(αMe)Val$]_n$ peptide where n was as low as 6, using the solvent system MeOH/HFA. Identification of the

different structures was achieved through the use of FTIR and circular dichroism techniques. The two secondary structures are separated by a very low conformational energy barrier resulting in the system functioning as a molecular switch. Most of the work to date on the electrical properties of peptides is carried out on synthetic peptides, however, there have also been recent studies on the immobilization of naturally occurring peptides on a gold surface using cysteine linkers.[20]

5.3 Aims

The aims of the following experiments are to study the effect that different linker groups have on the conductance through the short peptide sequences A_5C and C_5A. Various methods to determine the single molecule conductance were used to establish whether or not these molecules conform to a standard conductance value depending on the circumstances and environment in which they are measured. *I*(*s*), break junction and monolayer techniques have all been used.

The second part of the chapter deals with the single molecule conductance measurements of a pH responsive peptide. The aim here was to develop the *I*(*s*) technique in order to measure one peptide in two completely different conformations in a pH solution.

5.4 CAAAAA and AAAAAC

The two six mer peptide sequences were purchased from Anaspec. Purity was > 90% as confirmed by Mass Spec and HPLC data.

The structure of each of the peptide sequences are illustrated in Figure 5.4.

AAAAAC

a)

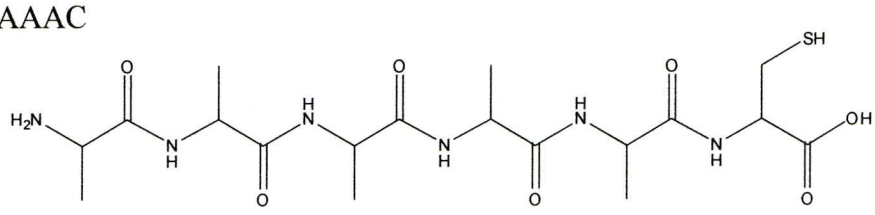

CAAAAA

b)

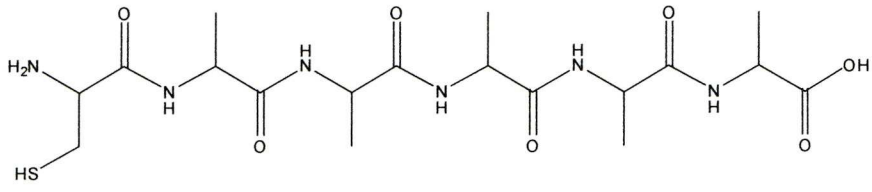

Figure 5.4 a) structure of A_5C, b) structure of C_5A.

In the first, A_5C, the cysteine is located at the C- terminus, so the thiol and the carboxyl group are at the C- terminus and the free amine group at the N- terminus. The second peptide CA_5 has the thiol and amine groups at the N- terminus and just a COOH at the C- terminus. It has already been established that incorporating a cysteine residue enables bonding to a gold tip or substrate via the thiol moiety and amine groups are also able to form contacts to gold.[34,42] Carboxyl groups are also capable of forming contacts with gold leads via coordination of both oxygen atoms,[42,43] although the strength of the COO(H) bond to the surface is less than that of the gold-sulfur and gold-amine bonds.

Due to the design of the peptides, we can study the effects of the two different contacts, the carboxylic group and the amine group to discover if the contact affects the conductance through the molecule. The $I(s)$[43,44] and break junction technique[42] have both been applied successfully to the measurement of carboxylic acid terminated alkanes. So, both of these linker groups should work well when studied with these two techniques.

The CA_5 peptide has been shown to form a low coverage of flat lying molecules on a Hg surface following low adsorption times. Longer adsorption times result in a high coverage layer with the molecules in an upright position and both are a result of the formation of Hg-S bonds. From the experiments carried out by Doneux *et al.*[45] it is suggested that

the high coverage layer is composed of dimers. As the thiol group in peptides is known to readily bind to gold, we are assuming similar assembly features in the following experiments.

These peptide sequences will not have a defined secondary structure as they are too short to form stable helical structures associated with alanine based peptide sequences. It can be assumed, therefore, that their dipole moments are not aligned with the molecular axis. When compared with the helical peptide studied in the course of the chapter, the electric field generated by the dipole will be relatively small and we would expect a very small rectification ratio. Tao *et al.*[38] reported small current voltage asymmetry for extremely short peptides just two and three residues in length.

Also, the pathway of the electron transport is unknown and it is possible that it could occur mainly through the peptide backbone structure if there is insufficient hydrogen or intermolecular bonding. Peptide sequences incorporating helical favouring amino acids generally need to contain at least 12 – 15 [4] residues to establish the rotation angles necessary for helix formation. Sequences shorter than this generally encounter difficulties in adopting the helix. An exception is 3_{10} helixes which have been synthesised with sequences as short as 8 residues.[35] Ma *et al.*[4] also showed that it was possible to use ruthenium and palladium metal complexes to induce helicity in short pentapeptides composed of alanine and histidine residues and they followed these structural changes using NMR and CD. Helix formation in short peptides can also be encouraged by the use of non competing, aprotic solvents. This is because water is often used as a solvent and therefore competes directly with the peptide with respect to hydrogen bonding.[4,21] The short sequences used in this study are soluble in water, since a longer version of this peptide sequence would result in the peptide becoming very insoluble due to the alanine residues. For experiments on longer alanine chains it would be necessary to insert hydrophilic residues such as Lys or Glu periodically within the sequence.[1,21]

The lack of defined secondary structure also means that it is not possible to calculate precisely the length of the peptides, using the SPARTAN

molecular modelling program (Figure 5.5) However, using this program it can be estimated that the peptides are between 0.96 and 1.96 nm long corresponding to helical and fully extended forms respectively. As neither of these forms is likely to be adopted, a value roughly between the two would be expected.

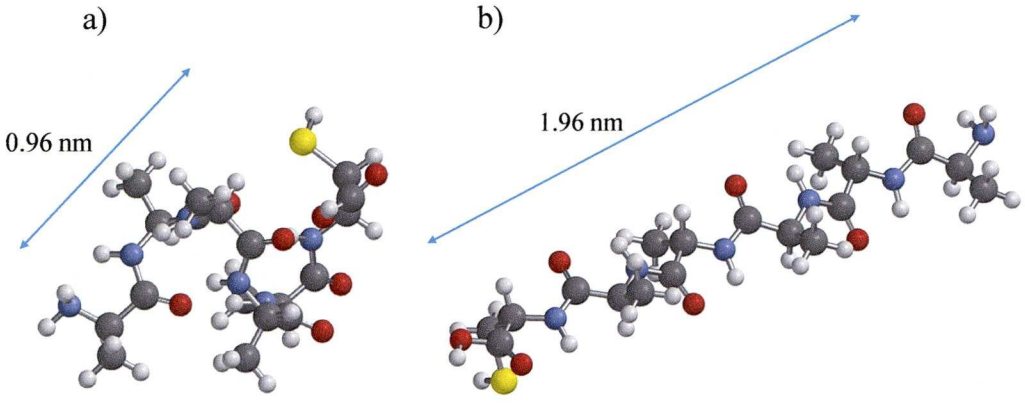

Figure 5.5. Spartan simulations of the A_5C peptide in a) α-helix conformation and b) fully extended conformation.

The solutions of the two peptides were prepared in water/trifluoroethanol; There is evidence that the addition of TFE increases the helical propensity of amino acids in water, due to a decrease in the dielectric constant of the solvent, which decreases the hydration of the peptide backbone.[21,22]

5.5 Experimental

XPS was performed at NCESS, Daresbury Laboratory, UK using a Scienta ESCA 300spectrometer. Take off angles were 10^0 and 90^0. The spectra were referenced to the Au 4d 5/2 line positioned at 335.0 eV.

5.4.1 High Coverage Substrates

2,2,2,-Trifluoroethanol 99% was purchased from Sigma Aldrich and used as received. SAMs of the peptide were prepared by immersion of a flame annealed gold substrate in a 1mM H_20/TFE (60/40) solution of peptide for

~24 hours. The substrates were rinsed with MilliQ® water and dried in a stream of N_2.

5.5.2 Low Coverage Substrates.

Flame annealed gold substrates were immersed in 1 x10^{-4} M H_20/TFE (60/40) solutions of peptides for around three minutes. Again these immersion times were the result of systematic experiments. Shorter immersion times resulted in few or no plateaus observed during measurements. The substrates were then rinsed with Milli Q water and dried in a steam of N_2.

5.6 Results

5.6.1 XPS A_5C

Figure 5.6 shows the spectra recorded for A_5C at 90^0 TOA.

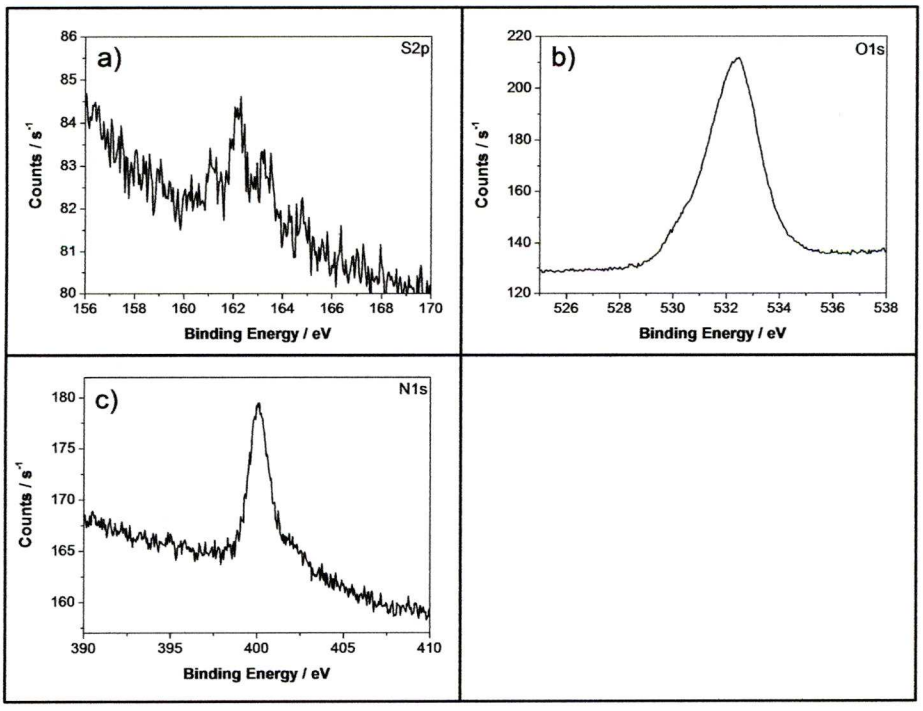

Figure 5.6. XPS spectra for A_5C peptide at 90^0.a) S2p, b) O1s and c) N1s.

The main peak at 162 eV in the S2p region (a) is due to the Au-S bond.[46, 47] The peak at 163.5 eV can be attributed to unbound thiol or disulfide.[47] Unbound thiol groups may result from inadequate rising of the sample before measurement. The peak at 161 eV is generally attributed to atomic or alternatively bound sulfur.[48] The oxygen peak in (b) between 532 and 533 eV is consistent with the carbonyl groups of the peptide backbone[49] and the N1s peak in (c) at 400 eV with the nitrogen contained in the back bone.

Figure 5.7 shows an STM image of one of the surfaces used in the following experiments with a low coverage of A_5C. This image is 150 x 150 nm in size and shows steps and terraces on the Au(111) textured surface. Again, molecular structure would not be seen at this magnification and ordered layers were not expected due to the low concentrations and immersion times used.[50]

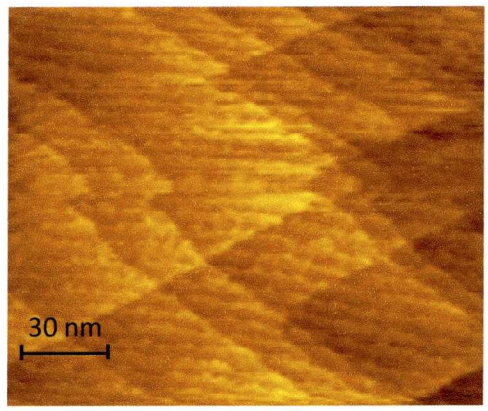

Figure 5.7 Image of flame annealed gold on glass substrates with a low coverage of A_5C. $U_{tip} = 0.1V$, $I_0 = 0.5nA$.

5.6.2 *I*(*s*) Measurements

The *I*(*s*) technique was carried out in air as described previously with 120 scans taken. A set point current of 20 nA was eventually chosen as lower values produced little or no results. Examples of *I*(*s*) scans obtained for this peptide sequence are shown in Figure 5.8. The success rate for obtaining scans displaying a clear plateau was low ~ 1%.

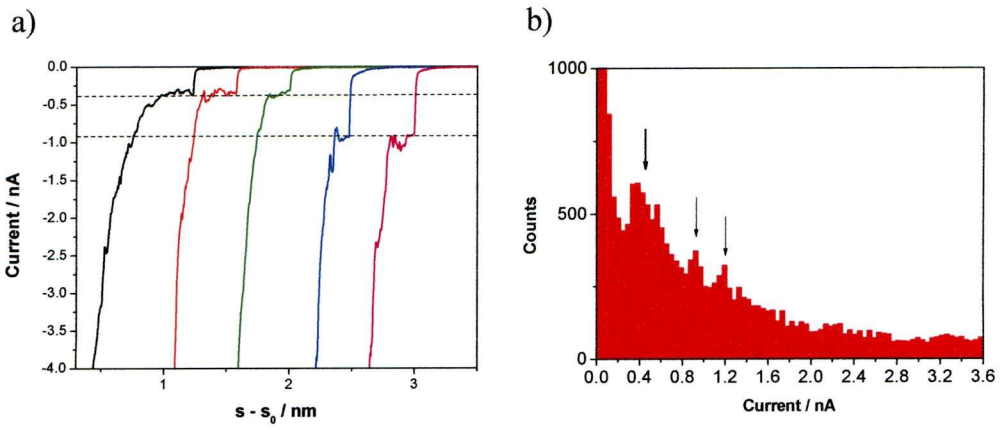

Figure 5.8 a) Examples of *I*(*s*) scans obtained for AAAAAC b) All data current histogram constructed from 120 *I*(*s*) scans at 0.2V, I_0 = 20nA.

There is a clear peak on the histogram giving a conductance of (2.23 ± 0.51) nS or (5.97 x 10^{-5}) G_0. There is also a small second peak just below 1 nA that gives a conductance of (4.62 ± 0.19) nS which is slightly more than double the first; this can be attributed to the A_2 group. The third small peak appears at 1.2 nA giving a conductance of around 6 nS. Although it is a little low to be the A_3 group

Break off distance

The distances at which the current value dropped to zero were measured by hand to construct the histogram shown in Figure 5.9.

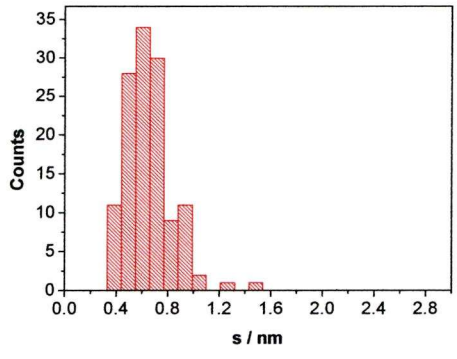

Figure 5.9. Histogram to show measured break off distances for A_5C.

From the main peak the average break off distance was determined to be 0.63 nm. The initial tip sample separation was calculated to be 0.71nm. This gives an overall distance of (1.34 ± 0.2) nm.

5.6.3 Break Junction

Although over 100 scans were collected using this method at 0.2 V, the resulting histogram was unclear. The peak observed suggested a conductance of around 3.12 nS.

5.6.4 Monolayer Results

The initial set point current was set at 5 nA. Figure 5.10 shows example *I*(*s*) data and current histograms for A_5C.

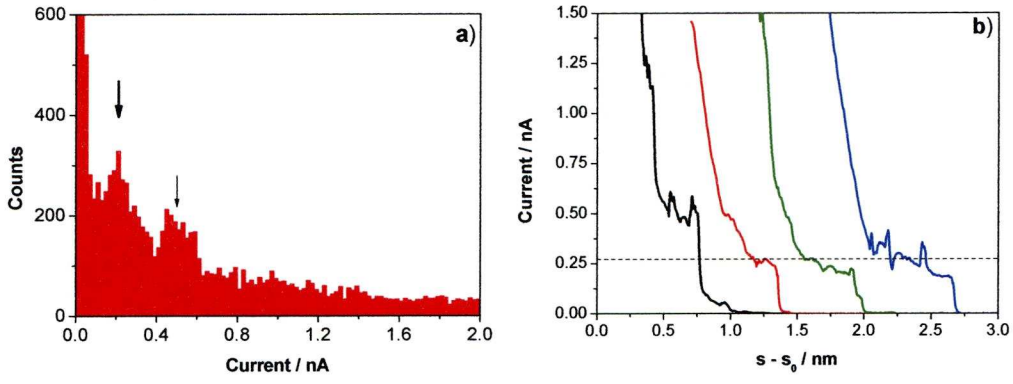

Figure 5.10 a) All current data histogram constructed from 75 scans at -0.2V, I_0 = 5nA, b) Example *I*(*s*) curves

There is a clear peak around 0.21 nA giving a conductance of (1.05 ± 0.21) nS or (1.36 x 10^{-5}) G_0. There is also a second A_2 peak apparent at (2.53 ± 0.26) nS, just over double the value of the first. A conductance of 1.05 is less than half the value obtained using the *I*(*s*) method (2.23 nS). It has been a common feature of these experiments that the conductance calculated using the Sek method is slightly lower than that of other techniques. In the case of the ethers measured in chapter four, although the value was lower, it was still within error limits. With this peptide molecule, however, it is clear that the conductance from the Sek and *I*(*s*) methods are not consistent. This may be because the peptide is more

complex that a simple ether molecule and it can be assumed that when assembled in the monolayer the peptide molecules may be subject to substrate-molecule and neighbouring molecule interactions which may affect their conformation. As illustrated in Figure 5.5, changes in peptide conformation can produce large changes in the overall end to end distance of the peptide which may in turn affect its electrical properties.

5.6.5 *I*(*s*) C_5A

Experiments on this peptide sequence were performed identically to the first. However the success ratio for obtaining acceptable *I*(*s*) scans were considerably lower with an approximate 0.5 % success rate. This is undoubtedly due to difficulty in creating the COOH-gold contact with the STM tip. The percentage of acceptable *I*(*s*) scans was higher at positive potentials than at negative potentials. Nevertheless a full data set was obtained and the results are shown in Figure 5.11.

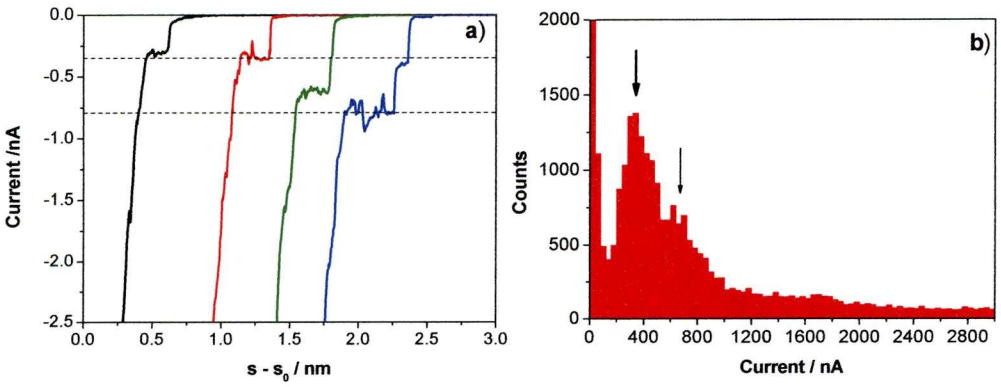

Figure 5.11. a) *I*(*s*) scans for C_5A, b) All data current histogram constructed from 120 *I*(*s*) scans at 0.2V, I_0 = 20nA.

As shown in Figure 5.11 (a), the plateaus were fairly well defined with a sharp drop in current as the molecule detaches. The histogram in (b) shows a clearly defined peak with a conductance of (1.81 ± 0.43) nS or

(2.34 x 10^{-5}) G_0. A large spread of break off values was obtained shown in Figure 5.12.

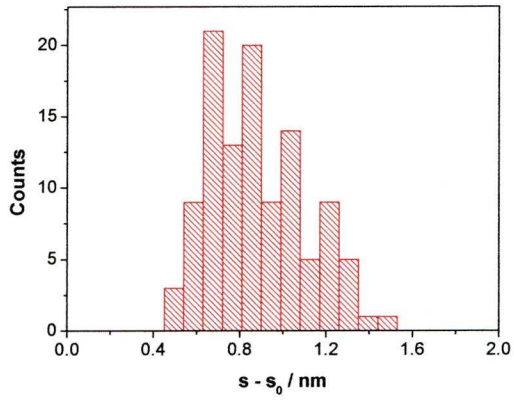

Figure 5.12. Measured break off distances for C_5A using I(s) technique. 0.2V, I_0 = 20nA.

The initial tip-sample separation was calculated to be 0.68 nm. The histogram gives an average distance of (0.858 ± 0.19) nm. This gives an overall value of 1.53 nm. This figure is higher than that obtained for A_5C.

5.6.6 Monolayer Method

Despite several attempts, experiments using the monolayer method on this peptide were unsuccessful. Again this can surely be attributed to the difficulty in creating the carbonyl – gold contact, indicating that the COOH group is situated at the exposed side of the monolayer as we expect.

5.6.7 Break Junction

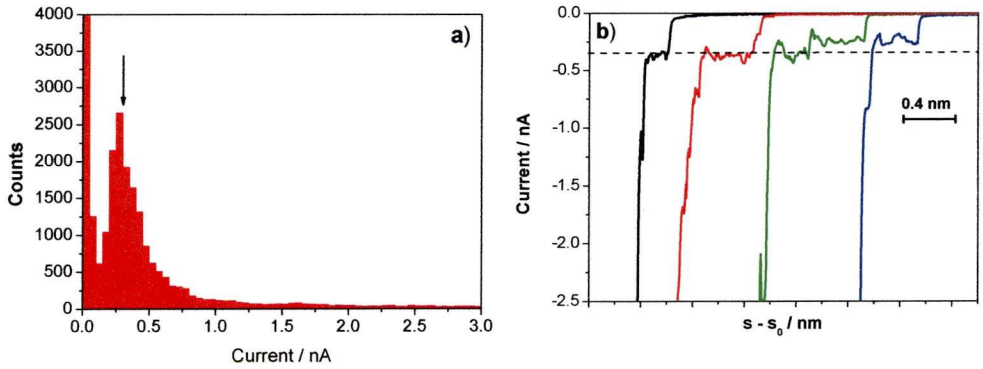

Figure 5.13.a) All data break junction histogram for C_5A, b) Example BJ scans.

The break junction method was used to confirm the measured conductance using the *I*(*s*) technique. The histogram in Figure 5.13 (a) shows that this method was successful in obtaining the A group values for the molecule. The peak is very distinct and gives a conductance of (1.51 ± 0.33) nS or (1.95 x 10^{-5}) G_0. This value is close and within error limits to the *I*(*s*) peak of (1.81 ± 0.43) nS. The example BJ scans in (b) are also well defined with long plateaus, so we can say with some confidence that this is indeed the low conductance value of the peptide.

5.6.8 Current-Voltage Data A_5C

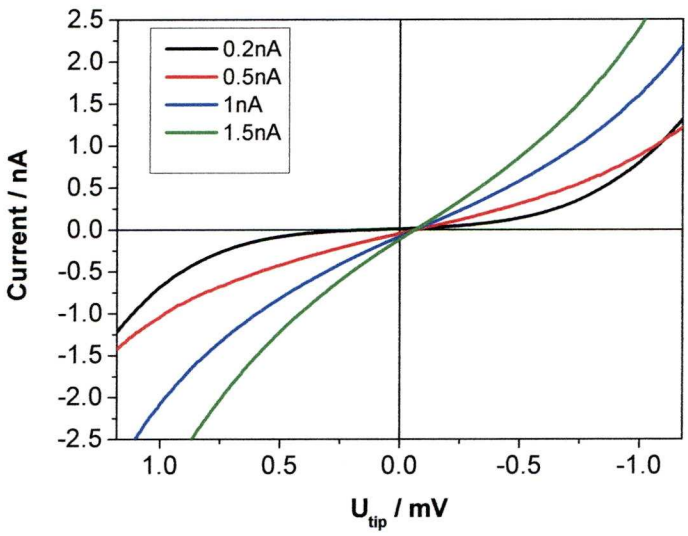

Figure 5.14. Current voltage curves for A_5C.

I-V curves were taken for A_5C high coverage layer at 0.6V at varying set points from 1.2 to -1.2 V (Figure 5.14). Each curve is representative of an average of 10 curves. At 1.5 nA (green line) the linear part of I-V curve corresponds to 2 nS – conductance determined from *I*(*s*) measurements. At a set point of 1 nA (blue line), the curve corresponds to 1.2 nS, closer to the value obtained from the monolayer measurements, this indicates that at this set point the tip has made contact with the monolayer. From the exponential decay, and the equation presented in Chapter 2, it is

possible to calculate that at this bias and set point, the tip is 1.14 nm from the gold surface, where 9.3988 is the average value of $d \ln (I) / ds$.

$$\frac{\ln((77400 \times 0.6)/1}{9.3988} = 1.14\text{nm}$$

This value is not representative of the length of the peptide in the monolayer but estimates the thickness of the film. The length of the molecule calculated from the $I(s)$ technique was (1.34 ± 0.2) nm. When assembled, the peptides will be orientated on the surface at a specific angle. Without the value of this tilt angle it is difficult to calculate the exact length of the peptide.

5.7 Discussion

The two peptides conductance values are (2.23 ± 0.51) nS for A_5C and (1.81 ± 0.43) nS for C_5A, with both values being determined by the $I(s)$ technique. Although overall the peptide with the carboxylic linker appeared to give a lower conductance, the values lie within the error limits. This indicates that the different linking groups do not have a large influence on the electron transport through these molecules.

The measured break-off distances for the two peptides are (1.34 ± 0.2) nm and (1.53 ± 0.2) nm respectively. It is appropriate that the peptide with the slightly lower conductance gave the higher distance value. As the two peptides have different terminal linkers, their conformations and orientation may be slightly different in the gap accounting for the difference in length.

Examination of the I-V traces produced for A_5C shows no rectification behaviour for measurements carried out at $I_0 \leq 1$nA. I-V curves for 1 and 1.5 nA (blue and green lines), on the other hand, show a very small asymmetry with a current increase at positive potentials of approximately 39 and 42% respectively which is consistent with contact to the peptide monolayer. As predicted, the degree of asymmetry is low for due to the

lack of defined secondary structure of the peptide. Also it is possible that the molecules are not uniformly orientated within the junction which will affect the I-V curves.

Without the measured conductance for the C_5A monolayer it is difficult to obtain a good picture of the effects of conductance through single molecules to that through self assembled films. It would also be useful to obtain some characterisation data for the peptides in the SAM using FTIR or peptides in solution with CD. Both of these measurements would give information on the percentage of secondary structure, if any, adopted by the peptide. Calculated tilt angles of the peptide in the film would also contribute to rationalising the distance determined from the monolayer conductance measurements.

5.8 $H(EL)_5C$

Investigations into single molecule conductance were carried out on the peptide sequence $H(EL_5)C$, the structure of which is shown in Figure 5.14. The peptide possesses a cysteine residue (C) at the C-terminus and a histidine residue (H) at the N-terminus. The peptide backbone is comprised of alternating glutamic acid and leucine residues, labelled E and L respectively.

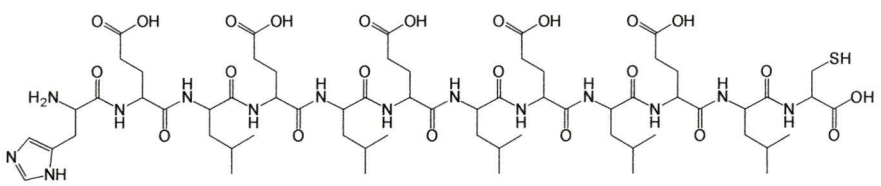

Figure 5.15. Structure of $H(EL)_5C$ sequence

This peptide was used following the 2009 paper by Doneux *et al.*[16] where the same sequence was employed to fabricate pH responsive monolayers through self assembly. They investigated the properties of the monolayer as a function of pH using electrochemical measurements. They found that

at low pH, i.e. pH 2, the peptide was present in a stable α-helix conformation. On the other hand, a random coil structure was dominant at pH 7. The helix-coil transition of polyglutamic acid has been well studied,[17,51,52] both in solution and grafted onto surfaces. Koga *et al* report a structural transition at a pH of around 5.[53] The glutamic acid in the $H(EL_5)C$ peptide is responsible for the relationship between structure and pH and the structure of glutamic acid is shown in Figure 5.16 (a). With its acidic side chain, glutamic acid is a hydrophilic amino acid and leucine (b) with its aliphatic side chain is hydrophobic.[1]

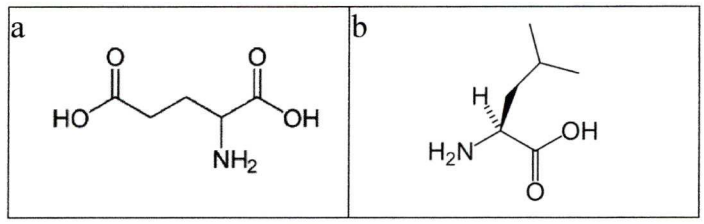

Figure 5.16 a) structure of glutamic acid b) leucine

The carboxylic acid group in the side chain is sensitive to pH. At low pH it is protonated which results in the peptide forming a helical structure. At higher pH values, the carboxyl group is deprotonated, producing negatively charged carboxylates. Electrostatic repulsions between these negative charges prevent the peptide from remaining in a helical state and the sequence adopts an anionic random coil formation. Doneux *et al.* used molecular dynamics and circular dichroism to identify the structures at the two pH values. It should be noted however that not all of the residues will have exactly the same conformation and the α-helical structure is an average structure, also, the random coil will have many possible configurations and is generally formed from bends and turns. By performing single molecule measurements on this particular sequence, it was expected that if, at pH 2, the peptide forms a helical structure then it would be possible to form molecular junctions. On the other hand, at pH 7, an extended random coil conformation would be more difficult to measure.

There have been several studies performed to determine the interaction of histidine with an Au(111) surface. Feyer *et al.* [53] used XPS and

NEXAFS to study the adsorption of histidine and histidine containing peptide sequences; they did so using both monolayer coverage and a low coverage phase. Their XPS analysis of histidine adsorbed on gold showed that the interaction was via chemisorption rather than physisorption and that bonding between the His residue and the Au proceeded via the imino nitrogen atom with only a weak bond existing between the amino nitrogen and the surface. They also concluded that the adsorbed species contained a carboxylate COO^- group, which at high coverage was stronger than that of the imino group. Marti *et al.* [54] used to RAIRS to conclude that it was chiefly the deprotonated carboxylate group that interacted with the surface with the imidazole ring perpendicular to the surface and older studies by Liedberg et al[55] agree with this notion. However, these experiments were performed at a neutral pH and changing the pH can alter the way in which amino acids interact with a surface. It would be expected that the bonding interaction would be different at pH 2.

Figure 5.17 shows a SPARTAN model of the peptide in an α-helical conformation. As reported the presence of intramolecular hydrogen bonds should facilitate electron transport. The model gives an estimation of the length of this peptide as 2.22nm.

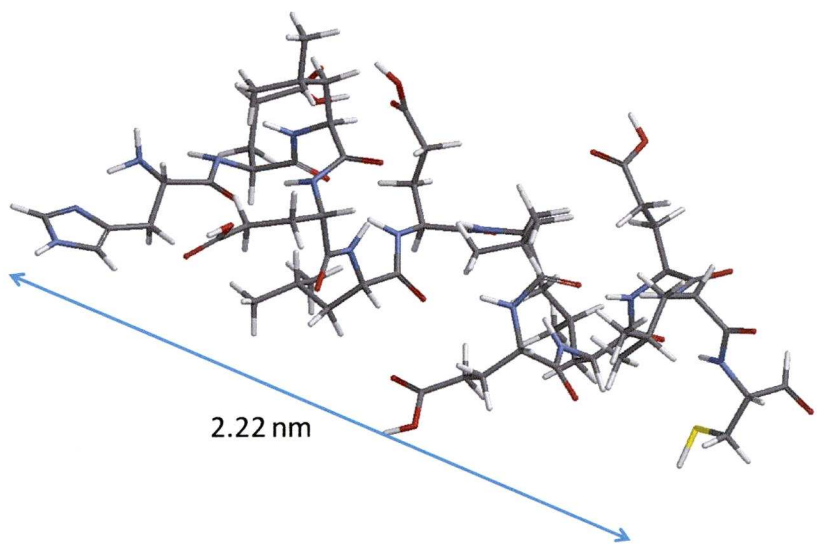

Figure 5.17. SPARTAN model of $H(EL)_5C$.

It is difficult to predict the length of the peptide in a random coil conformation but using SPARTAN a full extension would give a value of around 4.23 nm.

5.9 Experimental

The peptide sequence $H(EL_5)C$ was purchased from Anaspec >90%. Purity was determined using HPLC and Mass Spectrometry, it was used without further purification. $HClO_4$ was purchased from Merck, 70% and K_2HPO_4 and KH_2PO_4 were purchased from Fisons, all chemicals were used as received. All pH measurements were performed on a Hanna 2211 bench pH meter. Calibration was carried out just prior to experiments using pH 2 and pH 7 buffer solutions.

Samples for $I(s)$ measurements were prepared in the same manner as described in Chapter 2. A pH 2 solution was made using Milli-Q® water and perchloric acid and his was used to make a 1×10^{-4} M solution of the peptide. Following immersion of the gold substrate for two minutes, the sample was rinsed with Milli-Q® water and dried in a stream of nitrogen. It was then placed on the STM sample plate and covered with a Teflon cell (See Chapter 2 for cell preparation). It was subsequently filled with the pH2 solution and a cut, coated STM tip was used for $I(s)$ measurements. Samples for high pH measurements were prepared in the same way using pH 6.9 solutions of freshly prepared K_2HPO_4/KH_2PO_4.

5.10 $I(s)$ Results

5.10.1 pH 2 Results

Measurements were carried out at +0.2 and -0.2 V using a set point current of 10 nA. The choice of set point resulted from a systematic increase from 5nA to the point where plateau formation was observed.

Figure 5.18 shows examples of *I*(*s*) scans produced at a bias voltage of 0.2V.

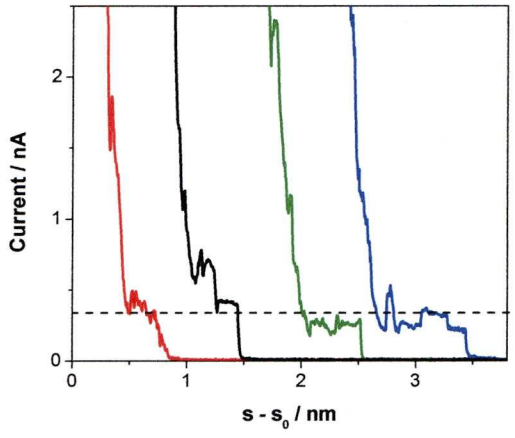

Figure 5.18 *I*(*s*) scans for H(EL$_5$)C at -0.2V I_0 = 10nA

The success ratio for molecular bridging events for this peptide was approximately 1 – 2 %. This ratio is very low, however, when events did occur they were of high quality and a full data set was eventually obtained. The plateaus shown in Figure 5.18 are clearly defined and many were over 0.5 nm in length. The lack of two terminal sulphur groups undoubtedly contributed to the difficulty in creating single molecule junctions. Figure 5.19 shows the resultant histogram compiled from over 100 *I*(*s*) curves showing current plateaus.

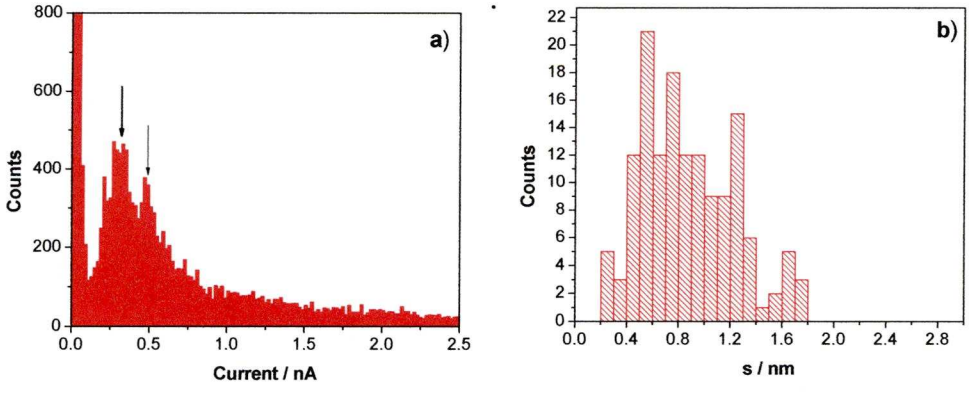

Figure 5.19. a) All data *I*(*s*) histogram for H(EL$_5$)C at -0.2 V b) Break off distance measurements.

The main peak gives a conductance of (1.76 ± 0.50) nS or (2.27 x 10^{-5}) G_0, with an A_2 group at 2.49 nS. The value of the A_2 group is fairly low and may in fact be due to conformational changes rather than two molecules in

the junction. Although the measurements were carried out in pH2 solution to maintain the helical structure throughout, as stated earlier, the α-helical structure is an experimentally determined average structure. It is possible the helix was compressed or modified in the junction giving the second conductance peak or alternatively there may be two current values corresponding to slightly different local conformations of the peptide. Similarly, in the break off distance measurements Figure 5.19 (b) we see a large deviation in the average break off distance value.

Alternatively, as helical peptides show directional dependence, the second peak may be due to the orientation of the peptide in the junction. Although the likely orientation of the molecule in the junction is the sulphur bound to the substrate, it is possible that binding to the tip may occur through either the cysteine or the histidine residue.

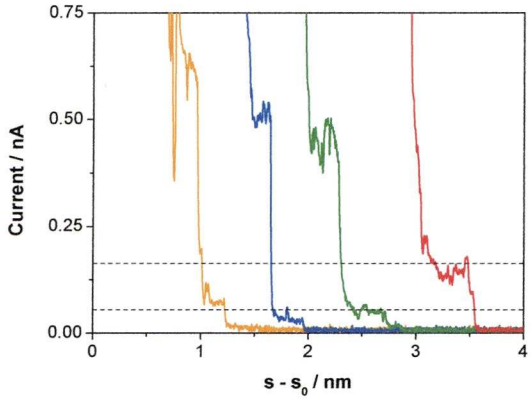

Figure 5.20 *I*(*s*) scans for H(EL$_5$)C displaying low current plateaus.

Close examination of some *I*(*s*) scans (Figure 5.20) show a very low current plateau around 0.05 nA corresponding to ~ 0.3 nS with a length of over 1 nm, however, these currents are obscured in the all data histogram. There are several reasons for the presence of the lower value plateau. Several groups have proposed that the mechanical extension of an α-helical peptide proceeds via 3_{10} helices[13,56] and the low current plateau may be indicative of an occasional structural conformation change as the tip is retracted, as the 3_{10} helix is about 0.4 Å per reside longer than the α-helix.[5] The break off distances over 1.2 nm were plotted against the associated current value to reveal that the longer break off distances

correlate to low currents, around 0.03 nA. If we discount the distance measurements due to these low current values we have a break off distance of around 0.81 nm. We can calculate that at 10 nA the STM tip is 0.803 nm from the surface giving a total length of ~1.61 nm. Sek et al also proposed a similar explanation for their observed non-zero current drops when performing *I*(*s*)-like measurements on helical peptides. They concluded that low-conductive conformations of the peptide may be responsible.[10]

5.10.2 pH 7 Results

As previously described, it is expected that at pH 7 the peptide adopts an irreversible random coil formation. It is unlikely that conduction through the molecule will be possible at this point due to the extended length and lack of electron transfer pathways through the molecule. Measurements were again carried out at 0.2 and -0.2 V and as predicted, no plateaus were observed during measurements. *I*(*s*) scans were performed over several hours on three different samples and at different sample locations. The histogram in Figure 5.21 (a) shows an all data histogram constructed from over 1000 *I*(*s*) measurements with representative scans shown in Figure 5.21 (b)

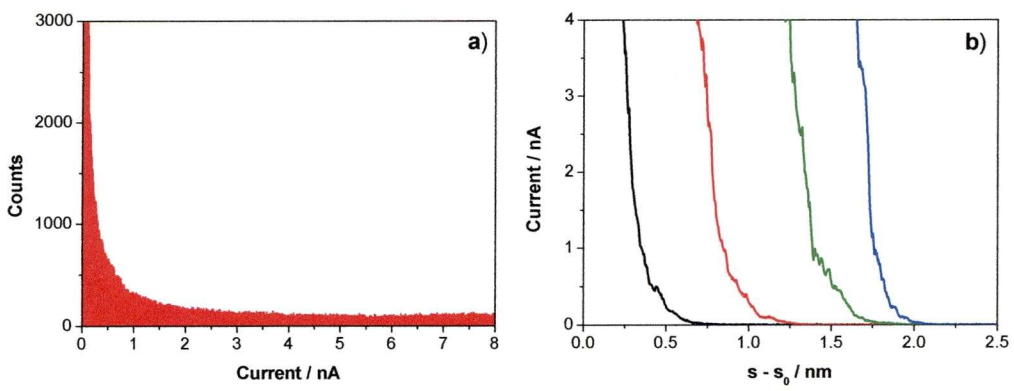

Figure 5.21 All data histogram of H(EL$_5$)C at pH 7, -0.2 V. I$_0$ = 10 nA, b) *I*(*s*) scans.

There is no discernable peak visible within the data, indicating that tip was not able to pick the molecule up or that there was little or no conductance through the peptide in its extended configuration. Throughout the measurements, only around five or six scans were taken that displayed a current plateau, examples of which are shown in Figure 5.22. The jumps appear around 0.1 to 0.3 nA, giving a conductance of between 0.5 and 1.5 nS. There are not enough of these measurements to produce a reliable data set and by examining the break off distance for each it is likely that they can be attributed to occasional structural fluctuations or lifting of the molecule by creation of a bond between any one of the central residues.

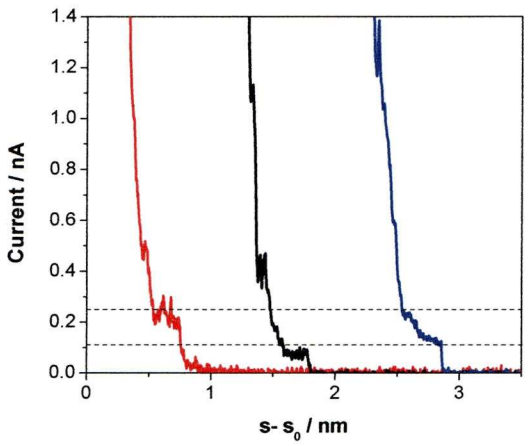

Figure 5.22. Low current plateaus for $H(EL)_5C$.

5.11 Discussion

The ability to measure the peptide single molecule conductance at low pH but not at high pH is in agreement with the helix-random coil transition proposed. The results from the $I(s)$ measurements at pH 2 give a conductance of (1.76 ± 0.50) nS. This value is comparable to the one determined in Chapter 3 for HDTA, demonstrating the enhanced electron transport properties of the α-helix conformation, being more than double the length with a difference of at least 1.17 nm.

This is consistent with the model presented by Cristancho *et al.*[41] When the group performed theoretical calculations on α-helical forms of fifteen

mer polyglycine and polyL-alanine, discussed earlier, they also performed the calculations on the corresponding linear configuration of the polyglycine. They predicted that the linear configurations would have extremely small conductance values and show no current-voltage dependence due to the extended electron transfer pathway which seems to be the case here.

Experiments on self-assembled monolayers would allow a more detailed study of the electron transport through this particular peptide in its helical form and monolayers prepared from the pH 2 solution have been shown to be stable in the potential range +0.45 to -0.5V. It is likely that the peptide would be immobilized via the thiol linker of the cysteine[16] allowing the STM tip to interact with only the histidine group, thus removing the question of the orientation of the molecule within the junction. It would then be possible to obtain current-voltage data for the peptide to investigate the directional dependence.

The peptide in its helical form corresponds to a minimum length of around 2.2 nm, according to the literature [8,9] the critical distance at which tunnelling is no longer possible is between 14 and 20Å, suggesting that electron hopping may be a possible conduction mechanism through the peptide.

5.12 Conclusions

STM techniques including *I*(*s*), break junction and monolayer methods have been used successfully to determine the single molecule conductance through the C_5A and A_5C peptides. The different linkers on each peptide were not observed to have an impact on the resulting values however more detailed study is needed including the characterisation of these peptides present in monolayers.

The $H(EL)_5C$ peptide showed that conformational changes as a function of pH can be monitored using the *I*(*s*) technique. At low pH values, the peptide has been reported to have an α-helical secondary structure which allowed the determination of its single molecule conductance. At high pH

values the peptide has a random coil structure which is considerably longer and lacks the electron transport capabilities of the helical form. The peptide in this form could not therefore be measured using the STM techniques presented here.

References

1. Grant, G. A. Synthetic Peptides. W. H. Freeman and Company. (1992).
2. Doonan S. Peptides and Proteins. Cambridge : Royal Society of Chemistry, (2002).
3. Zagrovic, B.; Jayachandran, G.; Millet, I.; Doniach, S and Pande, V. S. *J. Mol. Biol.* **353**, 232-241. (2005).
4. Ma, M. T.; Hoang, H. N.; Scully, C.; Appleton, T and Fairlie, D. P. *J. Am. Chem. Soc.* **131**, 4505-4512. (2009).
5. Moretto, A.; Formaggio, F.; Kaptein, B.; Broxterman, Q. B.; Wu, L.; Keiderling, T. A and Toniolo, C. *Biopolymers.* **90** (4), 567-574. (2008).
6. Okamoto, S.; Morita, T and Kimura, S. *Langmuir*, **25**. 3297-3304. (2009).
7. Watanabe, J.; Morita, T and Kimura, S. *J. Phys. Chem. B.* **109**, 14416-14425. (2005).
8. Cordes, M and Giese, B. *Chem. Soc. Rev.* **38** 892-901. (2009).
9. Arikuma, Y.; Takeda, K.; Morita, T.; Ohmae, M and Kimura, S. *J. Phys. Chem. B.* **113**, 6256-6266. (2009).
10. Sek, S.; Misicka, A.; Swiatek, K and Maicka, E. *J. Phys. Chem. B.* **110.** 19671-19677. (2006).
11. Elliott, W. H and Elliott, D. C. Biochemistry and molecular biology. 3rd edition. OUP: UK. (2005).
12. Santhanamoorthi, N.; Kolandaivel, P and Senthilkumar, K. *Chemical Physics Letters*. **440**. 302-307. (2007).
13. Afrin, R.: Takahashi, I.; Shiga, K.; and Atsushi, I. *Biophysical Journal*, **96**, 1105-1114. (2009)
14. Floudas, G. and Spiess, H. W. *Macromol. Rapid Commun.* **30**, 278-298. (2009)
15. Impellizzeri, G.; Pappalardo, G.; Purrello, R.; Rizzarelli, E. and Santoro, A. *Chem. Eur. J.* **4** (9), 1791-1798. (1998)

16. Doneux, T.; Bouffier, L.; Mello, L. V.; Rigden, D. J.; Kejnovska, I.; Fernig, D. G.; Higgins, S. J and Nichols, R. J. *J. Phys. Chem. C*, **113** (16), 6792-6799. (2009).
17. Zimmermann, R.; Kratzmuller, T.; Erickson, D.; Li, D.; Braun, H. G and Werner, C. *Langmuir*. **20**, 2369-2374. (2004).
18. Takeda, K.; Morita, T and Kimura, S. *J. Phys. Chem. B*. **112**, 12840-12850. (2008).
19. Higashi, N.; Kawahara, J and Niwa, M. *J. Coll. Inter. Sci*. **288**, 83-87. (2005).
20. Uzarski, J.; Tannous, A.; Morris, J and Mello, C. *Colloiid and Surfaces B: Biointerfaces*. **67**, 157-165. (2008).
21. Vila, J. A.; Ripoll, D. R and Scheraga, H. A. *Proc. Natl. Acad. Sci*. **97** (24), 13075-13079. (2000).
22. Higuchi, M.; Ushiba, K and Kawaguchi, M. *J. Coll. Intf. Sci*. **308**, 356-363. (2007).
23. Pace, G.; Venanzi, M.; Castrucci, P.; Scarselli, M.; De Crescenzi, M.; Palleschi, A.; Stella, L.; Formaggio, F.: Toniolo, C.; Marletta, G. *Materials Science and Engineering* (2005)
24. Bieri, M.; Bürgi, T. *J. Phys. Chem. B*. **109**, 22476-22485. (2005)
25. Mendelsohn, R. and Flach, C. R. *Handbook of Vibrational Spectroscopy 2*. 1028-1041. (2001).
26. Sek, S.; Moszynski, R.; Sepiol, A.; Misicka, A and Bilewicz, R. *Journal of Electroanalytical Chemistry*. **550**, 359-364. (2003).
27. Morita, T.; Yanagisawa, K and Kimura, S. *Polymer Journal*. **40**(8), 700-709. (2008).
28. Gatto, E.; Venanzi, M.; Palleschi, A.; Stella, L.; Pispisa, B.; Lorenzelli, L.; Toniolo, C.; Formaggio, F and Marletta, G. *Materials Science and Engineering C*. **27**, 1309-1312. (2007).
29. Mandal, H. S and Kraatz, H. *Chemical Physics*. **326**, 246-251. (2006).
30. Sek, S.; Tolak, A.; Misicka, A.; Palys, B.; Bilewicz, R. *J. Phys. Chem. B*. (2005) need voume
31. Sek, S.; Swiatek, K.; Misicka, A. *J. Phys. Chem. B*, **109** (49), 23121-23124. (2005)

32. Long, Y.; Abu-Irhayem, E.; Kraatz, H. *Chem. Eur. J,* **11**, 5186-5194. (2005)

33. Santhanamoorthi, N.; Kolandaivel, P and Senthilkumar, K. *Journal of Molecular Graphics and Modelling.* **27**, 784-791. (2009).

34. Sek, S. *J. Phys. Chem. C.* **111**, 12860-12865. (2007).

35. Kai, M.; Takeda, K.; Morita, T and Kimura, S. *J. Pep. Sci.* **14**, 192-202. (2008).

36. Kitagawa, K.; Morita, T and Kimura, S. *J. Phys. Chem. B*, **109**, 13906-13911. (2005).

37. Wackerbarth, H.; Tofteng, A.; Jensen, K.; Chorkendorff, I and Ulstrup, J. *Langmuir*. **22**, 6661-6667. (2006).

38. Xiao, X, Xu, B and Tao, N. *Angew. Chem. Int. Ed.* **43**, 6148-6152. (2004).

39. Kitagawa, K.; Morita, T.; Kawasaki, M.; Kimura, S. *J. Polymer Science. A*. **41** (22). 3493-3500. (2003).

40. Shin,Y. K.; Newton, M. D and Isied, S. S. *J. Am, Chem, Soc.* **125,** 3722-3732. (2003).

41. Cristancho, D and Seminario, J. M. *J. Chem. Phys*. **132**, 065102 (2010).

42. Chen, F.; Li, X.; Hihath, J.; Huang, Z and Tao, N. *J. Am. Chem. Soc.* **128**, 15874-15881. (2006).

43. Martin, S.; Haiss, W.; Higgins, S.; Cea, P.; Carmen Lopez, M and Nichols, R. J. *J. Phys. Chem. C.* **112**, 3941-3948. (2008).

44. Martin, S.; Manrique, D. Z.; Garcia-Suarez, V. Haiss, W.; Higgins, S.; Lambert, C. J and Nichols, R. J. *Nanotechnology*. **20**, 125203. (2009).

45. Doneux, Th.; Dorcak, V and Palecek, E. *Langmuir*.**26** (2), 1347-1353. (2010)

46. Wirde, M.; Gelius, U and Nyholm, L. *Langmuir*. **15**, 6370-6378. (1999).

47. Castner, D. J. *Langmuir*, **12** (21), 5083–5086. (1996).

48. Zharnikov, M. *J. Electr. Spec. Rel. Phenom*, **178-179**, 380-393. (2010).

49. Lopez, G.; Castner, D. G and Ratner, B. D. *Surface and Interface Analysis*. **17**, 267-272. (1991).

50. Haiss, W.; Nichols, R.; Zalinge, H. V.; Higgins, S. J.; Bethell, D.; Schiffrin, D.J. *Phys. Chem. Chem. Phys*, **6**, 4330-4337. (2004).

51. Koga, T.; Nagaoka, A.; Higashi, N. *Colloids and Surfaces A*, **284**, 521-527. (2006).

52. Zimmermann, R.; Osaki, T.; Kratzmuller, T.; Gauglitz, G.; Dukhin, S and Werner, C. *Anal. Chem*. **78**, 5851-5857. (2006).

53. Feyer, V.; Plekan, O.; Tsud, N.; Chab, V.; Matolin, V and Price, K. *Langmuir*. **26** (11), 8606-8613. (2010).

54. Marti, E. M.; Quash, A.; Methivier, C.; Dubot, P and Pradier, C. M. *Colloids and Surfaces A.* **249** 85-89. (2004).

55. Liedberg, B.; Carlsson, C and Lundstrom, I. *Journal of Colloid and Interface Science.* **120**, 64-75. (1986).

56. Rohs, R.; Etchebest, C. and Lavery, R. *Biophys. J.* **76**, 2760-2768. (1999)

Chapter 6. Conclusions

The single molecule conductance of several different "molecular wires" has been determined experimentally. One of the aims of this thesis was to investigate the effect of simple atom substitution on the single molecule conductance of polymethylene chains. The results of the subsequent experiments have led to the observation that even small changes to the structure of a molecule can affect its electrical properties and these effects have been discussed in terms of various tunnelling models and DFT calculations of molecular orbital energies. Environmental effects on the conductance of molecular junctions have also been investigated; the results from these studies indicated that the electron transport through certain molecular sequences can be sensitive to the conditions in which they are measured.

Peptide sequences provide interesting ways with which to study single molecule conductance. Their ability to exist in defined secondary structures and the ease with which they can be functionalised has made them attractive systems for molecular electronic applications. Conduction through such molecules as a function of their sequence and secondary structure has been discussed and the electron transfer through short peptide sequences chemically bound to gold has been investigated. Also a peptide that can act as a switch in different pH surroundings has been examined.

Heptanedithioacetate has been synthesised and its electrical properties determined experimentally using the $I(s)$ and $I(t)$ techniques developed by Haiss. This is the first reported single molecule conductance value for the C_7 methylene chain. This value of (1.42 ± 0.05) nS was found to fit well with the previously measured conductance values of the *n*-alkanedithiols. These results were then used as part of a wider to study to investigate the anomalous length dependence of alkanedithiols and it was demonstrated that short alkanedithiols do not conform to the length dependence characteristics of longer molecules in the series. This was

found to be the case for all the fundamental conductance groups that can be observed in single molecule studies.

Table 1 provides a summary of all the A_1 conductance group data for each molecule measured using either the $I(s)$ or the $I(t)$ technique The A_1 single molecule conductance as determined by break junction or monolayer methods is also presented where the data exists. Octane- and nonanedithiol are also included to provide a comparison with the TEG and DBE respectively.

Molecule	**I(s) and I(t)**	**Break Junction**	**Monolayer**
DBE	1.26 ± 0.09	1.46 ± 0.53	0.99 ± 0.22
NDT	0.50 ± 0.07[(1)]		
TEG	2.93 ± 0.16	3.54 ± 1.02	3.22 ± 0.55
ODT	0.99 ± 0.07[(1)]		
DPTE	4.10 ± 0.29		
HDTA	1.42 ± 0.05		
A_5C	2.23 ± 0.51		1.05 ± 0.21
C_5A	1.81 ± 0.43	1.51 ± 0.33	
$C(EL)_5H$ (pH 2)	1.76 ± 0.50		

Table 1. Summary of single molecule conductance values determined through the work presented in this thesis.

The DBE molecule was synthesised using a two step process starting from ring opening of THF that resulted in the production of a dichlorobutylether. This was then reacted with potassium thioacetate to produce the target structure which was characterised using ^{1}H NMR, ^{13}C NMR and mass spectrometry. The molecule was designed with a central oxygen atom to determine whether the incorporation of the oxygen affected the electronic properties of the molecule. A number of techniques were employed to determine the single molecule conductance for DBE and it was observed that the central oxygen did significantly increase electron transport along the molecular backbone. A double tunnelling barrier model was applied to this system after SPARTAN® DFT calculations revealed that the HOMO -2 orbital for this molecule was located exclusively on the oxygen and was lower in energy and therefore closer to the Fermi energy of the gold contacts than the orbital located on the whole chain, the HOMO -5. The HOMO -5 orbital had energy similar to that of the frontier orbital of nonanedithiol the alkane analogue to this single ether. This difference may help to explain why the ether was more conductive than the nonanedithiol when measured with the same STM techniques.

Similar studies were performed on the ether with two oxygen bridges. This was synthesised directly from a tosylated version of the molecule using KSAc and NaI as a catalyst. Again the single molecule conductance observed for this molecule was higher than its analogue, octanedithiol. The I-V data for this molecule, however, could not be fit to a simple tunnelling barrier model and the DFT calculations displayed no evidence of a similar double tunnelling barrier mechanism.

A thioether was also prepared which exhibited enhanced conductance capabilities compared to simple alkanes. This observation was attributed to electron transfer enhancement by the central sulfur moiety. The molecule proved difficult to measure with the available techniques, however, due to the strong affinity the central sulfur for the gold surface. It is likely that this molecule can 'stick' to the gold surface and prevent lifting and extension by the STM tip, this theory was supported by the

large spread of both conductance and break off values obtained whilst using the *I*(*s*) technique.

Molecular junctions formed by the oxygen containing molecules in water environments showed increased conductance compared to ambient and argon environments. This may be due to the hydrogen bonding capabilities of the central oxygens. Ambient environments result in films of water forming on the substrate, however, so these observations cannot be rationalised by the simple presence or absence of water within the junction.

A comparable study of popular techniques used to calculate single molecule conductance was also presented, a summary of which is presented below

Break Junction

As reported in the literature, the STM break junction technique can result in slightly higher recorded current values for the low conductance A groups. It also allows for a higher probability of observing B and sometimes C group events due to the different contact geometries resulting from contact of the STM tip with the substrate, for example, adsorption on top or hollow sites. The break junction method was used successfully throughout these studies and gave A and B conductance group values for the ether molecules as shown in table 1. The current values for the B group events were approximately four times larger than that those recorded for A group events.

Monolayer method

The monolayer measurements produced consistently lower conductance values than those obtained using *I*(*s*), *I*(*t*) and break junction methods. This may be a result of intermolecular effects or slight changes in conformation upon self-assembly and packing. It would be advantageous to perform these monolayer measurements on a series of alkanedithiols as all the measurements presented here are performed on SAMs of molecules with a specific functionality whether it be bridging atoms or peptide bonds and side groups. As SAMs of alkanedithiols are stabilized

mainly by Van der Waals interactions, this may help to distinguish between intermolecular effects.

Peptides

The single molecule conductance for C_5A and A_5C were determined experimentally using a combination of STM techniques including *I*(*s*) and break junction methods. Although the literature predicted a difference in single molecule conductance between molecules with terminal sulfur and amine linkers, only a slight difference in conductance was measured in these studies. This may be a consequence of the lack of secondary structure of the two peptide sequences as the length of the molecule in the gap can only be estimated due to many possible conformations of the random coil structures. Also, although the sulfur group is predicted to preferentially bind to the gold surface, the actually orientation of the peptides could not be confirmed without further characterisation.

Performing *I*(*s*) like measurements on high coverage substrates produced some interesting results. The observed single molecule conductance values for the oxygen containing molecules measured using the monolayer technique were within error limits with the values determined from *I*(*s*), break junction and *I*(*t*) methods. This was not the case for the peptides studied. Here, the high coverage measurements produced a lower conductance value than for the other techniques. This highlights the additional parameters that need to be taken into account when dealing with peptide sequences. When assembled in a monolayer, the amide bonds and/or functional groups along the peptide backbone may interact with neighbouring molecules via hydrogen bonding and these lateral interactions mean that the possibility of intermolecular electron transfer within peptide films cannot be discounted.

The *I*(*s*) technique was adapted to perform experiments in different pH environments. Measurement of the $C(EL)_5H$ peptide sequence was possible at low pH values as the peptide is predicted to adopt an α-helical secondary structure under these conditions. In this form the peptide

should be just over 2 nm in length. At high pH values however, the molecule formed a random coil and conductance measurements could not be performed as the peptide was too extended for efficient electron transport. Thousands of $I(s)$ scans were performed at this pH value to ensure the reliability of this claim.

A hopping mechanism is predicted for the $C(EL)_5H$ in its helical form due to the large observed conductance relative to the molecular length. A simple alkane chain of over 2 nm would have a conductance significantly lower and outside the measurable current region of the STM. The literature on electron transport through helical peptides provides support for this theory; however, length dependence studies would further elucidate the mechanism involved. As the main sequence consists of just two alternating residues, it may be possible to synthesis longer versions of this peptide with which to carry out such experiments to probe the limits of electron transport through such a system.

There is still much work to do in the field of molecular electronics as disparity still remains between different groups experimental results and also with theoretical calculations. However the field is advancing quickly and progress in translating these studies of single molecule conductance into functional devices is anticipated.

References

1. Haiss, W.; Nichols, R.; Zalinge, H. V.; Higgins, S. J.; Bethell, D.; Schiffrin, D.J. Measurement of Single Molecule Conductivity Using the Spontaneous Formation of Molecular Wires. *Phys. Chem. Chem. Phys*, **6**, 4330-4337. (2004).

Appendix 1

Data analysis using LabVIEW™

Once the LabVIEW™ program is loaded, raw data from STM $I(s)$ measurements can be selected from any file. Once the data has been selected, various parameters can be set. For example, for the data presented in this thesis, the signal to noise ratio was usually set between 5 and 7. The deviation on the plateau was generally set to 25, giving a 12.5% possible current deviation on either side of the plateau. Once the parameters have been chosen the program is set to run. The program then analyses all the data from that particular folder and the number of files analysed can be monitored using the progress window.

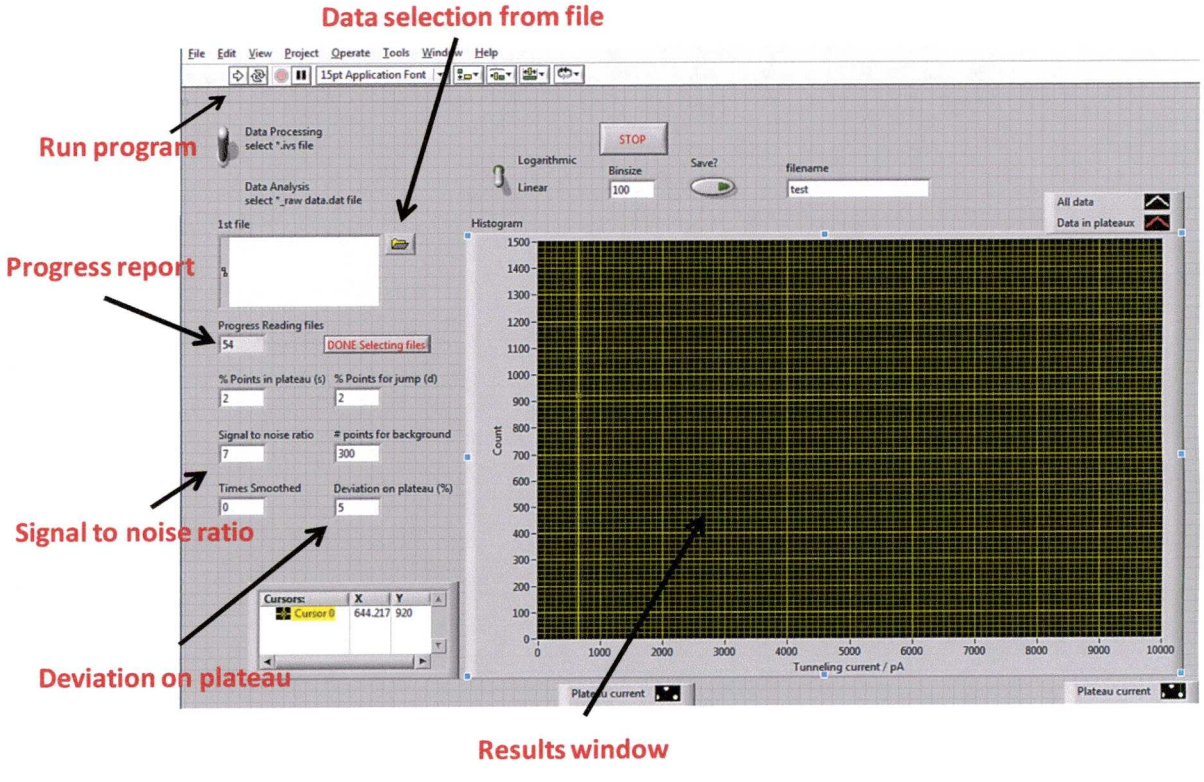

Results

When all the data has been analysed, two histograms will appear in the results window as shown. The large histogram shown in white corresponds to all the data points, while the red histogram shows just the plateau data. With the program still running, the bin size can be altered to obtain the best resolution of the histogram peaks. The line histograms can then be saved to present results. As all the data has then been analysed, the program creates a file containing every data point recorded. This ASCII file can then be imported into Origin™ and is used to construct an all data histogram, numerous examples of which are shown throughout this thesis.

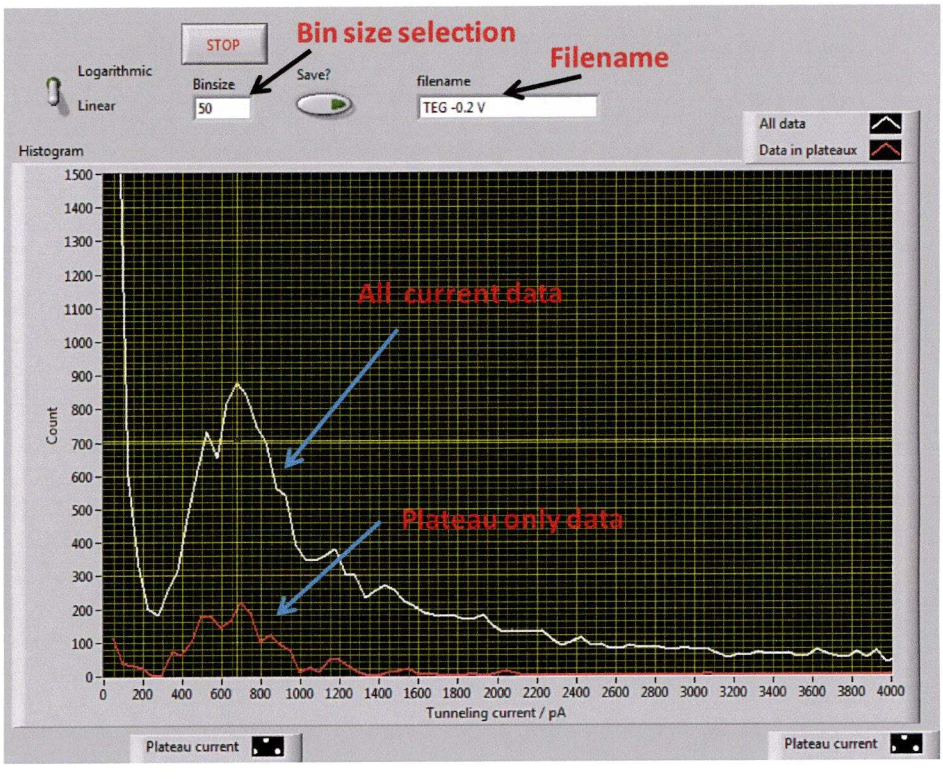

Appendix 2

^{1}HNMR of HDTA

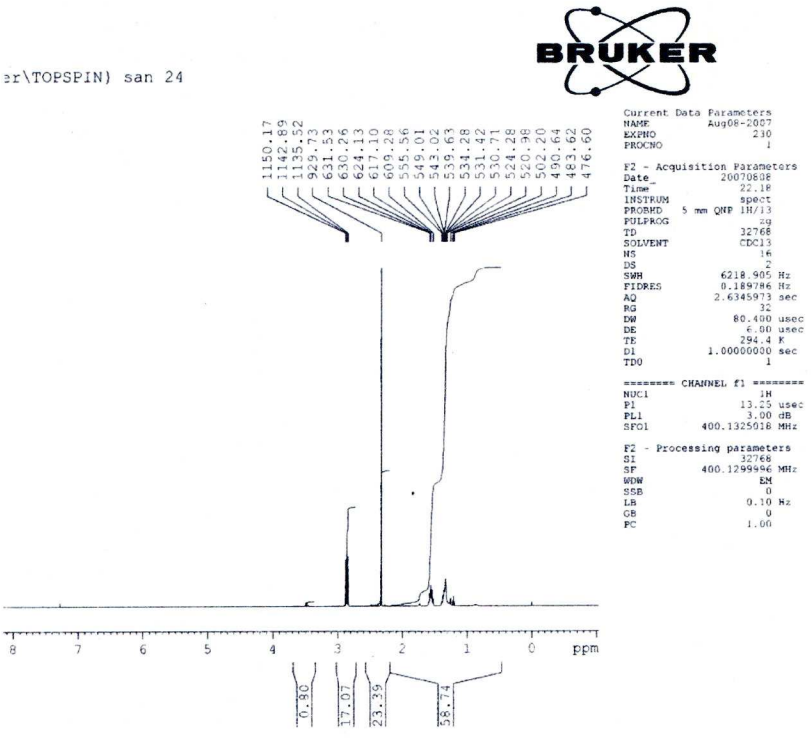

^{13}C NMR for HDTA

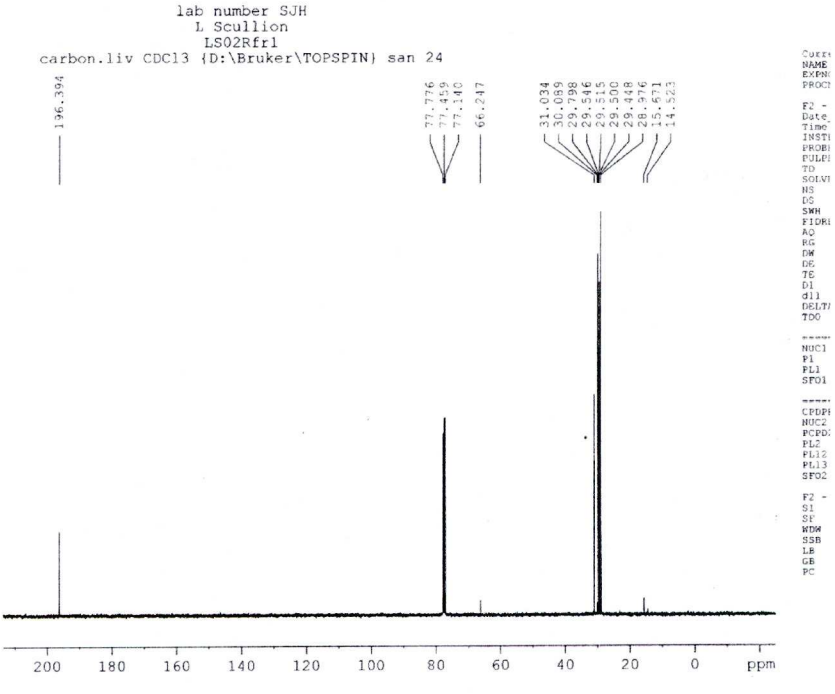

Mass Spec data for HDTA

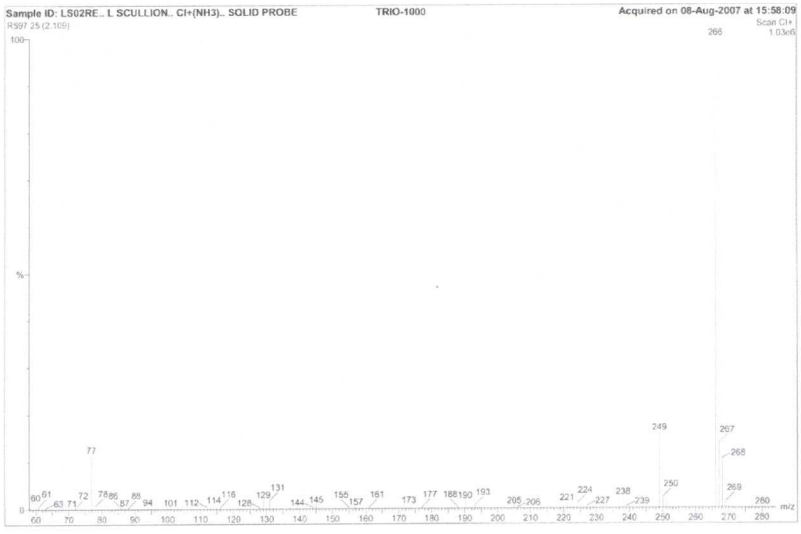

Appendix 3

^{1}H NMR DBE

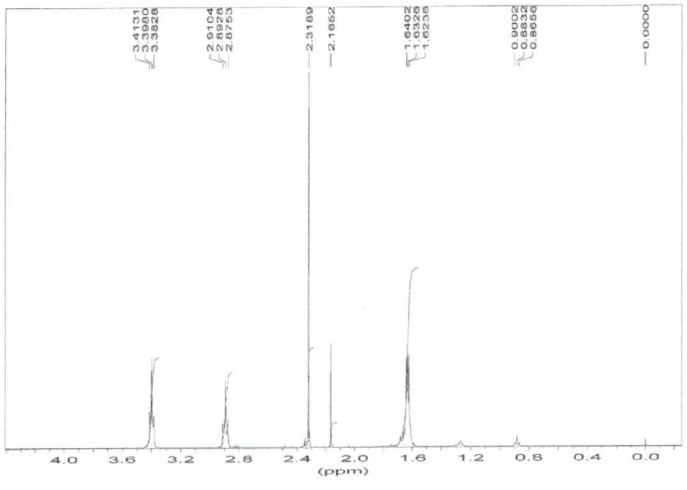

^{13}C NMR for DBE

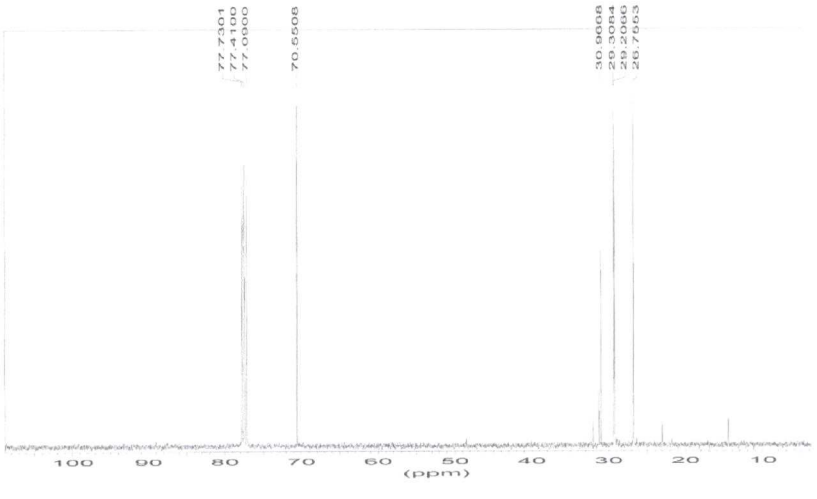

Mass Spec data for DBE

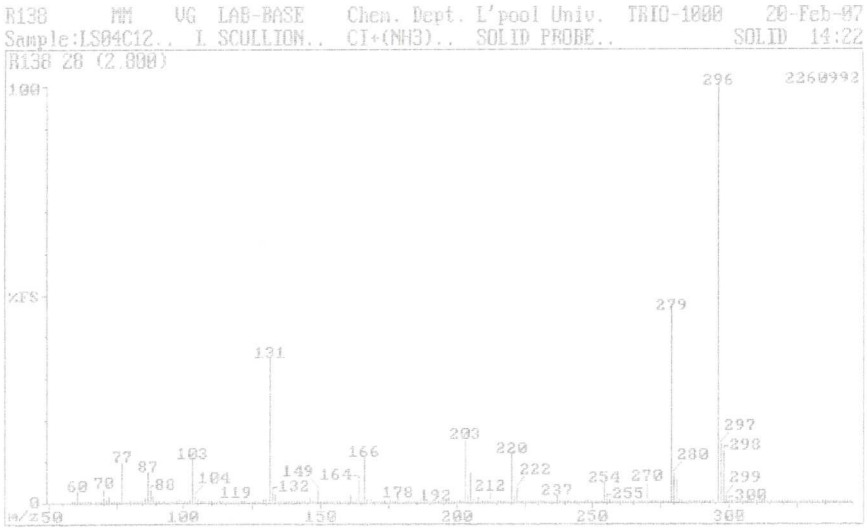

Appendix 4

^{1}H NMR TEG

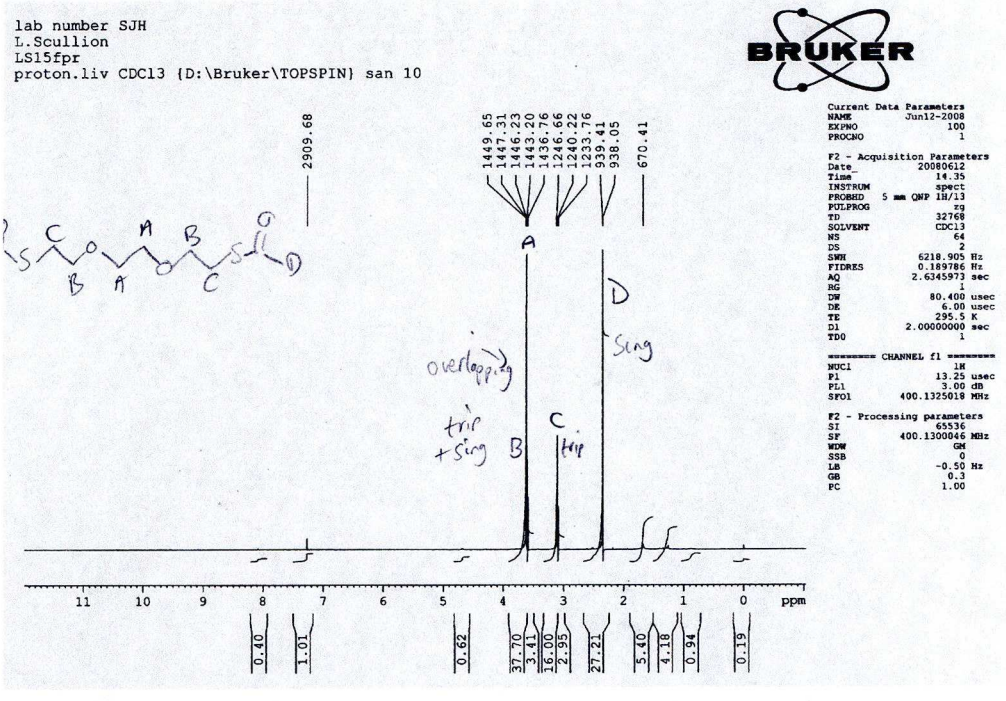

^{1}H NMR TEG – expanded view

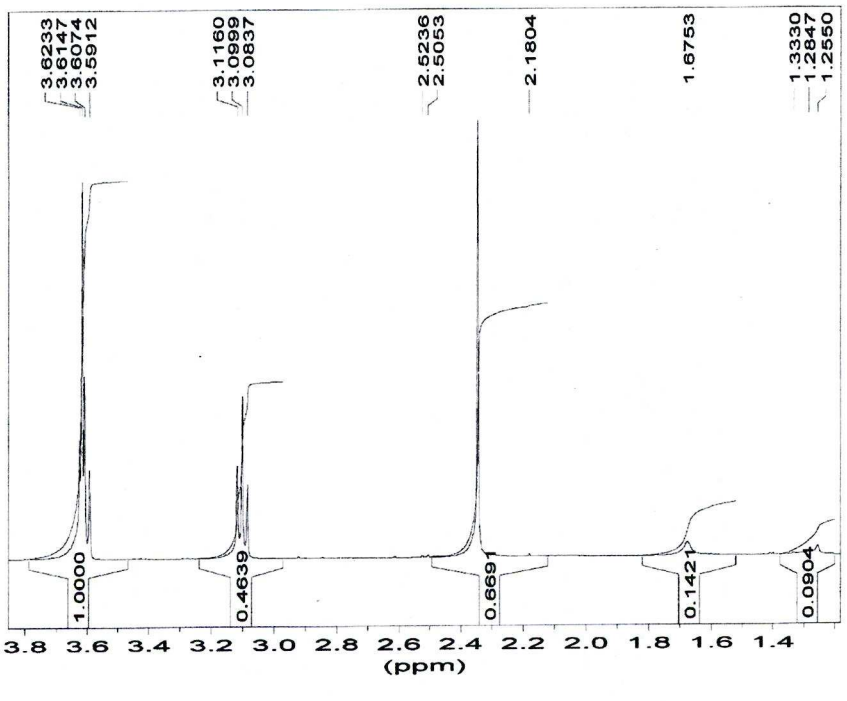

^{13}C NMR TEG

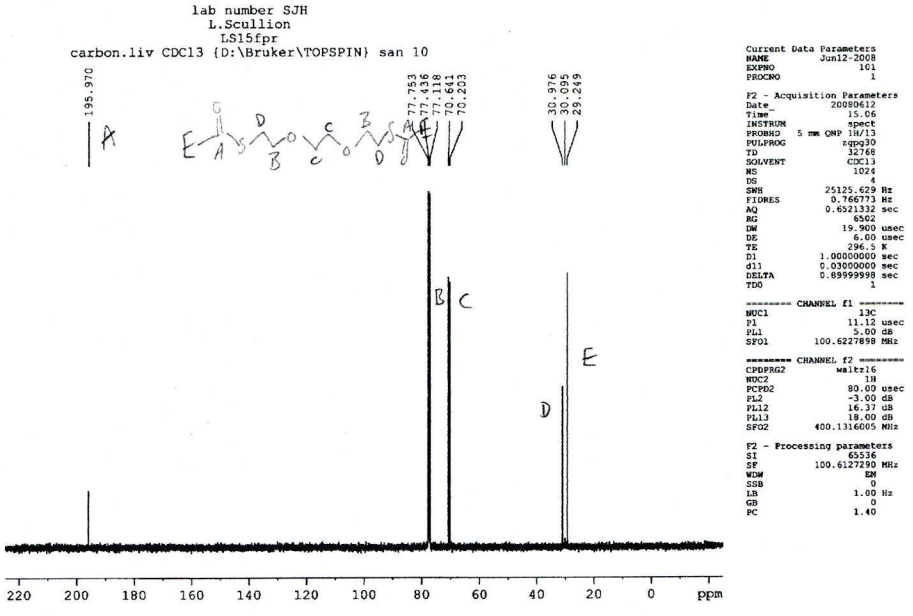


```
Current Data Parameters
NAME            Jun12-2008
EXPNO                  101
PROCNO                   1

F2 - Acquisition Parameters
Date_             20080612
Time                 15.06
INSTRUM              spect
PROBHD   5 mm QNP 1H/13
PULPROG          zgpg30
TD                  32768
SOLVENT              CDCl3
NS                    1024
DS                       4
SWH              25125.629 Hz
FIDRES               0.766773 Hz
AQ                0.6521332 sec
RG                     6502
DW                  19.900 usec
DE                   6.00 usec
TE                  296.5 K
D1                1.00000000 sec
d11               0.03000000 sec
DELTA             0.89999998 sec
TD0                      1

======== CHANNEL f1 ========
NUC1                   13C
P1                  11.12 usec
PL1                  5.00 dB
SFO1            100.6227898 MHz

======== CHANNEL f2 ========
CPDPRG2            waltz16
NUC2                    1H
PCPD2               80.00 usec
PL2                 -3.00 dB
PL12                16.37 dB
PL13                18.00 dB
SFO2            400.1316005 MHz

F2 - Processing parameters
SI                    65536
SF              100.6127290 MHz
WDW                     EM
SSB                      0
LB                    1.00 Hz
GB                       0
PC                    1.40
```

Mass Spec data for TEG

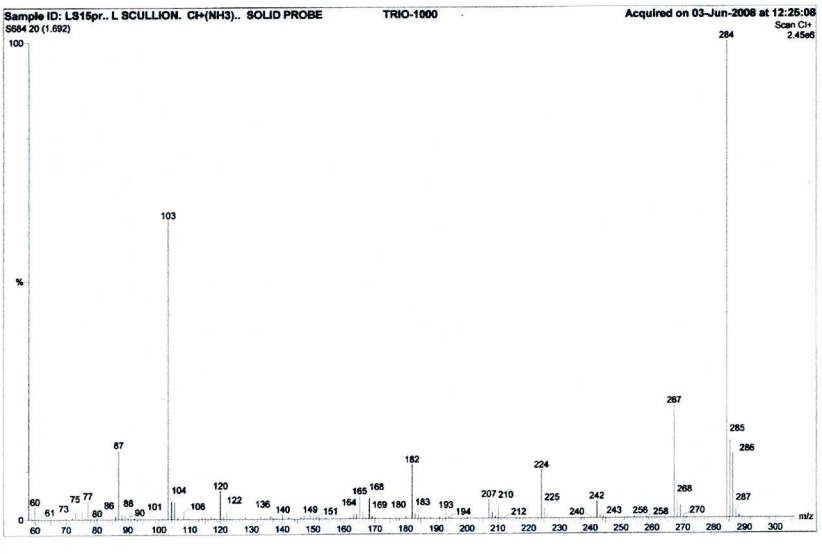

Appendix 5

Synthesis of *S,S'*-(thiobis(propane-3, 1-diyl))diethanethioate. (DPTE).

3, 3'-thiodipropanol (2.54 g, 0.017 mol) was added to 20 cm^3 of dichloromethane. The mixture was stirred and then cooled to 0^0C. Pyridine (3.15 g, 0.04 mol) and TsCl (7.64 g, 0.04 mol) were added slowly and the mixture was brought back to room temperature and stirred for 24 hrs. The reaction mixture was quenched with 200 cm^3 distilled water and extracted with dichloromethane (2 x 100 cm^3). The extracts were washed with distilled water (2 x 125 cm^3) distilled water followed by 1M HCl (30 cm^3) and saturated $NaHCO_3$ solution (100 cm^3) and a further 100 cm^3 distilled water. The organic layer was dried over $MgSO_4$ and filtered under gravity. The solvent was removed and the crude product purified by column chromatography (hexane/EtOAc/MeOH 3:1:1) to give the 3,3□thiobis(propane-3,1-diyl) bis(4-methylbenzenesulfonate). (1.60g, 20.6%).

This product was then refluxed with KSAc (5 Eq, 1.91g, 0.01.6 mol), NaI (0.06g) and acetone (30 cm^3). The reaction was quenched with distilled water (100 cm^3) followed by extraction with EtOAc.(3 x 100 cm^3). The product was dired under high vacuum to give the final product, *S,S'*-(thiobis(propane-3, 1-diyl))diethanethioate. (70 %). ^1H NMR ($CDCl_3$) δ 2.34 (s, 6H), 2.52-2.6 (t), 1.8-1.92 (qu) and 2.94 (t). ^{13}C NMR 28.4, 29.7, 31.1 and 31.4. $[M+NH_4]^+$ 284.